Journal of Drug Delivery Science and Technology 33 (2016) 136–142

Contents lists available at ScienceDirect

Journal of Drug Delivery Science and Technology

journal homepage: www.elsevier.com/locate/jddst

Research paper

The effect of the release behavior of simvastatin from different PLGA particles on bone regeneration *in vitro* and *in vivo*: Comparison of simvastatin-loaded PLGA microspheres and nanospheres

Takayuki Terukina [a], Yoshihito Naito [b], Tatsuaki Tagami [a], Yoshinori Morikawa [a], Yoko Henmi [c], Widyasri Prananingrum [d], Tetsuo Ichikawa [d], Tetsuya Ozeki [a, *]

[a] *Drug Delivery and Nano Pharmaceutics, Graduate School of Pharmaceutical Sciences, Nagoya City University, 3-1 Tanabe-dori, Mizuho-ku, Nagoya, Aichi, 467-8603, Japan*
[b] *Oral Implant Center, Tokushima University Hospital, 3-18-15 Kuramoto-cho, Tokushima, 770-8504, Japan*
[c] *Department of Biomaterials and Bioengineering, Institute of Biomedical Sciences, Tokushima University Graduate School, 3-18-15 Kuramoto-cho, Tokushima, 770-8504, Japan*
[d] *Department of Oral and Maxillofacial Prosthodontics and Oral Implantology, Institute of Health Biosciences, The University of Tokushima Graduate School, 3-18-15 Kuramoto-cho, Tokushima, 770-8504, Japan*

ARTICLE INFO

Article history:
Received 3 February 2016
Received in revised form
7 March 2016
Accepted 7 March 2016
Available online 10 March 2016

Keywords:
Bone regeneration
Simvastatin
poly(lactic-co-glycolic acid) (PLGA) particles
Drug delivery system
Controlled release

ABSTRACT

Simvastatin is a cholesterol-lowering drug known to affect bone formation *in vivo* and its sustainable administration into localized areas is of particular interest in the dental field. Two simvastatin-loaded poly(lactic-co-glycolic acid) (PLGA) formulations (PLGA microspheres and PLGA nanospheres) were compared to investigate whether a sustainable supply of simvastatin from a PLGA-based carrier is effective for bone regeneration. PLGA microspheres successfully presented sustained release of simvastatin for one month, whereas simvastatin was continuously released from PLGA nanospheres for one week. The difference of drug release pattern between two PLGA particles was confirmed by Korsmeyer–Peppas mathematical model. PLGA microspheres and simvastatin alone (no carrier) induced the proliferation MC3T3-E1 cells and increased alkaline phosphatase (ALP) activity, a differentiation marker of MC3T3-E1 cells, whereas PLGA nanospheres did not. These results suggested that PLGA nanospheres had an adverse effect on bone generation *in vitro* due to the production of PLGA metabolized products. Both PLGA microspheres and PLGA nanospheres provided a bone formation effect in an *in vivo* rat calvaria bone defect model and PLGA microspheres were superior to PLGA nanospheres. Our data suggest that simvastatin-loaded PLGA microspheres can release simvastatin sustainably and induce bone formation more efficiently than PLGA nanospheres, thus promoting bone regeneration.

1. Introduction

Dental implant therapy is one of the most reliable options for restoring the teeth of edentulous patients [1,2]. The success of implant therapy depends partly on the status of the patient's alveolar bone, and placing implants in a fully healed alveolar ridge provides the most predictable clinical outcome [3,4]. However, unfavorable local conditions of the alveolar ridge caused by, for example, periodontal disease, malnutrition, or trauma, can result in insufficient bone volume, rendering implant placement unstable or impossible [5,6]. The use of agents to facilitate and increase bone formation, and the use of anti-microbial agents, are useful strategies for addressing these unfavorable conditions. Implantable drugs and drug-loaded carriers for use in the oral cavity have been developed to allow sustainable and localized drug delivery with less drug distribution [7–9].

Simvastatin (SMV), a 3-hydroxy-3-methylglutaryl-coenzyme A (HMG-CoA) reductase inhibitor, is widely used as a cholesterol-lowering drug. It has been suggested that SMV can increase the mRNA expression of bone morphogenetic protein (BMP-2) in osteoblasts when injected subcutaneously over the murine calvaria, resulting in a subsequent increase in bone formation [10]. Several animal studies have been performed to clarify the clinical

* Corresponding author.
E-mail address: ozekit@phar.nagoya-cu.ac.jp (T. Ozeki).

http://dx.doi.org/10.1016/j.jddst.2016.03.005
1773-2247/

importance of SMV [11,12]. Most epidemiological and experimental studies have shown that statins such as SMV have beneficial effects on bone metabolism, as evaluated by bone mineral density and fracture risk [13–15]. SMV has therefore been proposed as a potential agent in dentistry to treat and regenerate the alveolar bone [16–18].

Poly(lactic-co-glycolic acid) (PLGA) is one of the most widely used biodegradable polymers. PLGA can be metabolically hydrolyzed into the monomers lactic acid and glycolic acid. These monomers are endogenous and are easily metabolized by the human body via the citric acid cycle, and thus PLGA is approved by both the US FDA and the European Medicine Agency for use in various drug delivery systems for humans. PLGA-based drug-carriers and biomaterials have been extensively investigated for drug delivery and biomaterial applications. The chemical degradation of PLGA is well characterized [19–21]. The stability of PLGA is affected by various factors such as the polymer molecular weight, the ratio of lactic to glycolic acid in the co-polymers, the polymer-drug ratio, pH, the environmental temperature, and preparation process. SMV-loaded hybrid PLGA particles are made by blending PLGA and materials such as hydroxyapatite, tri-calcium phosphate, or gelatin hydrogel, and many studies have demonstrated that these blends are effective for promoting bone regeneration [22,23]. However, to our knowledge, it remains unclear whether the release behavior of SMV from PLGA-based particles affects bone regeneration.

The present study aimed to determine the release characteristics of SMV from PLGA-based particles and to observe biological responses to this release. SMV-loaded PLGA particles of two sizes (and thus with different drug release profiles) were prepared and compared. We investigated the influence of different degradation mechanisms and drug release behavior of SMV-loaded PLGA particles on bone formation *in vitro* and *in vivo*.

2. Materials and methods

2.1. Reagents

PLGA (ratio of lactic acid:glycolic acid of 75:25, molecular weight 15,000–30,000 Da), polyvinyl alcohol (PVA), and all organic solvents (dichloromethane, acetonitrile, ethanol and acetone; analytical grade) were purchased from Wako Pure Chemical Industries (Osaka, Japan).

2.2. Preparation of SMV-loaded PLGA microspheres (MSPs) & nanospheres (NSPs)

MSPs were prepared using the oil/water (O/W) single emulsion/solvent evaporation method, with modifications [24]. Briefly, 10 mg SMV and 500 mg PLGA were dissolved in 3 mL dichloromethane (DCM). This mixture was dropped into 300 mL of 0.25% (w/v) PVA solution at room temperature with homogenization for 3 min at 10,000 rpm using a PT 3100 homogenizer (Polytron, Kinematica AG, Luzern, Switzerland). The O/W emulsion was then stirred for 6 h to remove DCM by organic solvent evaporation. The resulting MSP suspension was centrifuged at 6000 rpm for 5 min, then washed 3 times with distilled water. The MSPs were frozen at −80 °C for 30 min, then freeze-dried for 24 h using a FD-1 freeze dryer (Tokyo Rikakikai Co., Ltd., Tokyo, Japan).

NSPs were prepared using the O/W single emulsion/solvent diffusion technique, with modifications [25]. Briefly, 100 mg of PLGA was dissolved in 10 mL of acetone, then 1 mg SMV was added and the mixture was sonicated at 180 W for 1 min in an ultrasonic wave cleaner (US-4R; Asone Co., Ltd., Osaka, Japan) to produce the oil phase. This solution was then added to 10 mL of 1% PVA-50% ethanol solution and sonicated again at 180 W for 15 min to form the O/W emulsion. The resulting NSP suspension was centrifuged at 15,000 g for 30 min to remove residual solvent. Then the samples were centrifuged for 5 min, then washed 3 times with distilled water. The NSPs were frozen at −80 °C for 30 min, then freeze-dried for 24 h using a FD-1 freeze dryer (Tokyo Rikakikai Co., Ltd., Tokyo, Japan). The MSP and NSP preparations were stored at −80 °C until further use.

2.3. Characterization of MSPs & NSPs

The morphologies of the MSPs and NSPs were visualized using a scanning electron microscope (S-4300, Hitachi High-Technologies Corporation, Tokyo, Japan). The mean particle size of the MSPs was calculated by measuring the Feret diameter of each particle from the scanning electron microscopy images. In contrast, the lyophilized NSPs were dispersed in 5% PVA solution in an ultrasonic wave cleaner (US-4R; Asone Co., Ltd.) for 5 min and the mean particle size was measured using a Zetasizer Nano-S (Malvern Instruments Ltd, Worcestershire, UK). Samples were measured in triplicate.

The encapsulation efficiency of SMV in the MSPs and NSPs was calculated as described previously [26]. In brief, an appropriate amount of MSPs or NSPs was dissolved in acetonitrile and the SMV concentration was measured by high performance liquid chromatography (HPLC, LC-20 series; Shimadzu, Kyoto, Japan) on a reverse phase column (Inertsil® ODS-80A column; GL Science, Tokyo, Japan). The HPLC conditions were: mobile phase, 100% acetonitrile; flow rate, 0.1 mL/min; wavelength, 238 nm. The encapsulation efficiency was calculated by the formula: Encapsulation efficiency (%) = amount of SMV loaded into the MSPs or NSPs/the initial amount of SMV in the preparation.

2.4. In vitro release profile of SMV from MSPs & NSPs

The release profile of SMV from the MSPs and NSPs was obtained as described previously [26]. Briefly, 3 mL of MSPs (1 mg SMV/sample) dispersed in phosphate-buffered saline (PBS) was loaded into a dialysis tube (Spectrum Laboratories, Inc., Rancho Dominguez, CA, USA; MWCO 12,000–14,000) and stirred in 500 mL of PBS at 37 °C. At set time-points (1, 2, 3, 5, 7, 14, 21 and 28 days for MSPs; 1, 3, 6, 12, 24, 48, 72, 96 and 120 h for NSPs), 1 mL of the dialysis buffer was collected and filtered, and the concentration of SMV was determined by HPLC as described above. Same volume of PBS was added to adjust the volume in dialysis.

2.5. Analysis of drug release kinetics (Korsmeyer-Peppas model)

The mechanism of SMV release from the MSPs and NSPs was analyzed using a mathematical model, as previously described [27,28]. Data corresponding to first 60% of SMV released from the particles were fitted to the Korsmeyer-Peppass equation: $Mt/M\infty = kt^n$. The value of "n" is calculated from the slope of the plot of the log of drug release (M_t/M_∞) vs. the log of time. Mt and M∞ correspond to the percentage of drug released at time t and ∞, respectively, k is the kinetic constant, t is the release time, and n is the diffusional component for drug release.

2.6. Cell culture

The pre-osteoblast murine cell line MC3T3-E1 was obtained from the American Type Culture Collection (ATCC; Manassas, VA, USA). The cells were cultured in MEM-α (Wako Pure Chemical Industries, Osaka, Japan) supplemented with 10% fetal bovine serum (FBS; Biowest, Nuaille, France) and 1% penicillin/streptomycin (Wako Pure Chemical Industries) in an incubator at 37 °C in a 5% CO_2 atmosphere.

2.7. Cell proliferation assay

Cell proliferation was measured using a WST-8 assay kit (Cell Counting Kit-8, Dojindo, Kumamoto, Japan) according to the manufacturer's instructions. MC3T3-E1 cells were seeded in 96-well plates (5000 cells/well). After 24 h, 100 μL of medium containing SMV alone, SMV-loaded MSPs, or SMV-loaded NSPs (SMV concentration: 1 μM) was added to the wells and the cells were cultured for 1, 2, 3, and 4 weeks. The medium in wells containing SMV alone, MSPs, or NSPs was changed five times per week. Before the assay, 10 μL of WST-8 solution was added to each well, then the plate was placed in a CO_2 incubator for 4 h. Cell proliferation was assessed by measuring the absorbance at 450 nm using a microplate reader (Wallac 4000 ARVO multi-label counter; PerkinElmer, Waltham, MA, USA).

2.8. Detection of alkaline phosphatase (ALP) activity

ALP activity was measured using an ALP staining kit (TRACP & ALP double-stain kit; Takara Bio Inc., Ohtsu, Japan) according to the manufacturer's protocol. MC3T3-E1 cells were seeded in 96-well plates (5000 cells/well) and then cultured. After 24 h, the medium was changed to 100 μL of medium containing SMV alone, SMV-loaded MSPs or SMV-loaded NSPs (SMV concentration: 1 μM). After 1, 2 or 3 weeks, the level of *p*-nitrophenyl phosphate was determined by measuring the absorbance at a wavelength of 405 nm using a microplate reader (Wallac 4000 ARVO multi-label counter; PerkinElmer).

2.9. Animals and rat bone-defect model

Wistar rats (12 weeks old, Charles River Laboratories Japan Inc., Yokohama, Japan) were used. The animal experiments were approved by the Tokushima University Animal Care and Use Committee and all surgical procedures were performed under general anesthesia using ketamine chlorate. The heads of nine rats were shaved and disinfected with iodine solution, then two defects were created on the calvaria bone using a hollow trephine bur with a 5-mm outer diameter [29]. The right side of the defect of six rats was filled with MSPs, and the left side of the defect was filled with NSPs. The MSPs powder or NSPs powder (42 ng SMV to obtain 1 μM SMV in bone defect after complete dissolution) was gently and carefully loaded onto the defect, respectively. In the other three rats, the two defects in each rat served as a control (surgery only as sham).

Four weeks after the treatment, the levels of bone regeneration were evaluated using micro-computed tomography (SkyScan 1176, Bruker Micro-CT; Kontich, Belgium). Newly formed bone volume in the defect area was measured using image software (Data Viewer, CT-Analyser, Bruker Micro-CT). Briefly, the image files were opened in the software and a calibration was set to conduct the measurements at the same magnification. The entire defect was chosen, then all bright objects in the defect were counted. The sum of the area of all the bright objects in the defect were observed and used to calculate the newly formed bone volume. The area of the total defects was observed and used to calculate the total defect volume. The percentage of newly formed bone in each defect area was calculated using the formula: The percentage of newly formed bone (%) = newly formed bone volume (μm^3)/total defect volume (μm^3), and expressed as mean values ± standard error (SEM).

2.10. Statistical analysis

The results were expressed as mean ± SEM. One-way ANOVA models were used to compare expression levels with Dunnett's Multiple Comparisons Test as post hoc analysis for the cell proliferation and ALP activity assays. One-way ANOVA models were used to compare expression levels with Tukey's Multiple Comparisons Test as post hoc analysis for the animal experiments. Differences were considered significant at $^*P < 0.05$.

3. Results

3.1. Characterization of MSPs and NSPs

The appearance of the MSPs and NSPs was observed by scanning electron microscopy (Fig. 1) and the images indicated that both have a smooth morphology. As shown in Table 1, the mean particle sizes of the MSPs and NSPs were approximately 25 μm and 318 nm, respectively. The encapsulation efficiencies of SMV in the MSPs and NSPs were 89.82 ± 0.78% and 14.72 ± 0.11%, respectively. We speculate that the low encapsulation efficiency pf NSPs may be related with higher specific surface area and SMV are easy to go through aqueous phase in the process of emulsion/solvent diffusion method. Additionally, the low encapsulation of NSPs suggest that the encapsulation of SMV into nanoparticle is very difficult because SMV has highly insoluble and the crystal growth seems to be fast.

3.2. Release profiles of SMV from MSPs and NSPs

The *in vitro* release profiles of SMV from MSPs and NSPs are shown in Fig. 2 and are quite different. NSPs showed an initial burst release of SMV (approximately 78% within 24 h), followed by extended drug release over 5 days. In contrast, MSPs showed a lower initial burst release (approximately 7% within 24 h), followed by sustained release for 4 weeks. The release rate of SMV from MSPs was fast during the first week, then decreased, indicating that MSPs can release SMV sustainably compared to NSPs.

3.3. Release analysis using the Korsmeyer-Peppas model

We used the Korsmeyer–Peppas mathematical model, which is commonly used to determine the kinetics of drug release from polymeric matrices [27,28]. MSPs and NSPs gave a good fit to the model, with $R^2 = 0.9907$ and $R^2 = 0.9988$, respectively. MSPs provided $n = 1.08$, indicating that the drug release follows the super case-II·transport mechanism. However, NSPs provided $n = 0.51$, which lies within the range 0.43 and 0.85; this range is indicative of anomalous behavior during drug release, where swelling, diffusion, and erosion play important roles.

3.4. Effect of MSPs and NSPs on cell proliferation in vitro

The effects of MSPs and NSPs on cell proliferation were evaluated using MC3T3-E1 cells, a model of the pre-osteoblast. In order to partially simulate *in vivo* condition, the medium in wells containing SMV alone, MSPs, or NSPs was changed five times per week *in vitro* experiments. It has been reported that the blood components which is similar to high density lipoprotein such as apolipoprotein E can interact with PLGA particles [30]. So the FBS components in medium may interact with MSPs (or NSPs) and we assume that the interaction may slightly change the drug release pattern which was shown in Fig. 2.

As shown in Fig. 3, cell proliferation in the presence of SMV-loaded MSPs and SMV alone was similar to that of untreated cells (control), although cell proliferation increased irregularly during the first week. However, SMV-loaded NSP-treated cells showed remarkably decreased cell proliferation compared with the other three groups after two weeks, suggesting that the NSPs had a negative effect on cell proliferation.

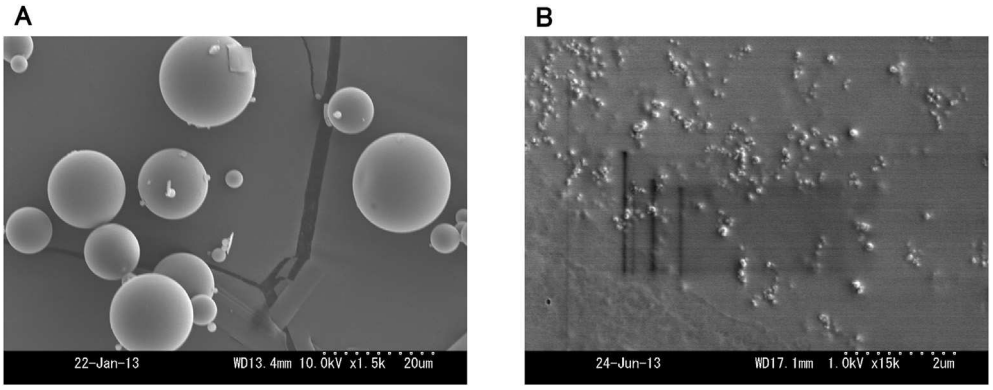

Fig. 1. A. Image of MSPs (A) and NSPs (B) observed by scanning electron microscopy.

Table 1
Characterization of MSPs and NSPs.

	MSPs	NSPs
SMV:PLGA	1:50	1:100
Encapsulation efficiency (%)	89.8 ± 0.8	14.7 ± 0.1
Average particle size	24.6 μm	317.7 nm

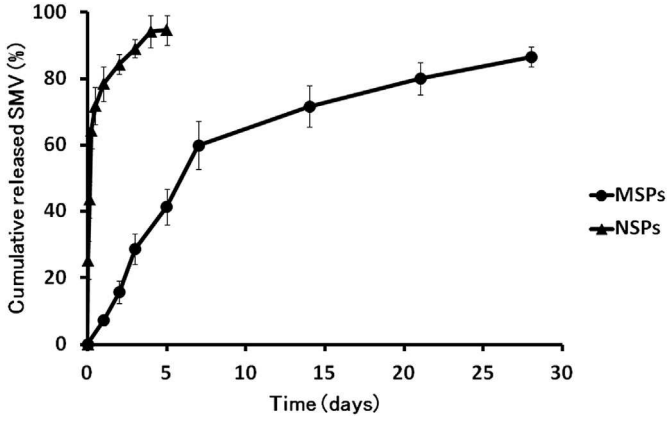

Fig. 2. Release profiles of SMV from MSPs and NSPs. Each value represents the mean ± SEM (n = 3, *P < 0.05 compared with control).

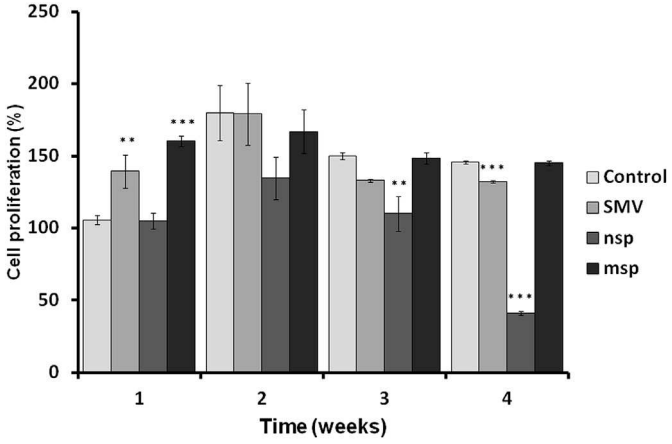

Fig. 3. Influence of SMV treatment on the proliferation profile of MC3T3-E1 cells. The data represent the mean ± SEM (n = 3, *P < 0.05 compared with control).

3.5. Effect of MSPs and NSPs on cell differentiation in vitro

The activity of ALP, a marker of osteoblast differentiation, was investigated to evaluate if MSPs and NSPs affect osteoblast differentiation. SMV- and SMV-loaded MSP-treated cells enhanced ALP activity compared with untreated cells (control), indicating differentiation into osteoblasts at one week and two weeks during the treatment (Fig. 4). In contrast, the ALP activity of SMV-loaded NSP-treated cells remained unchanged. However, no significant differences were observed between all groups at three weeks.

3.6. Effect of MSPs and NSPs on bone formation in vivo

The effects of MSPs and NSPs on bone formation *in vivo* were investigated further by implantation into calvarial defects created in our rat model (Fig. 5). The calvarial defect model has been used to assess the topical bone regeneration effect and SMV showed bone regeneration effect in the model [31]. Micro-CT images were taken 4 weeks post-implantation to visualize and quantify bone formation (Fig. 6) and showed less new bone formation in the defect areas of the NSPs-treated group (Fig. 6A). Significant new bone formation was confirmed in the defect area of the MSPs-treated group (approximately 12%) compared with the NSPs-treated group (approximately 8%) (Fig. 6C).

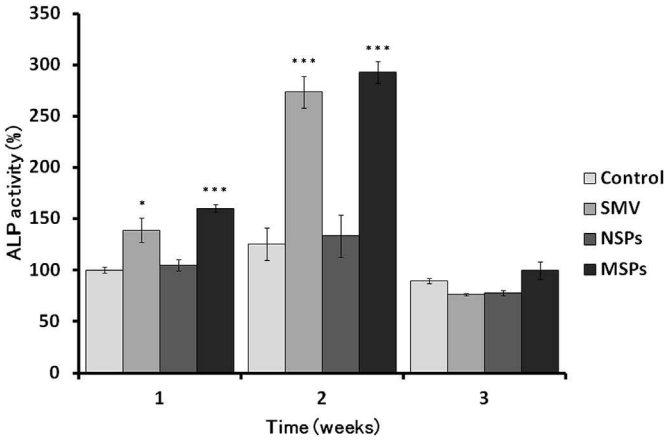

Fig. 4. Influence of MSPs and NSPs on ALP activity in MC3T3-E1 cells. The data represent the mean ± SEM (n = 3, *P < 0.05 compared with control).

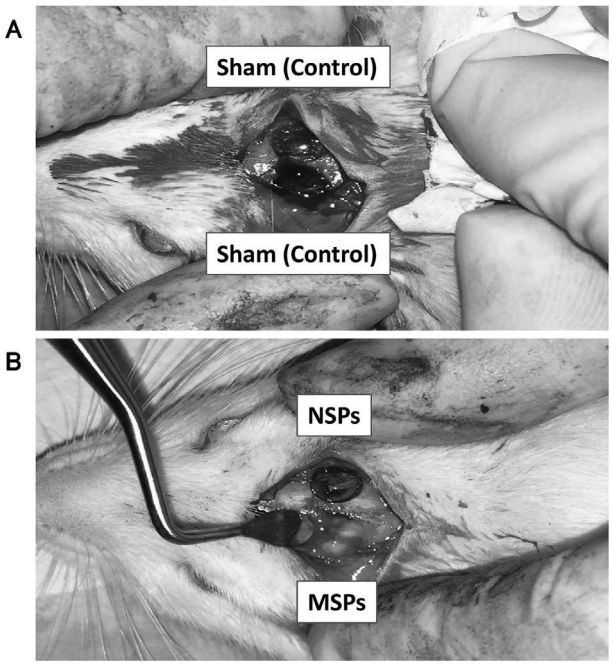

Fig. 5. Photos of the surgical procedure in the rat calvarial defect model. A flap was raised, two bone defects 5 mm in diameter were created, and the defects were filled with MSPs or NSPs. The control group defects were left unfilled.

4. Discussion

The first report that SMV can enhance bone regeneration, by Mundy et al. [10], led to studies demonstrating that SMV plays a crucial role in bone formation *in vivo* and that SMV-loaded modified biomaterials and SMV/mineral complex can enhance bone regeneration *in vivo* [22,23,31]. We previously showed that calcium-aluminate bone cement containing SMV-loaded PLGA microspheres enhances bone formation in rabbit calvarial bone defects [26]. However, to our knowledge, there have been few reports on the influence of the characteristics of SMV release from PLGA-based biomaterials on bone regeneration. The aim of the present study was to provide evidence that sustainable release of SMV can effective for enhancing bone formation.

PLGA has been widely used as a drug delivery carrier because of its biocompatibility and biodegradability, and the release profile of a drug from a PLGA carrier can be controlled by parameters such as molecular weight, the ratio of lactic acid to glycolic acid, and particle size. We therefore used PLGA to develop MSPs and NSPs as SMV carriers and observed that they exhibited different SMV release profiles (Fig. 2). MSPs (approximately 20 μm in diameter) showed a slow release of SMV release that continued up to 28 days. On the other hand, NSPs (approximately 300 nm in diameter) showed much faster release, with an initial burst release of approximately 60% SMV in the first day. The release data must be fit to a suitable mathematical model in order to predict and correlate the release behaviors of SMV from the two types of PLGA particles. The first 60% of the drug released from the MSPs and NSPs correlated well with the Korsmeyer-Peppas model [27,28]. In spherical matrices, if $n < 0.43$, Fickian diffusion-mediated drug release occurs, whereas if $0.43 < n < 0.85$, non-Fickian diffusion occurs; erosion-mediated release corresponds to $n > 0.85$. The MSPs showed $R^2 = 0.9907$ and an n value of 1.08, suggesting that the release rate of SMV was independent of time. In contrast, the NSPs showed $R^2 = 0.9988$ and an n value of 0.51, suggesting non-fickian diffusion. Therefore, the two types of SMV-loaded PLGA particles differed both in particle size and SMV release behavior.

SMV was previously reported to promote the ALP and collagen type I gene expression and mineralization of MC3T3-E1 cells [32,33]. In this study, we evaluated the effects of SMV-loaded MSPs and NSPs on the proliferation and differentiation of MC3T3-E1 cells to evaluate their utility as carrier systems. The MSPs induced significant proliferation and ALP activity of MC3T3-E1 cells as differentiation (Figs. 3 and 4), suggesting that SMV released from the MSPs promoted the differentiation of MC3T3-E1 cells into osteoblasts. In contrast, the NSPs inhibited cell proliferation and ALP activity. Meyer et al. reported that lactic acid and glycolic acid, the products of PLGA degradation, had adverse effects on osteoblast proliferation and differentiation *in vitro* [34]. Thus, the presence of high concentrations of these acids could reduce the proliferation and differentiation of MC3T3-E1 cells. The encapsulation efficiency of the NSPs was lower than that of the MSPs and required the use of a large amount of PLGA. The dissolution of NSPs is much faster than that of MSPs due to their larger surface area, and the resulting exposure of the cells to a large amount of degradation product could be detrimental. The metabolite of PLGA, lactic acid and glycolic acid might partially change the pH of medium and the presence of PLGA metabolite may affect the cell growth and cell differentiation. Additionally, other reason that NSPs have inhibitory effect *in vitro* might be due to excess amount of intracellular uptake of NSPs. NSPs prepared in current study had submicron size (317.7 nm, Table 1). Hydrophobic submicron particle are preferably taken up by phagocytic cells via endocytosis. Submicron pulverized particles were remarkably preferably taken up by cells with phagocytic property compared to micron bulk particles, resulting in the improved cytotoxic effect [35]. Although all osteoblasts does not have phagocytic property, the excess intracellular uptake might affect the function differentiation. On the other hand, there was no significant difference in the ALP activity of the NSP group and that of the control group after 1 and 2 weeks. We speculate that SMV released from NSPs might neutralize the adverse effects of the acids.

The results from the *in vitro* cell proliferation and differentiation experiments were reflected in the results of the effect of SMV-loaded MSPs and NSPs on bone formation *in vivo* (Fig. 6): PLGA degraded from NSPs and SMV released from MSPs affect bone formation. In the current study we did not investigate the effect of SMV alone *in vivo*. However, we believe that the maintaining appropriate drug concentration is a key factor. Garrett et al., mentioned that the treatment with SMV at low concentration increased BMP-2 promoter activity on 2T3 cells [36]. We also found that 1 μM SMV improved differentiation with cell proliferation *in vitro* (Figs. 3 and 4). From these results, sustained SMV release from PLGA microsphere could maintain relatively low concentration in the bone defect area *in vivo*, resulting in the improved therapeutic effect, while burst release from PLGA nanosphere did not. Eventually, our studies support the conclusion that the sustained release of SMV to osteoblasts in bone defect areas is useful for bone regeneration.

5. Conclusion

The influence and mechanism of SMV release from polymeric carrier particles on osteoblast activity and bone regeneration were investigated by comparing two SMV-loaded PLGA particles differing in particle size. SMV was released slowly from MSPs over a period of approximately 1 month, whereas NSPs released their cargo of SMV within 1 week. MSPs exhibit sustained drug release and stimulate MC3T3-E1 cell proliferation and differentiation *in vitro* and promote bone formation in a bone defect area *in vivo*. Cell proliferation, differentiation, and bone mineralization are

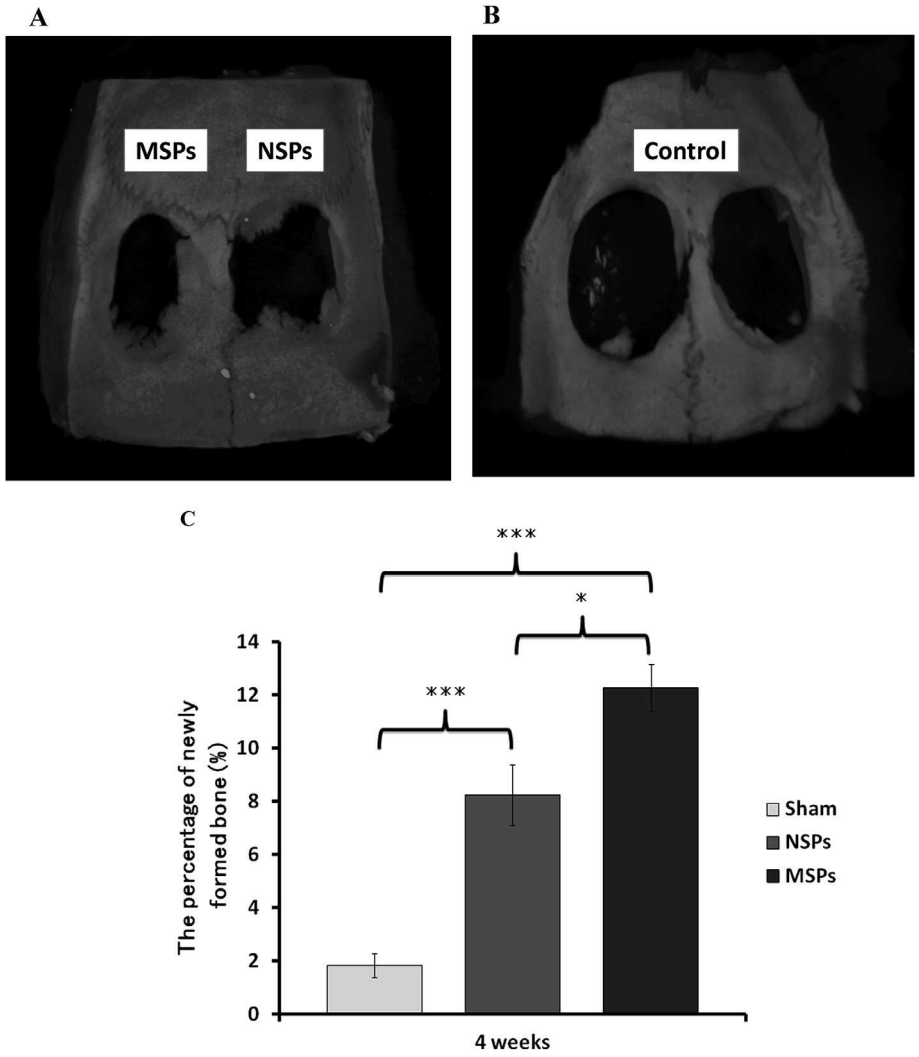

Fig. 6. Bone generation effect of MSPs and NSPs *in vivo*. Micro-CT images of MSP or NSP treated (A) and untreated (B) bone, and quantification (C) after 4 weeks. The data represent the mean ± SEM (n = 6, *P < 0.05 compared with control).

important for bone healing. Thus the use of SMV-loaded MSPs, alone or in combination with other osteoconductive or osteoinductive biomaterials, would be beneficial for patients with alveolar bone deficiency due to periodontal disease or unsuccessful dental implant surgery.

References

[1] R.M. Cibirka, M. Razzoog, B.R. Lang, Critical evaluation of patient responses to dental implant therapy, J. Prosthet. Dent. 78 (6) (1997) 574–581.
[2] R.R. Resnik, Surgical techniques to increase bone augmentation success, Dent. Today 34 (11) (2015), 114–116-9.
[3] M. Clementini, et al., Success rate of dental implants inserted in horizontal and vertical guided bone regenerated areas: a systematic review, Int. J. Oral Maxillofac. Surg. 41 (7) (2012) 847–852.
[4] F. Javed, et al., Role of primary stability for successful osseointegration of dental implants: factors of influence and evaluation, Interv. Med. Appl. Sci. 5 (4) (2013) 162–167.
[5] M. Esposito, et al., Biological factors contributing to failures of osseointegrated oral implants. (I). Success criteria and epidemiology, Eur. J. Oral Sci. 106 (1) (1998) 527–551.
[6] K. Kiyokawa, et al., Treatment outcomes of implants performed after regenerative treatment of absorbed alveolar bone due to the severe periodontal disease and endoscopic surgery for maxillary sinus lift without bone grafts, J. Craniofac. Surg. 24 (5) (2013) 1599–1602.
[7] R.M. Gruber, et al., Mandibular reconstruction using a calcium phosphate/polyethylene glycol hydrogel carrier with BMP-2, J. Clin. Periodontol. 41 (8) (2014) 820–826.
[8] U.W. Jung, et al., The efficacy of BMP-2 preloaded on bone substitute or hydrogel for bone regeneration at peri-implant defects in dogs, Clin. Oral Implants Res. 26 (12) (2015) 1456–1465.
[9] S.K. Yadav, G. Khan, B. Mishra, Advances in patents related to intrapocket technology for the management of periodontitis, Recent Pat. Drug Deliv. Formul. 9 (2) (2015) 129–145.
[10] G. Mundy, et al., Stimulation of bone formation in vitro and in rodents by statins, Science 286 (5446) (1999) 1946–1949.
[11] H. Namazi, Effects of simvastatin on osseointegration in a canine total hip arthroplasty model an experimental study: a novel molecular mechanism, J. Arthroplast. 27 (1) (2012) 162–163 author reply 163.
[12] J. Rutledge, et al., Simvastatin application to augment facial jaw bone in a dog model: pilot study, J. Periodontol. 82 (4) (2011) 597–605.
[13] Y. Zhang, et al., Statins, bone metabolism and treatment of bone catabolic diseases, Pharmacol. Res. 88 (2014) 53–61.
[14] A. Montagnani, et al., Effect of simvastatin treatment on bone mineral density and bone turnover in hypercholesterolemic postmenopausal women: a 1-year longitudinal study, Bone 32 (4) (2003) 427–433.
[15] A. Thabit, et al., Effect of simvastatin and atorvastatin on serum vitamin d and bone mineral density in hypercholesterolemic patients: a cross-sectional study, J. Osteoporos. 2014 (2014) 468397.
[16] Z. Wu, et al., The effect of simvastatin on remodelling of the alveolar bone following tooth extraction, Int. J. Oral Maxillofac. Surg. 37 (2) (2008) 170–176.
[17] H. Seto, et al., Topical administration of simvastatin recovers alveolar bone loss in rats, J. Periodontal Res. 43 (3) (2008) 261–267.
[18] C.A. Nassar, et al., Evaluation of the effect of simvastatin on the progression of alveolar bone loss in experimental periodontitis—an animal study, J. Int. Acad. Periodontol. 16 (1) (2014) 2–7.
[19] H. Okada, H. Toguchi, Biodegradable microspheres in drug delivery, Crit. Rev.

Ther. Drug Carr. Syst. 12 (1) (1995) 1–99.
[20] S. D'Souza, et al., A short term quality control tool for biodegradable microspheres, AAPS PharmSciTech 15 (3) (2014) 530–541.
[21] A. Schoubben, P. Blasi, P.P. Deluca, Effect of agitation regimen on the in vitro release of leuprolide from poly(lactic-co-glycolic) acid microparticles, J. Pharm. Sci. 101 (3) (2012) 1212–1220.
[22] I.C. Tai, et al., Local delivery of controlled-release simvastatin/PLGA/HAp microspheres enhances bone repair, Int. J. Nanomed. 8 (2013) 3895–3904.
[23] S.D. Nath, et al., Encapsulation of simvastatin in PLGA microspheres loaded into hydrogel loaded BCP porous spongy scaffold as a controlled drug delivery system for bone tissue regeneration, J. Biomater. Appl. 28 (8) (2014) 1151–1163.
[24] H. Okada, et al., Preparation of three-month depot injectable microspheres of leuprorelin acetate using biodegradable polymers, Pharm. Res. 11 (8) (1994) 1143–1147.
[25] H. Murakami, et al., Preparation of poly(DL-lactide-co-glycolide) nanoparticles by modified spontaneous emulsification solvent diffusion method, Int. J. Pharm. 187 (2) (1999) 143–152.
[26] Y. Naito, et al., The effect of simvastatin-loaded polymeric microspheres in a critical size bone defect in the rabbit calvaria, Int. J. Pharm. 461 (1–2) (2014) 157–162.
[27] R.W. Korsmeyer, et al., Mechanisms of potassium chloride release from compressed, hydrophilic, polymeric matrices: effect of entrapped air, J. Pharm. Sci. 72 (10) (1983) 1189–1191.
[28] P. Costa, J.M. Sousa Lobo, Modeling and comparison of dissolution profiles, Eur. J. Pharm. Sci. 13 (2) (2001) 123–133.
[29] H.C. Kim, et al., Combined effect of bisphosphonate and recombinant human bone morphogenetic protein 2 on bone healing of rat calvarial defects, Maxillofac. Plast. Reconstr. Surg. 37 (1) (2015) 16.
[30] K. Sempf, et al., Adsorption of plasma proteins on uncoated PLGA nanoparticles, Eur. J. Pharm. Biopharm. 85 (1) (2013) 53–60.
[31] M. Nyan, et al., Bone formation with the combination of simvastatin and calcium sulfate in critical-sized rat calvarial defect, J. Pharmacol. Sci. 104 (4) (2007) 384–386.
[32] T. Maeda, et al., Simvastatin promotes osteoblast differentiation and mineralization in MC3T3-E1 cells, Biochem. Biophys. Res. Commun. 280 (3) (2001) 874–877.
[33] M.S. Walter, et al., Simvastatin-activated implant surface promotes osteoblast differentiation in vitro, J. Biomater. Appl. 28 (6) (2014) 897–908.
[34] F. Meyer, et al., Effects of lactic acid and glycolic acid on human osteoblasts: a way to understand PLGA involvement in PLGA/calcium phosphate composite failure, J. Orthop. Res. 30 (6) (2012) 864–871.
[35] T. Tagami, et al., Simple and effective preparation of nano-pulverized curcumin by femtosecond laser ablation and the cytotoxic effect on C6 rat glioma cells in vitro, Int. J. Pharm. 468 (1–2) (2014) 91–96.
[36] I.R. Garret, et al., Statins and bone formation, Curr. Pharm. Des. 7 (2001) 715–736.

Materials Research, Vol. 6, No. 3, 359-365, 2003.

Blendas Biodegradáveis de Poli(3-Hidroxibutirato)/Poli(ε-Caprolactona): Obtenção e Estudo da Miscibilidade

Nilton Vogelsanger[a], *Michele Cristina Formolo*[a], *Ana Paula Testa Pezzin*[a]*, *Andréa Lima dos Santos Schneider*[a], *Sandra Aparecida Furlan*[a], *Heloísa Pinna Bernardo*[a], *Sérgio Henrique Pezzin*[b], *Alfredo Tibúrcio Nunes Pires*[c], *Eliana Aparecida de Rezende Duek*[d]

[a]*Universidade da Região de Joinville - UNIVILLE*
Campus Universitário, C.P. 246, 89201-972 Joinville - SC, Brasil
[b]*Universidade do Estado de Santa Catarina - UDESC, Joinville - SC, Brasil*
[c]*Universidade Federal de Santa Catarina - UFSC, Florianópolis - SC, Brasil*
[d]*Pontifícia Universidade Católica - PUC-SP, Sorocaba - SP, Brasil*

Received: October 30, 2002; Revised: May 29, 2003

Due to its biodegradability, poly(3-hydroxybutyrate) P(3-HB) has attracted much attention in the environmental sector. However, some characteristics of this polymer, such as high crystallinity, poor processability and high brittleness, have lead several research groups to study polymeric blends in order to modify P(3-HB) properties. Poly(ε-caprolactone) (PCL) is a synthetic polyester which is completely degraded after about one year when buried in soil. In general, it acts as a polymeric plasticizer lowering the elastic modulus and enhancing the processability of the blend. Blends of two biodegradable polymers, P(3-HB) and PCL have been prepared by casting in different compositions. Miscibility, thermal behavior and morphology of these blends were studied using modulated differential scanning calorimetry (MDSC), scanning electron microscopy (SEM) and polarizing light microscopy (PLM). The two glass transition temperatures, detected by MDSC, suggest the immiscibility of the system. Phase separation was confirmed by PLM.

Keywords: *blends, miscibility, P(3-HB), PCL*

1. Introdução

Dentre os maiores problemas ambientais relacionados à utilização de materiais poliméricos, tais como o polipropileno, poliestireno, polietileno e poli(cloreto de vinila) pode ser destacado o tempo necessário para que ocorra degradação e a utilização de recursos não renováveis derivados do petróleo[1]. Os poli(hidroxialcanoatos) (PHA), poliésteres naturais e biodegradáveis, podem sofrer degradação hidrolítica ou enzimática[2-4] e sob ação de microrganismos degradam completamente produzindo dióxido de carbono e água[5,6]. Devido a biodegradabilidade, o estudo de PHA tem despertado bastante interesse em aplicações na área ambiental. O poli(3-hidroxibutirato) P(3-HB) é produzido através de fermentação bacteriana, com predominância de utilização da bactéria *Raltonia eutropha*[7]. A biossíntese deste polímero permite um processo cíclico sustentável através de fontes renováveis, substituindo tecnologias de ponta ligadas à produção e ao uso de materiais poliméricos sintéticos[8]. Entretanto, a baixa processabilidade, o elevado grau de cristalinidade e fragilidade do P(3-HB) limitam suas aplicações. A fim de se obter materiais com melhores características, misturas físicas de P(3-HB) com outros polímeros (blendas) também biodegradáveis podem ser preparadas. O estudo dos sistemas P(3-HB)/poli(propiolactona), P(3-HB)/poli(adipato de etileno) e P(3-HB)/poli(3-hidroxibutirato-co-3-hidroxivalerato) (PHBV) mostrou que a cinética de degradação das blendas é mais acelerada quando comparada com os polímeros puros, sendo atribuído ao processo de separação de fases dos componentes nas blendas[9]. Trabalhos anteriores mostraram que é possível

*e-mail: paulapezzin@univille.edu.br
Trabalho apresentado no 1º Congresso da Sociedade Brasileira de Pesquisa em Materiais, Rio de Janeiro, julho de 2002.

controlar a taxa de degradação hidrolítica dos componentes das blendas, por exemplo, acelerando a degradação de poli(L–ácido láctico) (PLLA) através da adição poli(*p*-dioxanona) (PPD) [10, 11]. Poli(ε-caprolactona) (PCL) pode agir como plastificante polimérico, diminuindo o módulo de rigidez e melhorando a processabilidade da blenda[12]. Neste trabalho foram preparadas blendas de P(3-HB)/PCL e avaliadas a miscibilidade, buscando obter materiais flexíveis e biodegradáveis, para aplicações na área agrícola.

2. Parte Experimental

Materiais

O P(3-HB) utilizado foi gentilmente fornecido pela PHB Industrial (lote FE-67 ESF) identificado por espectroscopia no infravermelho (FTIR) da Perkin Elmer Spectrum One, no intervalo de 4000 a 650 cm^{-1} pela técnica de reflectância difusa e difratometria de raios-X (DRX) da SHIMATZU modelo XRD 6000, variando o ângulo 2θ de 15 a 35° e utilizando fonte de CuKα.

A massa molar viscosimétrica foi determinada em clorofórmio a 30 °C a partir da equação de Mark-Houwink (Eq. 1):

$$[\eta] = k\, M^{\alpha} \qquad (1)$$

onde [η] é a viscosidade intrínseca e k e α são as constantes para o sistema polímero-solvente. Utilizando os valores de $k = 1{,}18 \times 10^{-4}$ e $\alpha = 0{,}78$ [13], foi obtido a massa molar média do P(3-HB) igual a 342.000 g/mol. A PCL da Sigma-Aldrich com M_w igual a 60.000 g/mol, segundo o fabricante. As fórmulas estruturais das unidades monoméricas dos polímeros são apresentadas nas Fig. 1. O clorofórmio, utilizado como solvente foi fornecido pela Synth.

Preparação das Blendas

Inicialmente, foram preparadas soluções de P(3-HB) a 1% m/v sob aquecimento e PCL na mesma concentração a temperatura ambiente, utilizando clorofórmio como solvente

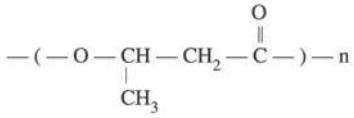

(a)

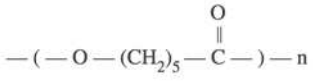

(b)

Figura 1. Estruturas químicas: a) poli(3-hidroxibutirato); b) da poli(ε-caprolactona).

comum. Em seguida foram misturadas diferentes proporções de cada uma das soluções e mantidas sob agitação durante 2 h, de maneira a obter as composições de 0/100, 20/80, 50/50, 80/20 e 100/0 m/m de P(3-HB)/PCL. Os filmes foram obtidos por evaporação do solvente em atmosfera saturada de clorofórmio por 48 h, mantidos sob vácuo durante 24 h e armazenadas em dessecador.

Caracterização das Blendas

Calorimetria Diferencial de Varredura Modulada (MDSC)

As medidas no MDSC foram feitas no equipamento TA Instruments, modelo 2920. As amostras foram seladas em recipientes de alumínio, aquecidas de 25 a 200 °C a 10 °C/min e mantidas nesta temperatura por 5 min. Em seguida, as amostras foram resfriadas a -100 °C numa taxa de 30 °C/min. Após 5 min a -100 °C as amostras foram submetidas a um segundo aquecimento até 200 °C, com taxa de 5 °C/min. A amplitude e o período de oscilação utilizados foram 0,5 °C e 60 s, respectivamente.

Microscopia Eletrônica de Varredura (SEM)

Os fragmentos da superfície superior e da superfície da fratura criogênica dos filmes foram fixados em suporte metálico e recobertos com ouro, utilizando-se um metalizador de amostras Sputer Coater BAL-TEC SCD 050 para obtenção das micrografias. Foi utilizado um microscópio eletrônico de varredura JEOL JXA 860A, utilizando tensão de 20 kV.

Microscopia Óptica com luz polarizada (PLM)

Filmes com cerca de 5 μm de espessura foram prensados a partir do fundido a 190 °C por 1 min e colocados entre duas lamínulas para observação no microscópio óptico. Antes de cristalizadas, as amostras foram primeiramente aquecidas a 190 °C por 1 min em um sistema de aquecimento da Mettler e em seguida resfriadas até a temperatura de cristalização de 83 °C e temperatura ambiente para o P(3-HB) e PCL, respectivamente. O microscópio óptico com luz polarizada Olympus BX-50 equipado com controle de aquecimento foi utilizado para avaliar as morfologias das blendas a diferentes composições.

3. Resultados e Discussão

O perfil de difração de raios-X (DRX) para o P(3-HB) é mostrado na Fig. 2. Como pode-se observar, o P(3-HB) apresenta picos de difração em 2θ igual a 13,5; 17; 22 e 25,5, sendo similar ao padrão mostrado por Ikejima e Inoue, 2000 [14]. O grau de cristalinidade (α_c) determinado para o polímero foi igual a 48,5%. O espectro de FTIR mostrado na Fig. 3 demonstra que o polímero doado pela PHB Industrial apresenta bandas características do P(3-HB), tais como as das deformações axiais da carbonila (C=O) a 1737 cm^{-1},

de O-H a 3438 cm^{-1} e de C-C a 978 cm^{-1}, além da banda de deformação angular simétrica no plano dos grupos CH_3 em 1380 cm^{-1} e a banda típica da conformação helicoidal das cadeias a 1227 cm^{-1}. As bandas a 1134 e 1187 cm^{-1} são atribuídas, respectivamente, aos estiramentos simétrico e assimétrico do grupo C-O-C [15].

Calorimetria Diferencial de Varredura Modulada (MDSC)

O primeiro aquecimento foi realizado para apagar a história térmica das blendas e poder compará-las em condições térmicas similares. A Fig. 4 mostra as curvas de MDSC para o resfriamento, as quais foram utilizadas para a determinação das temperaturas (T_c) e entalpias de cristalização (ΔH_c). Durante o resfriamento houve um decréscimo dos valores de T_c do P(3-HB) com o aumento da concentração de PCL nas blendas, sendo que para concentrações de PCL acima de 50% a T_c do P(3-HB) não foi detectada pela técnica utilizada. Por outro lado os valores de T_c do PCL e as entalpias de cristalização (ΔH_c) de ambos os polímeros não sofreram alteração em função da composição (Fig. 5a e 5b, respectivamente). Na Fig. 6 são apresentadas as curvas de MDSC para o segundo aquecimento referente aos componentes puros e blendas em diferentes composições, cujos valores obtidos para T_g foram 2 e -67 °C para o P(3-HB) e PCL, respectivamente, concordando com os valores da literatura[9,13]. A Fig. 7 mostra que as temperaturas de transição vítrea da PCL e P(3-HB) em função do aumento do conteúdo de PCL nas blendas permaneceram na mesma ordem de grandeza para todas composições estudadas, sugerindo que os polímeros são imiscíveis na fase amorfa. Esta observação concorda com os resultados de Kumagai e Doi para o mesmo sistema, sendo as blendas preparadas por moldagem por compressão. Neste estudo, a T_g do P(3-HB) permaneceu em torno de 1 °C, porém os autores não conseguiram observar a T_g da PCL na blenda, devido à alta cristalinidade deste polímero[9].

Nas curvas de MDSC (Fig. 6) foram observados dois picos endotérmicos a 168 e 55 °C, devido à fusão das fases cristalinas do P(3-HB) e da PCL, respectivamente. Quental e col[15] obtiveram dois valores de T_f do P(3-HB) a 167 e 147 ºC, sendo que o segundo pico não foi observado em

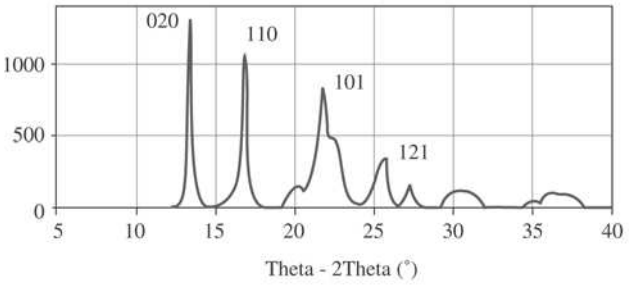

Figura 2. DRX do P(3-HB).

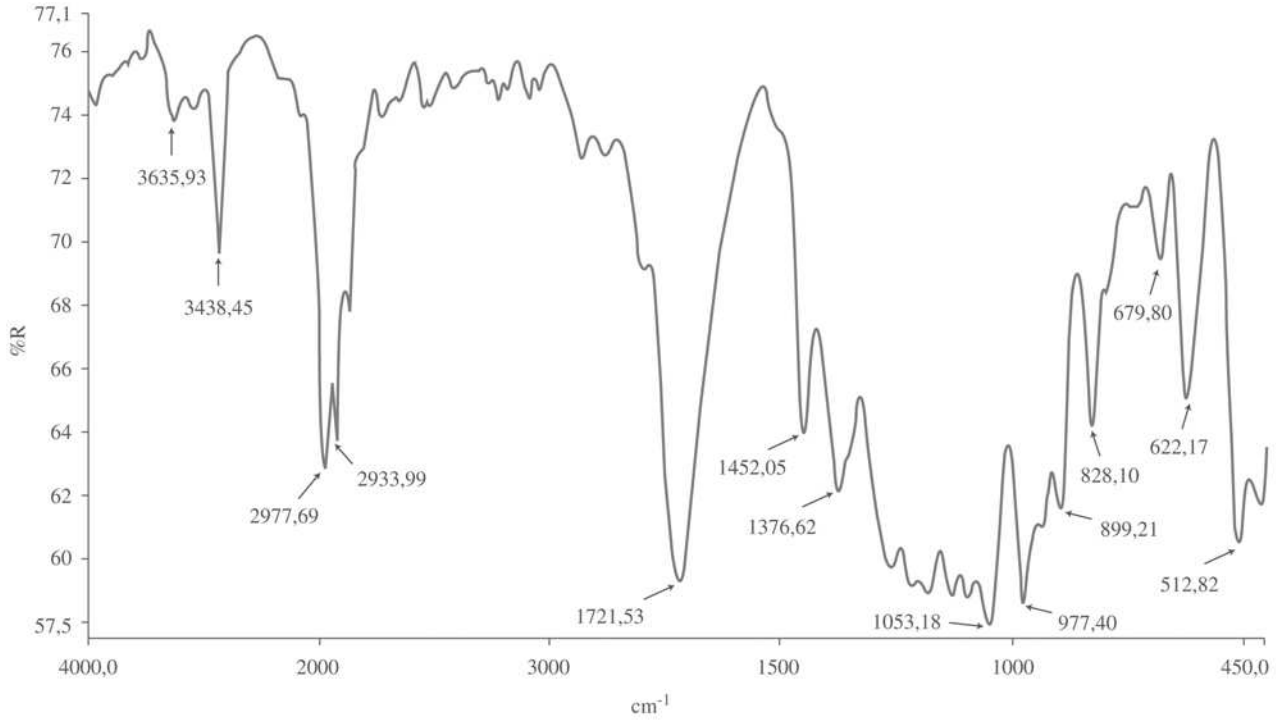

Figura 3. FTIR do P(3-HB).

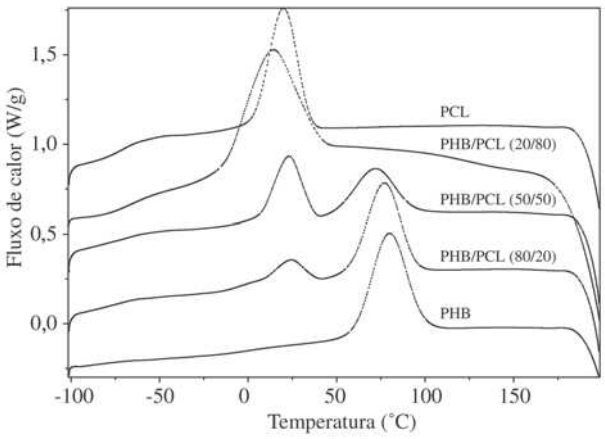

Figura 4. Curvas de fluxo de calor total, obtidas por MDSC para as blendas P(3-HB)/PCL no resfriamento.

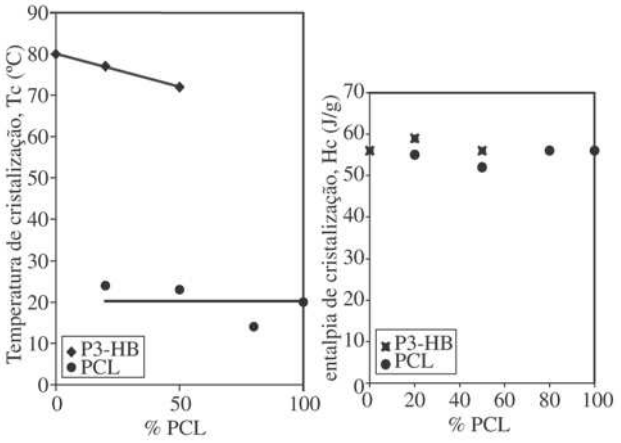

Figura 5. a) Temperaturas de cristalização do P(3-HB) e da PCL em função da % de PCL na blenda; b) Entalpias de cristalização do P(3-HB) e da PCL em função da % de PCL na blenda.

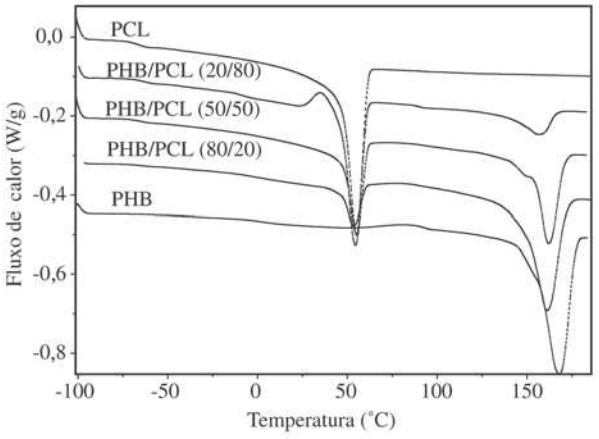

Figura 6. Curvas de fluxo de calor total, obtidas por MDSC para as blendas P(3-HB)/PCL no segundo aquecimento.

nosso experimento. O gráfico da Fig. 8a mostra para todas as composições que a T_f da PCL permaneceu constante e a T_f do P(3-HB) decresceu com o aumento da percentagem de PCL na blenda. A diminuição da T_f do P(3-HB) sugere que a composição da blenda influencia na cristalização do P(3-HB), podendo ser um reflexo da morfologia e das propriedades térmicas dos polímeros.

Como observado na temperatura de fusão, os valores de ΔH_f do P(3-HB) permaneceram inalterados para as diferentes composições das blendas, enquanto para o PCL foi verificado um decréscimo do ΔH_f em função do aumento da composição do PCL na blenda (Fig. 8b). A partir dos dados de ΔH_f e entalpia de fusão para o polímero 100% cristalino, ΔH_f^o = 146 J/g para o PCL [12] e ΔH_f^o = 142 J/g para o P(3-HB) [16], o grau de cristalinidade dos componentes na blenda foi calculado (α_c %), seguindo a Eq. 2:

$$\alpha_c = \frac{\Delta H_f}{\Delta H_f^o} \times 100 \qquad (2)$$

A Fig. 9 apresenta a variação do grau de cristalinidade do P(3-HB) e do PCL em função do aumento percentagem de PCL na blenda. Para os polímeros puros foi obtido α_c igual a 51% para o P(3-HB) e 45% para a PCL. Observa-se que os valores de cristalinidade obtidos por MDSC e DRX foram muito próximos, 51% e 48,5%, respectivamente. O grau de cristalinidade da PCL tende a diminuir com o aumento do conteúdo de PCL, enquanto o grau de cristalinidade do P(3-HB) permanece constante.

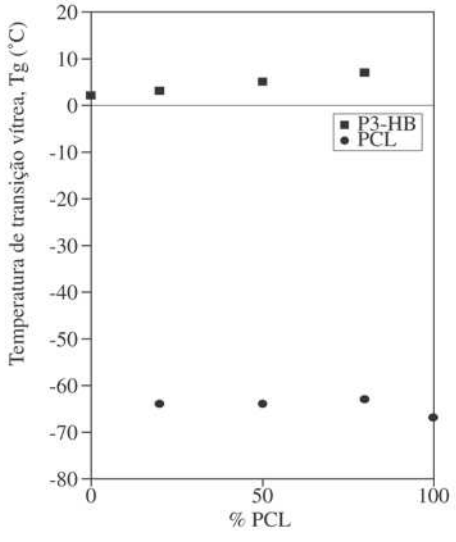

Figura 7. Temperaturas de transição vítrea do P(3-HB) e da PCL em função da % de PCL na blenda.

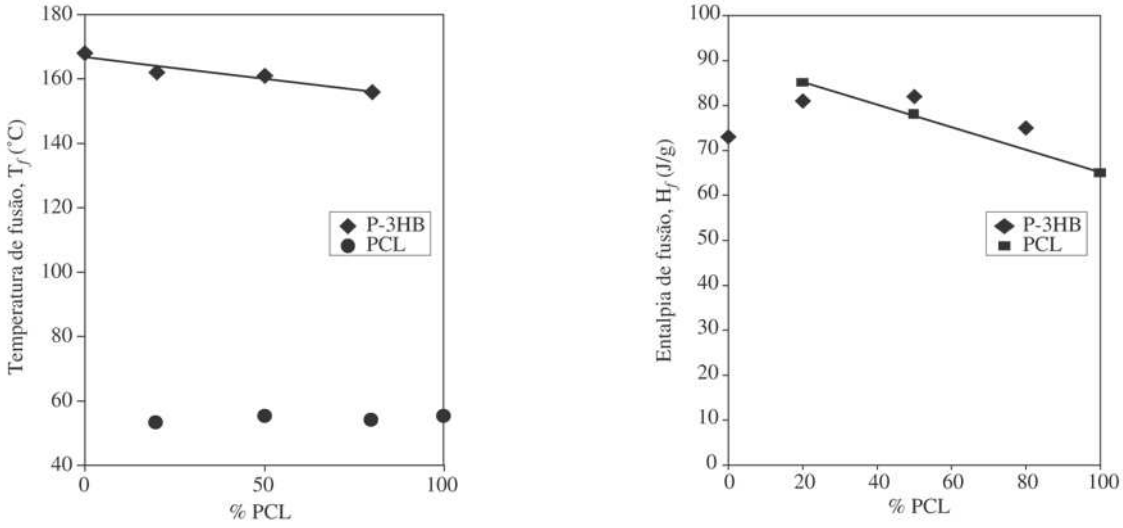

Figura 8. a) Temperaturas de fusão do P(3-HB) e da PCL em função da % de PCL na blenda; b) Entalpias de fusão do P(3-HB) e da PCL em função da % de PCL na blenda.

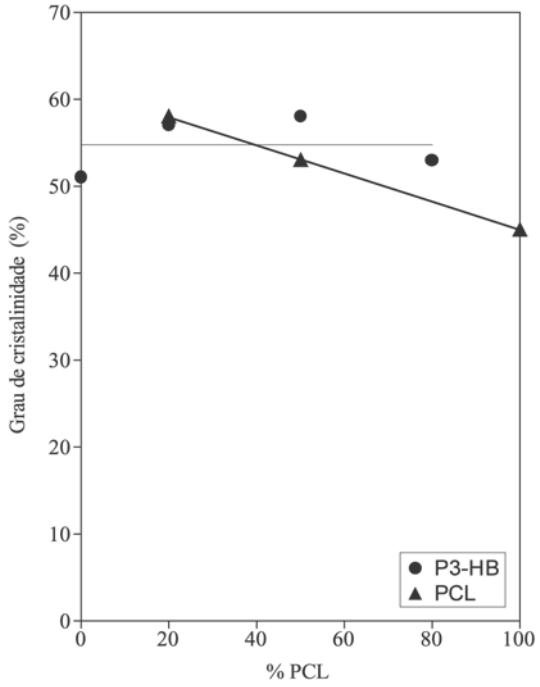

Figura 9. Grau de cristalinidade em função da % de PCL.

Microscopia Eletrônica de Varredura (SEM)

As micrografias de SEM da superfície superior dos polímeros puros mostram uma superfície rugosa e irregular para o P(3-HB) e para a PCL observa-se uma superfície lisa, descontínua, com cristais limitados pelos arranjos cristalinos vizinhos, formando polígonos (Figs. 10a, 10c). A morfologia variou bastante em função da composição das blendas, sendo que a composição 50/50, constituída por microesferas com cerca de 8 mm, foi a que apresentou a morfologia mais diferenciada (Fig. 10b).

Microscopia Óptica com luz polarizada (PLM)

A Fig. 11a apresenta a micrografia obtida por PLM com luz polarizada para o P(3-HB), mostrando um típico esferulito deste polímero, no qual se observam anéis concêntricos regulares. A porção externa apresenta pequenos cristais inseridos na massa fundida, que não fundiram a 190 °C, atribuídos provavelmente à impureza do polímero. A micrografia da PCL (Fig. 11f) apresenta os esferulitos da PCL, cristalizados a temperatura ambiente. Estes esferulitos são bem pequenos, pois uma enorme quantidade de núcleos foram formados com baixa velocidade de cristalização, devido ao fato da isoterma de cristalização ter sido realizada acima da temperatura de cristalização da PCL. A Fig. 11c corresponde à blenda P(3-HB)/PCL 50/50, onde foi realizada uma isoterma a 83 °C. A micrografia apresenta, nesta temperatura, o P(3-HB) já cristalizado formando esferulitos enquanto o PCL está ainda fundido, uma vez que sua temperatura de cristalização é bem abaixo da isoterma realizada. Já na Fig. 11d, correspondente a blenda P(3-HB)/PCL 50/50, observa-se uma total imiscibilidade entre os domínios de P(3-HB) e PCL, confirmando os dados observados por SEM. Nesta micrografia, nota-se a presença de esferulitos do P(3-HB) (anel na parte superior à esquerda) e de PCL (restante), pois foi realizada uma isoterma a 83 °C para cristalização do P(3-HB), seguida de resfriamento a

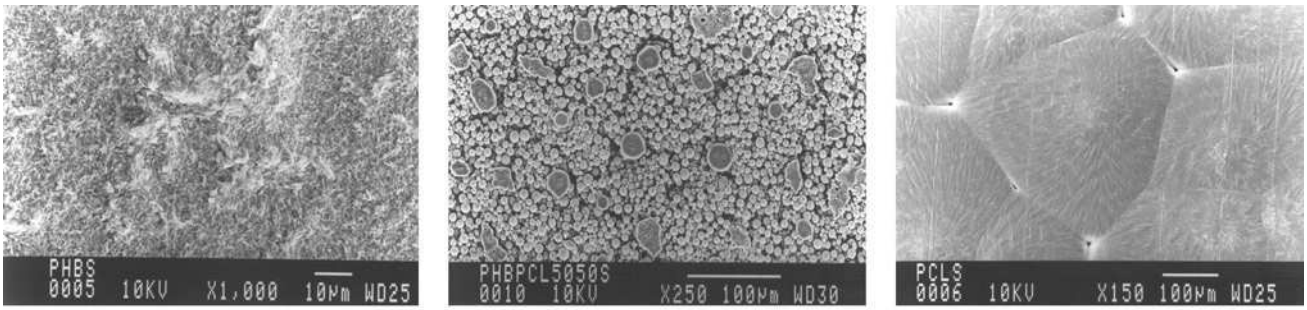

Figura 10. Micrografias de SEM da superfície superior das blendas de P(3-HB)/PCL e dos homopolímeros: a) P(3-HB); b) P(3-HB)/PCL (50/50); c) PCL.

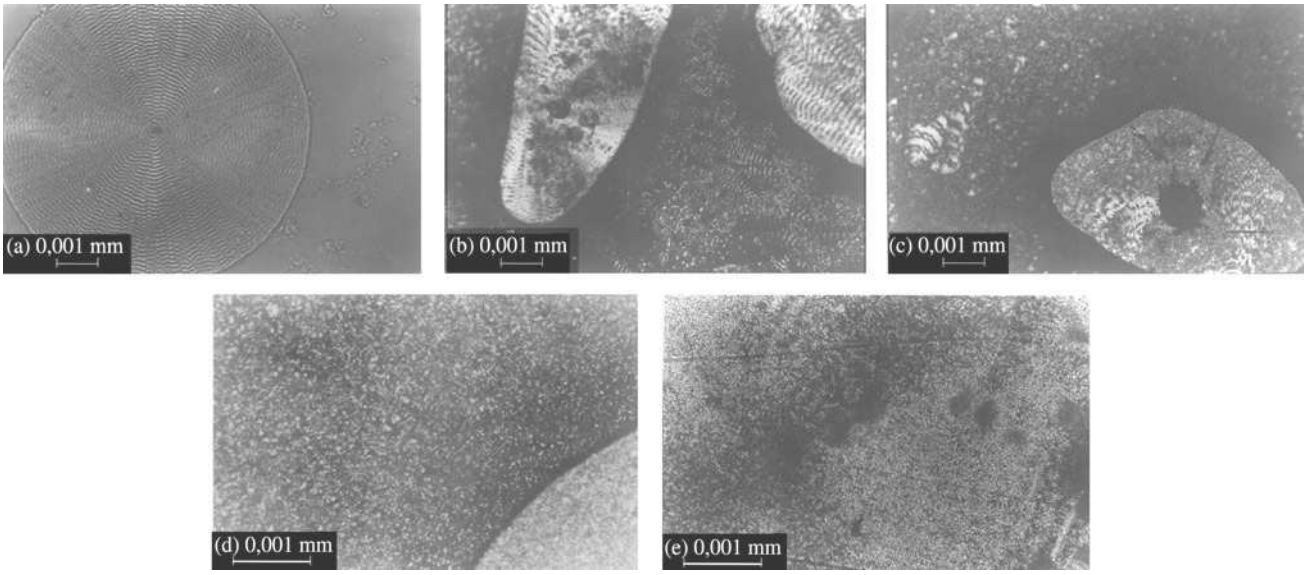

Figura 11. Micrografias de PLM com luz polarizada das blendas de P(3-HB)/PCL e dos homopolímeros: a) P(3-HB); b) P(3-HB)/PCL (80/20); c) P(3-HB)/PCL (50/50); d) P(3-HB)/PCL (20/80); e) PCL.

temperatura ambiente e outra isoterma a 25 °C para cristalização do PCL. A Fig. 11b corresponde a blenda P(3-HB)/PCL (80/20) é bem semelhante a blenda anterior, onde se observa separação de fases e a presença de esferulitos dos dois polímeros. A Fig. 11e, que corresponde a blenda P(3-HB)/PCL (20/80) também mostra separação de fases. Observa-se que a parte mais escura corresponde aos esferulitos da PCL, enquanto a parte mais clara é relativa aos esferulitos de P(3-HB).

4. Conclusões

A técnica de MDSC informa a presença de duas temperaturas de transição vítrea, que não se alteram, o que indica que as blendas são imiscíveis. Conforme observado por microscopia eletrônica de varredura, a morfologia variou de forma significativa em função da composição das blendas. As composições 20/80 e 80/20 apresentaram morfologia similar à do polímero presente em maior concentração. Com 50% de PCL, a morfologia da blenda mostra a presença microesferas. A microscopia óptica com luz polarizada mostrou a presença de esferulitos dos dois polímeros, que também se separam em duas fases distintas, concordando com os resultados da análise térmica.

Agradecimentos

Gostaríamos de agradecer ao Prof. Hugo Alejandro Gallardo Olmedo (UFSC) pelo uso do Microscópio Óptico, ao CNPq pela bolsa de recém doutor da Pesquisadora A.P.

T. Pezzin, ao FUNCITEC pelo financiamento do projeto e à UNIVILLE pelo financiamento do projeto e pelas bolsas de iniciação científica dos alunos Nilton Vogelsanger e Michele Formolo.

Referências Bibliográficas

1. Otake, Y.; Kobayashi, T.; Asabe, H.; Murakami, N.; ONO, K. *J. Appl. Polym. Sci*, v. 56, p. 1789-1796, 1995.
2. Abe, H.; Doy, Y. *International Journal of Biological Macromolecules*, v. 25, p. 185-192, 1999.
3. Darwis, D.; Minoto, H.; Enjoji, T.; Yoxhii, F.; Makuuchi, K. *Polymer Degradation and Stability*, v. 62, p. 259-265, 1998.
4. Satoh, H.; Yoshie, N.; Yoshio, I. *Polymer*, v. 35, n. 2, p. 286-289, 1994.
5. Yoshie, N.; Nakasato, K.; Fujiwara, M.; Kasuya, K.; Abe, H.; Doy, Y.I. *Polymer*, v. 41, p. 3227-3234, 2000.
6. Zhang, L.L.; Goh, S.H.; Lee, S.Y.; Hee, G.R. *Polymer*, v. 41. p. 1429-1439, 2000.
7. Marangoni, C.; Furigo Jr, A.; Aragão, G.M.F. *Biotechnology Letters*, v. 22, p. 1635-1638, 2000.
8. Braunegg, G.; Lefbvre, G.; Genser, K.F. *Journal of Biotechnology*, v. 65, p. 127-61, 1998.
9. Kumagai, Y.; Doi, Y. *Polymer Degradation and Stability*, v. 37, p. 253-256, 1992.
10. Pezzin, A.P.T.; Zavaglia, C.A.C.; Duek, E.A.R. *Polímeros: Ciência e Tecnologia*, v. 12, n. 4, p. 285-294, 2003.
11. Pezzin, A.P.T.; Duek, E.A.R. *Polymer Degradation and Stability*, in press, 2003.
12. Gassner, F.; Owen, A.J. *Polymer Report*, v. 35, p. 2233-2236, 1994.
13. Savenkova, L.; Gercberga, Z.; Bibers, I.; Kalnin, M. *Process Biochemistry*, v. 36, p.445-450, 2000.
14. Ikejima, T.; Inoue, Y. *Carbohydrate Polymers*, v. 41, p. 351-356, 2000.
15. Xu, J.; Guo, B.H.; Yang, R.; Wu, Q.; Chen, G.Q.; Zhang, Z.M. *Polymer*, v. 43, p. 6893-6899, 2002.
15. Quental, A.C.; Felisberti, M.I. *Anais do 6º Congresso Brasileiro de Polímeros,* p. 1260-1263, 2001.
16. Tsuji, H.; Ikada, Y. *Journal of Applied Science,* v. 60, p. 2367-2375, 1996.

In vivo performance of simvastatin-loaded electrospun spiral-wound polycaprolactone scaffolds in reconstruction of cranial bone defects in the rat model

Erhan Pişkin,[1] İ. Alper İşoğlu,[1] Nimet Bölgen,[1] İbrahim Vargel,[2] Sarah Griffiths,[3] Tarık Çavuşoğlu,[2] Petek Korkusuz,[4] Elif Güzel,[4] Sarah Cartmell[3]

[1]*Hacettepe University, Chemical Engineering Department and Bioengineering Division, Beytepe, Ankara and Biyomedtek, Beysukent, Ankara, Turkey*

[2]*Department of Plastic and Reconstructive Surgery, Faculty of Medicine, Kırıkkale University, Kırıkkale, Turkey*

[3]*Medical Research Unit, Institute for Science and Technology in Medicine, Keele University, Stoke-on-Trent-Staffordshire, United Kingdom*

[4]*Department of Histology and Embryology, Faculty of Medicine, Hacettepe University, Ankara, Turkey*

Received 3 January 2008; revised 3 April 2008; accepted 10 April 2008
Published online 31 July 2008 in Wiley InterScience (www.interscience.wiley.com). DOI: 10.1002/jbm.a.32157

Abstract: Reconstruction of large bone defects is still a major problem. Tissue-engineering approaches have become a focus in regeneration of bone. In particular, critical-sized defects do not ossify spontaneously. The use of electrospinning is attracting increasing attention in the preparation of tissue-engineering scaffolds. Recently, acellular scaffolds carrying bioactive agents have been used as scaffolds in "*in situ*" tissue engineering for soft and hard tissue repair. Poly(ε-caprolactone) (PCL) with two different molecular weights were synthesized, and the blends of these two were electrospun into nonwoven membranes composed of nanofibers/micropores. To stimulate bone formation, an active drug, "simvastatin" was loaded either after the membranes were formed or during electrospinning. The matrices were then spiral-wound to produce scaffolds with 3D-structures having both macro- and microchannels. Eight-millimeter diameter critical size cranial defects were created in rats. Scaffolds with or without simvastatin were then implanted into these defects. Samples from the implant sites were removed after 1, 3, and 6 months postimplantation. Bone regeneration and tissue response were followed by X-ray microcomputed tomography and histological analysis. These *in vivo* results exhibited osseous tissue integration within the implant and mineralized bone restoration of the calvarium. Both microCT and histological data clearly demonstrated that the more successful results were observed with the "simvastatin-containing PCL scaffolds," in which simvastatin was incorporated into the PCL scaffolds during electrospinning. For these samples, bone mineralization was quite significant when compared with the other groups. © 2008 Wiley Periodicals, Inc. J Biomed Mater Res 90A: 1137–1151, 2009

Key words: bone reconstruction; cranial defects; animal model; biodegradable scaffolds; poly(ε-caprolactone); electrospinning; spiral-wounding; simvastatin

INTRODUCTION

Reconstruction of large bone defects is still a major problem. Autogenic, allogenic, or xenogenic grafts are currently used clinically, with autogenic bone grafts being the gold standard in the reconstruction of large bone defect repair. However, there are significant disadvantages and limitations of this approach, including limited amount of tissue, donor site morbidity, additional pain, and longer rehabilitation time for patients in hospitals. Allografts also have disadvantages such as unpredictable degradation rates and integration extent, potential immunogenicity, disease transmission risks, conformal needs at the repair site, and ethical problems.[1] Novel approaches using materials with bioactive agents and biological compounds (e.g., growth factors, bone matrices, and cell transplants) have been proposed to repair larger defects.[2–5]

Tissue-engineering strategies have become a focus in regeneration of bone, in particular in the context

Correspondence to: E. Pişkin; e-mail: erhanpiskin@biyomedtek.com or piskin@hacettepe.edu.tr

Contract grant sponsor: Turkish Scientific and Technological Council (Turkish Scientific and Technological Research Council, TÜBİTAK, Project: Tissuebiomed); contract grant number: 105T509

Contract grant sponsor: Turkish Academy of Sciences (TÜBA)

Contract grant sponsor: Biyomedtek

of critical-sized defects, that do not ossify spontaneously.[6] Biodegradable scaffolds containing large interconnected openings ("pores"), allowing cell migration and 3D-growth are being used usually with primary cells (including stem cells) and bioactive agents in tissue engineering.[7,8] The ideal scaffold must satisfy a number of often conflicting demands: appropriate level and size of porosity allowing for cell migration; sufficient surface area and a variety of surface chemistries that encourage cell adhesion, migration, growth, and differentiation; and a degradation rate that closely matches regeneration rate of the desired natural tissue.[9,10] A broad range of tissue-engineering matrices have been fabricated from both synthetic and natural polymers by using solvent casting and particulate leaching, gas foaming, freeze drying, rapid prototyping, thermally induce phase separation, fiber bonding, melt molding, and electrospinning, as reviewed elsewhere.[11,12]

Electrospinning is attracting increasing attention for the processing of polymers into nanofibers and nonwoven structures. Almost all of the polymers soluble in a solvent or forming stable melts can be converted into nanofibers and nonwoven matrices by electrospinning.[13] Electrospun nanofiber meshes exhibit exceptional and unique properties. High porosity (openings between the nanofibers) and very high surface area per unit volume of the electrospun matrices (which affect the biodegradation rate and mode) are unique properties. Electrospun matrices have excellent elastic characteristics and are very soft and light, therefore, improving patient comfort. The nanofibrous structure of the electrospun matrices are biomimetic, simulating the size, geometry, and superior architecture of the natural extracellular matrix (ECM). It has been recently demonstrated by several groups that mammalian cells attach and proliferate on these nanofibrous structures.[14–17] However, cell migration and 3D cell growth are not optimal on these scaffolds. The pores of electrospun matrices simply cannot accommodate enough cells and do not easily allow cell migration. Pre- or post-procedures for further shaping of these matrices into 3D-structures are required to allow tissue engineering use, as we present in this study.

Several natural and synthetic polymers have been used as scaffolding materials for bone tissue engineering. Poly(α-hydroxy acids), mainly homo and copolymers of lactide and glycolide and also their copolymers with ε-caprolactone (ε-CL), are the most widely known and utilized biodegradable polymers among all others in medical applications.[18,19] Poly(ε-caprolactone) (PCL), which is selected also in this study to produce scaffolds, is getting an increasing amount of attention as a biodegradable biomaterial because of its controllable biodegradation rate (slower than other polymers) and also more suitable and tailor-made mechanical properties (usually more flexible and softer).[20–22] Several approaches including electrospinning, have been investigated to produce biodegradable materials from PCL.[23–25]

Recently, acellular scaffolds carrying bioactive agents have been used as active scaffolds in "*in situ*" tissue engineering for soft and hard tissue repair.[26–31] In this study, a statin drug has been applied as an active agent. Statins have recently attracted attention with their ability to stimulate/trigger bone regeneration.[32–36] There are several types of statin drugs available commercially, and they are widely used in patients as cholesterol-reducing agent, especially after cardiovascular "stent" applications.[37–42] Several *in vitro* and *in vivo* studies suggest that statins have an anabolic and antiresorptive effect on bone. Statins act by altering bone activation–resorption–formation cycles locally.[33,34,43,44] Orally administered statins also appear to increase bone density and in some studies decrease the incidence of bone fractures and increase bone density, although this effect is still contested.[33,45–50] Wong and Rabie investigated the use of simvastatin as a direct bone graft.[51,52] They quantitatively assessed the amount of new bone formed by statin collagen grafts comprising of simvastatin mixed with absorbable collagen sponge and compared it with that of absorbable collagen sponge alone. Maritz et al. found an inverse correlation between simvastatin dose and decrease in bone mineral density (BMD). They mentioned that the reason for the decrease in BMD remained speculative, and the two processes were operative in bone remodelling with differing dose–response curves.[53]

Considering the interesting information given earlier, in this study, we designed/attempted to prepare electrospun/spiral-wounded PCL-based biodegradable scaffolds with 3D-structure and loaded them with simvastatin as potential *in situ* tissue-engineering material for reconstruction of critical size calvarial bone defects. This paper reports the results of the animal model studies.

MATERIALS AND METHODS

Production of electrospun PCL membranes

Poly(ε-caprolactone) (PCL) was synthesized from ε-caprolactone (ε-CL, Aldrich, Germany) which was dried on a molecular sieve for about 24 h before use. The polymerization system and procedure were described in detail elsewhere.[54] Briefly, polymerization was conducted in a glass reactor under nitrogen atmosphere for 24 h at 120°C. PCL with two different molecular weights were produced. The monomer/catalyst (stannous octoate, Sigma) ratio was 1700:1 (mol/mol) for high-molecular-weight polymer, while it was 1700:3 (mol/mol) for the lower one. Low-

molecular-weight residuals were removed by a dissolution–precipitation method in which chloroform and methanol were used as the solvent and precipitant, respectively. The number and weight average molecular weight (M_n and M_w) and polydispersity index (PI) were determined by gel-permeation chromatography (GPC; Shimadzu, Japan) in chloroform (Sigma-Aldrich, Germany) at ambient temperature.

Electrospun PCL membranes were produced by the following protocol that was previously described.[25] The electrospinning solution containing 40 g/100 mL PCL with two different molecular weights was prepared in a mixture of chloroform and dimethylformamide (DMF; Sigma-Aldrich) with a DMF content of 50%. The ratio of high- to low-molecular-weight PCL in this solution was 20/80 (w/w). For electrospinning, this polymer solution was placed in a glass Pasteur pipette. The copper probe of the high voltage (HV) generator was inserted into the capillary. The grounded aluminum sheet was positioned opposite to the tip of the capillary at a distance of 10 cm. An electrical field of 15 kV was applied by a HV power supply (Gamma HVPS-ES40). The fluid jet was ejected from the capillary. As the jet accelerated toward the grounded collector, the solvent evaporated, and the polymer nanofibers were deposited on the collector in the form of a nonwoven fabric, that is, the electrospun PCL membrane. The prepared membranes were rolled (spiral-wound) to form disk-shaped spiral-wounded scaffolds with a diameter of 8 mm and height of 2 mm, and stuck using tissue glue (G.R.F., MICROVAL, France).

Simvastatin loading

The statin that was used in this study was a commercial product, that is, Simvastatin® (Zocor, Merck Sharp&-Dohme, USA) in tablet form, containing 10 mg active substance with cellulose, hydroxypropyl cellulose, hydroxypropyl methylcellulose, iron oxides, lactose, magnesium stearate, starch, talc, and titanium dioxide as reported in its prospectus. One hundred milligram tablets were dissolved in 2.5 mL absolute ethanol and 3.75 mL 0.1*M* NaOH solution at 50°C for 2 h. After cooling the mixture to room temperature, pH was adjusted to 7.2, and the final volume was adjusted to 25 mL with distilled water.

Two protocols were followed to load simvastatin to the scaffolds: (i) drug solution (containing 20 μg simvastatin) was embedded into the scaffolds by dropwise administration of the solution (to ensure an even distribution) for each specimen. Note that because of their unique structure, the electrospun membranes absorbed the whole drug solution. Here, these scaffolds were referred to as "simvastatin-embedded PCL scaffolds" ("Sim/Emb/PCL"). With this loading method we were expecting a "burst" release of drug in the very early stages after implantation.[55] Loading method (ii) involved a calculated dosage of simvastatin, which was dispersed within the PCL solution (to reach a final loading of 20 μg simvastatin/scaffold), and then membranes containing simvastatin were electrospun as described earlier. Here, these scaffolds were refered to as "simvastatin-containing PCL scaffolds" ("Sim/Con/PCL"). The loading protocol of this scaffold was designed in such a way that simvastatin molecules will be present in the bulk of nanofibers, and therefore, will most probably be released via a slow, long-term, controlled degradation.[55]

Animal model and surgical protocol

Ninety Wistar Albino rats weighing 250–300 g were used. All rats were fed with free access to food and water. They were maintained in a temperature- and humidity-controlled environment at the Animal Research Department of Hacettepe University. The following study was conducted after receiving permission/approval from the Animal Ethical Committee of the University (Approval number: 2007/007).

A sterile surgical technique was applied throughout the study. The electrospun matrices produced in the previous step were sterilized by ethylene oxide sterilization. Animals were anesthetized by intraperitoneal injection with a mixture of ketamine HCl (Parke Davis, 50 mg/mL, Taiwan) and Rompun (Bayer, 2%, 50 mL, Germany). The implantation region of the test animal was shaved and disinfected with Baticon solution (Droksan, 10%, Turkey). Cranial defects were created by removing 8 mm diameter's of the cranial bone, which was a critical size that cannot regenerate by itself.[56] Once the scalp was incised anterioposterior oblique line and after periosteum was elevated from the cranial bone surface, 8-mm diameter of the cranial bone was removed by using a circular saw, and critical-sized defect was created in calvarial bone. To allow possible cell migration from the sites toward the scaffolded area for bone regeneration, both the periosteum and duramater were preserved. Scaffolds were immediately placed in the defect; periosteum was laid over the scaffold. Periosteum and scalp was closed using a 5-0 silk suture. Figure 2 shows examples of the cranial bone removed, the defect just after removal, and after scaffold implantation within the defect.

The test animals were sacrificed at the selected time intervals (after 1, 3, and 6 months of postimplantation), and soft and hard tissue specimens were removed and placed in 10% phosphate buffered formalin (pH 7.0) at room temperature for fixation. They were analyzed first by microCT and then using standard histology, the results of which are given in the following sections.

MicroCT analysis

After euthanasia, calvarial specimens were removed from the animals after selected time periods (1, 3, and 6 months postimplantation), and placed in 10% phosphate buffered formalin (pH 7.0) at room temperature for fixation, and samples were then rinsed in buffer before analysis. Analyses were performed using X-ray microcomputed tomography (MicroCT40, Scanco Medical GmbH, Switzerland) to quantify mineralized matrix formation within the defect area, as an indicator of new bone formation, scanned at a resolution of 30 μm.[57–61] Samples were normalized to remove individual animal variations in bone-density, shape, and size of "old" bone surrounding the defect area. This was achieved by whole sample analysis

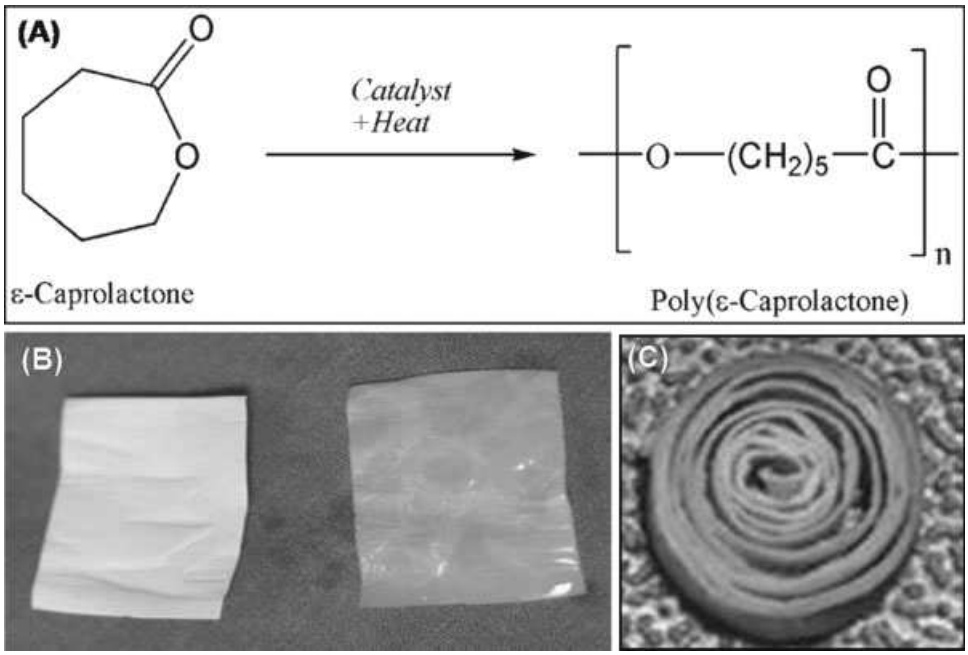

Figure 1. (A) Synthesis of PCL; (B) the PCL electrospun membrane before (left) and after simvastatin embedding (right); and (C) spiral-wound PCL scaffold with macrochannels and microporosity. Note that the nanofiber diameter is in the range of 600–800 nm, the nanofibrous structure is quite uniform, and the microporosity is about 80%. [Color figure can be viewed in the online issue, which is available at www.interscience.wiley.com.]

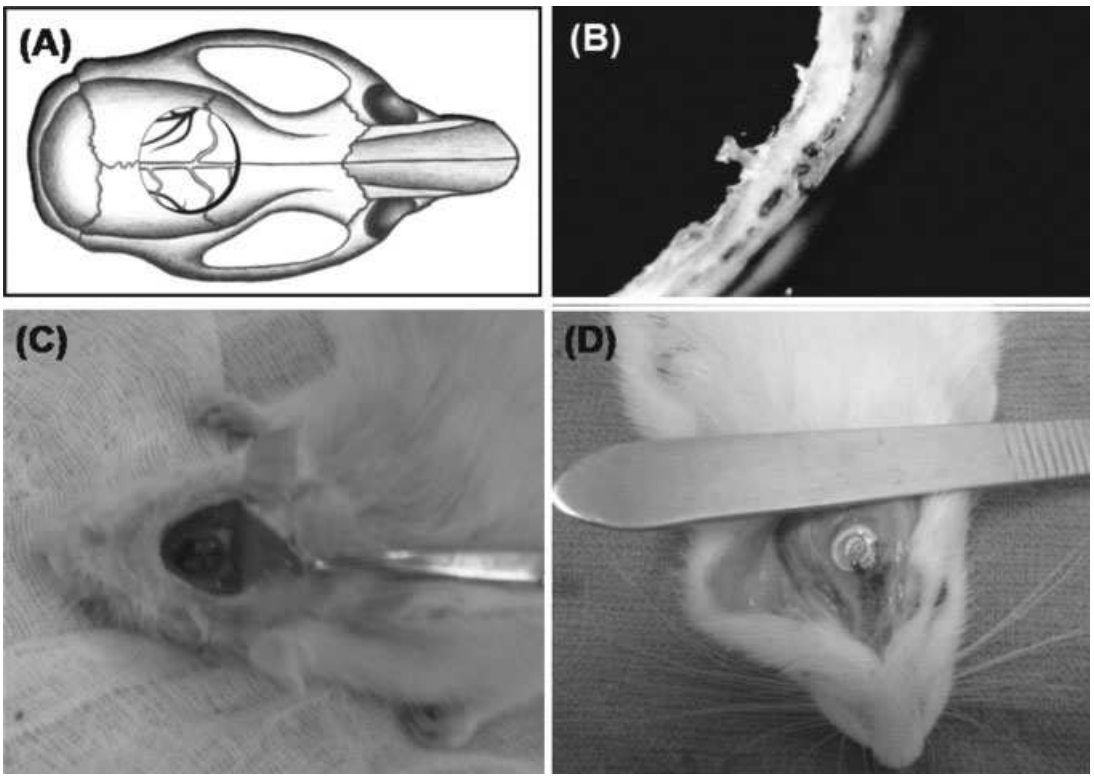

Figure 2. (A) Schematical cranial bone model; (B) cranial defect created rat; (C) the bone piece removed; and (D) scaffold implant in the cranial defect. [Color figure can be viewed in the online issue, which is available at www.interscience.wiley.com.]

to give a total bone volume (which includes the defect area and surrounding bone) before a second analysis was performed, which did not include the defect area, resulting in a value for the surrounding old bone alone. Removal of the volume for surrounding old bone, from the whole sample volume, results in a volume that should represent mineralization within the defect area alone. This is further normalized by using a specific threshold that excludes anything not falling within the specified range, determined for the mineralized matrix within the defect (i.e., air, polymer, and PBS are excluded). A threshold of 350 was chosen to give a good representation of both dense mineralized matrix and more osteoid-like less dense objects. This optimum threshold was determined via a combination of visual pixel alignment and histogram analysis.

Histological evaluation

Following the MicroCT analysis, the samples were decalcified by immersion in De Castro solution for 5–10 days before dehydration in a graded series of ethanol for embedding in paraffin. Five-micrometer-thick serial sections were cut parallel and perpendicular to the long axis of the defect site with a sliding microtome (Leica, Germany). Hematoxylin and eosin and Goldner's Masson Trichrome stained sections were evaluated for bone defect healing, and tissue response to and degradation of the biomaterial. Two independent investigators evaluated stained serial sections using the Leica DMR microscope (Germany). The images were captured by the Leica DC500 digital camera (Germany). Histological scoring system is summarized in Table I.

Statistical analysis

Histological scores and MicroCT data were analyzed using nonparametric tests (Student *t*-test, Kruskal Wallis, and Man Whitney-*U* with Bonferoni correction) to assess statistical significance between independent and dependent variables. Independent variables were time (1, 2, and 6 months) and control groups ("Ctrl"), PCL scaffolds without simvastatin ("PCL"), "simvastatin-embedded PCL scaffolds" ("Sim/Emb/PCL") and "simvastatin-containing PCL scaffolds" ("Sim/Con/PCL") groups. Spearman's test was used to assess correlations between continuous variables; microCT data and histological defect healing scores. Probability value of less than 0.05 was considered as significant. Descriptive statistical values were expressed as minimum, maximum, and medians. Statistical analysis was performed using the SPSS for Windows Release 11.5.

RESULTS AND DISCUSSION

Scaffold properties

PCL has been electrospun in nonwoven matrices formed of nanofibers for several potential biomedical applications.[23,24] In our previous studies, we prepared electrospun PCL membranes, characterized them by *in vitro* and *in vivo* studies, and applied their antibiotic releasing forms for prevention of postsurgery-induced intraabdominal adhesions in a rat model successfully.[17] Then we decided to use these nanofibrous structures for "*in situ*" tissue-engineered bone regeneration. We have observed two main drawbacks with our previous studies, which we have attempted to resolve in this study, as discussed later.

The first drawback was the rather slow degradation rates of PCL electrospun membranes *in vivo*. It has been shown by several groups that PCL is degraded rather slowly *in vivo* yielding ε-hydroxycaproic acid, mainly by simple hydrolysis. But the degradation products (both oligomers and monomers) carrying carboxylic acid end groups are responsible for the autocatalytic bulk degradation of the materials (similar to lactide and glycolide homo and copolymers), in which degradation rates are much faster than ordinary hydrolysis.[62–64] Different than lactide and glycolide homo and copolymers, enzymes (various lipases) also play a role in the degradation of the elastomeric homo and copolymers of ε-CL, which was documented by several authors.[65–67] It was generally agreed that enzymes may take a role at the later stages of degradation when chains fragmented, and then the smaller fragments can be phagocytosed and degraded intracellularly.[68,69] When we implanted the electrospun PCL membranes in an animal model,[25] we were expecting much faster degradation rates, because of the unique structure of these materials. Note that these membranes are formed from very fine nanofibers and have very high porosity. We thought that the microporosity would allow penetration of the degradation agents (water molecules) within the matrix easily. Combined with the very high surface area within the matrix, we hoped that together they would increase the degradation rate of these nanofibrous PCL materials significantly. However, this did not happen.[25] Therefore, when we designed this study, we decided to use blends of high- and low-molecular-weight PCL in preparation of electrospun PCL membranes for bone reconstruction. Low-molecular-weight PCL was included to increase the degradation rate, whilst higher-molecular-weight PCL was used to control the initial mechanical strength of the membranes and allow the material to undergo electrospinning. After preliminary efforts, we selected the recipe and conditions given in Production of Electrospun PCL Membranes section and synthesized two homopolymers of PCL with two different average molecular weights (M_w and M_n) and PIs, namely, M_w: 84,387; M_n: 51,172; PI: 1.64; and M_w: 14,321; 6715; PI: 2.13 (obtained by GPC).[55] The ratio of these two (high M_w to low M_w) was selected as

TABLE I
Histological Scoring System

Categories	Parameters		Scores			
			3	2	1	0
Category 1: Bone defect repair	New bone formation in the defect		Full bone formation in the defect	Moderate bone formation (>50%)	Mild bone formation (<50%)	No new bone
	Graft resorption		Full resorption	Moderate resorption (>50%)	Mild resorption (<)	No resorption
	Marrow changes		Adult type fatty marrow	>50% replaced by new tissue	<50% replaced by new tissue	Fibrous tissue or red
	Cortex remodelling		Full remodelling cortex	Moderate remodelling (>%50)	Mild remodelling (<50%)	No remodelling
		4	3	2	1	0
Category 2: Tissue response	Fibrous connective tissue formation	Severe deposition of dense collagenous connective tissue around implant	Disruption of normal tissue architecture and presence of moderately dense fibrous connective tissue	Presence of moderate connective tissue	Presence of delicate spindle-shaped cells or mild fibroplasia	No difference from normal control tissue, no presence of connective tissue at or around implant site
	Inflammatory cellular infiltration	Severe cellular infiltrate response to implant or tissue necrosis at or around the site	Presence of large numbers of lymphocytes, macrophages, and foreign body giant cells, also notable presence of eosinophils and neutrophils	Presence of several lymphocytes and macrophages with a few foreign body giant cells and a small foci of neutrophils	Presence of a few lymphocytes or macrophages, no presence of foreign body giant cells, eosinophil, or neutrophils	No difference from normal control tissue, and no presence of macrophages, foreign body cells, lymphocytes, eosinophils, or neutrophils at or around implant site

Bone defect repair and the tissue response are scored separately.

TABLE II
Histological and MicroCT Descriptive Statistical Data

Group	350 − Old 350	Tissue Response	Bone Defect Healing
Month 1.00			
Ctrl			
N	2	2	2
Mean	.6118	.0000	1.0000
Std. deviation	.41055	.00000	.00000
Median	.6118	.0000	1.0000
Minimum	.32	.00	1.00
Maximum	.90	.00	1.00
PCL			
N	5	5	5
Mean	.8701	3.4000	1.4000
Std. deviation	.10664	.54772	.54772
Median	.8338	3.0000	1.0000
Minimum	.74	3.00	1.00
Maximum	1.01	4.00	2.00
Sim/Con/PCL			
N	5	5	5
Mean	.5329	3.0000	1.4000
Std. deviation	.32585	.00000	.54772
Median	.4959	3.0000	1.0000
Minimum	.21	3.00	1.00
Maximum	1.05	3.00	2.00
Sim/Emb/PCL			
N	5	5	5
Mean	.8513	2.8000	2.0000
Std. deviation	.30450	.44721	.70711
Median	.8777	3.0000	2.0000
Minimum	.54	2.00	1.00
Maximum	1.27	3.00	3.00
Month 3.00			
Ctrl			
N	2	2	2
Mean	1.3994	.0000	1.5000
Std. deviation	.33750	.00000	.70711
Median	1.3994	.0000	1.5000
Minimum	1.16	.00	1.00
Maximum	1.64	.00	2.00
PCL			
N	5	5	5
Mean	2.1360	2.6000	2.4000
Std. deviation	2.37645	.54772	.54772
Median	1.2198	3.0000	2.0000
Minimum	.62	2.00	2.00
Maximum	6.33	3.00	3.00
Sim/Con/PCL			
N	5	5	5
Mean	3.4006	2.4000	3.4000
Std. deviation	5.03834	.54772	1.14018
Median	1.5006	2.0000	3.0000
Minimum	.34	2.00	2.00
Maximum	12.36	3.00	5.00
Sim/Emb/PCL			
N	5	5	5
Mean	1.6724	2.4000	3.2000
Std. deviation	.71418	.54772	.83666
Median	1.4948	2.0000	3.0000
Minimum	.94	2.00	2.00
Maximum	2.74	3.00	4.00
Month 6.00			
Ctrl			
N	2	2	2
Mean	1.6265	.0000	2.0000
Std. deviation	.02602	.00000	.00000
Median	1.6265	.0000	2.0000
Minimum	1.61	.00	2.00
Maximum	1.64	.00	2.00
PCL			
N	6	6	6
Mean	1.9118	1.6667	2.6667
Std. deviation	.65929	.51640	.81650
Median	1.7133	2.0000	2.5000
Minimum	1.36	1.00	2.00
Maximum	3.18	2.00	4.00
Sim/Con/PCL			
N	5	5	5
Mean	3.2608	1.2000	5.0000
Std. deviation	.71410	.44721	1.00000
Median	3.3601	1.0000	5.0000
Minimum	2.30	1.00	4.00
Maximum	3.95	2.00	6.00
Sim/Emb/PCL			
N	6	6	6
Mean	1.9813	1.6667	3.1667
Std. deviation	1.04218	.51640	.75277
Median	1.9295	2.0000	3.0000
Minimum	.63	1.00	2.00
Maximum	3.39	2.00	4.00

Ctrl, control; PCL, PCL scaffolds without simvastatin; Sim/Emb/PCL, "simvastatin-embedded PCL scaffolds"; Sim/Con/PCL, "simvastatin-containing PCL scaffolds."

20/80 (w/w) after preliminary electrospinning studies.[55] *In vivo* long-term (1 year) degradation studies of the electrospun membranes in animal models are still under investigation and will be reported elsewhere.[55]

The second drawback of electrospun materials for use as tissue-engineering scaffolds is their limited ability to give large openings that will allow cell migration and 3D-cell growth.[9,10] In this study, as a very simple innovative approach, we spiral-wound the membranes produced by electrospinning of the PCL blends mentioned earlier and created macro-channelled scaffolds in addition to microporosity within the electrospun PCL membrane (as shown in Fig. 1) and investigated their performances in the animal model described later. The final diameter and thickness of these scaffolds were 8 mm × 1.5 mm, which were adjusted to fit the cranial defects in these animals.

The National Institute of Biomedical Imaging and Bioengineering (NIBIB) defines tissue engineering as "a rapidly growing area that seeks to create, repair, and/or replace tissues and organs by using combinations of cells, biomaterials, and/or biologically active molecules."[70] Because of the limits/regulations placed upon cell therapies, scaffolds that incorpo-

rate/release bioactive agents are being used increasingly for *in situ* tissue engineering. Following this general trend, and considering the literature information,[26] we decided to include simvastatin in our biodegradable scaffolds to enhance the reconstruction of critical-size calvarial bone defects in an animal model, to stimulate osteoblast activity, which is the other important contribution of this study. Simvastatin is one of the most popular members of statin family and has the empirical formula $C_{25}H_{38}O_5$. Its molecular weight is 418.57 and the melting point is 135–138°C. The molecular structure of simvastatin is a white to off-white, nonhygroscopic, crystalline powder that is practically insoluble in water, and freely soluble in chloroform, methanol, and ethanol.[71] In this study, we incorporated simvastatin within the electrospun PCL membranes by two approaches, during electrospinning or after electrospinning to the matrices, as explained in Simvastatin Loading section. The matrices were then spiral-wound to obtain a 3D-structures, and used in the animal models described later.

Histological evaluation

Diverse intramembraneous, and in some areas, stages of endochondral ossification were observed within the critical size calvarial defect. Descriptive statistical data are presented in Table II for the bone defect healing scores and the tissue response to the implant. The PCL scaffold provided an osteoconductive environment causing only a mild inflammation, which was characterized mainly by mononuclear phagocyte cells, macrophages, lymphocytes, and fibroblasts. Some scattered polymorph nuclear leukocytes with foreign body giant cells were noted at 1 month; but the tissue reaction subsided in time leaving thin collagenous bands, fibroblasts with blood vessels near the degrading polymeric particles. Tissue response scores did not differ between groups. Neither necrosis nor foreign body reaction was noted in any of the samples at any time point. Tissue response scores decreased significantly from 1 month to 6 months in all PCL-implanted groups ($p < 0.05$). Therefore, we concluded that the PCL scaffolds were biocompatible (Figs. 3–5).

Bone defect healing scores increased with time at the critical size cranial bone defect model. Ossification procedure started from the edges of cortical bone toward to inside of the implant. Cartilage plates indicating endochondral ossification process were noted in implant groups. Active osteoblasts synthesizing new bone matrix were numerous at cortical bone edges, macrochannels walls near the cortical plates, and the cartilage islands in both types of simvastatin-loaded scaffolds. The number of samples in the control group (defect group) was limited, as previous studies showed that a 6-mm sized defect in rats was a critical size defect that cannot heal itself.[56] Moreover, in this case, the calvarial bone defect diameter was 8 mm. Ethical principles dictate that all efforts should be made to use the lowest number of animals to achieve meaningful results. In addition, the control group served for demonstration purposes only. Therefore, a limited number of animals were used in the control group. This was one of the reasons for the calvarial scores remaining almost invariable in the first 3 months for this group. Healing scores of the control group were significantly lower than that of implant groups at 6 months ($p < 0.05$). Histological bone defect healing scores were higher in simvastatin-loaded scaffolds compared with that of the PCL scaffolds without simvastatin. Healing significantly accelerated in the "simvastatin-containing PCL scaffolds" group. Six month bone defect healing scores for this group were significantly higher than that of the PCL scaffolds without simvastatin and the "simvastatin-embedded PCL scaffolds" scores ($p < 0.05$). Cortical bone remodeling was characterized by controlled osteoclastic activity, and the remodeling of the marrow cavity was better in this group compared with the other groups. Simvastatin had superior efficacy for accelerating critical size bone defect healing over a 3- to 6-month period, particularly when loaded to the scaffold during electrospinning. Six-month healing scores were significantly higher than that of the 3-month scores in the "simvastatin-containing PCL scaffolds" group ($p < 0.05$) (Figs. 4 and 5).

The implant has spirally shaped macrochannels allowing the ingrowth of connective tissue cells, and ECM elements including new blood vessels. Degradation started from the periphery expanding to the central parts of the implant after 1 month. However, at 6 months, PCL residues remained intact in the center, and the cavity was filled with a fibrous connective tissue rich in collagen fibers, fibroblasts, and blood vessels (Figs. 3–5).

MicroCT results

The microCT analysis found that the "simvastatin-containing PCL scaffolds" (in which simvastatin was loaded during electrospinning into the scaffolds) were the most effective at promoting mineralization within the defect (Table III). The increase in volume of mineralized matrix within the defect was significant at 6 months compared with critical defect alone ($p = 0.0068$), compared with PCL scaffolds without simvastatin ($p = 0.01$) and to the "simvastatin-embedded PCL scaffolds" ($p = 0.04$). At 3 months the results were more varied, with some showing signifi-

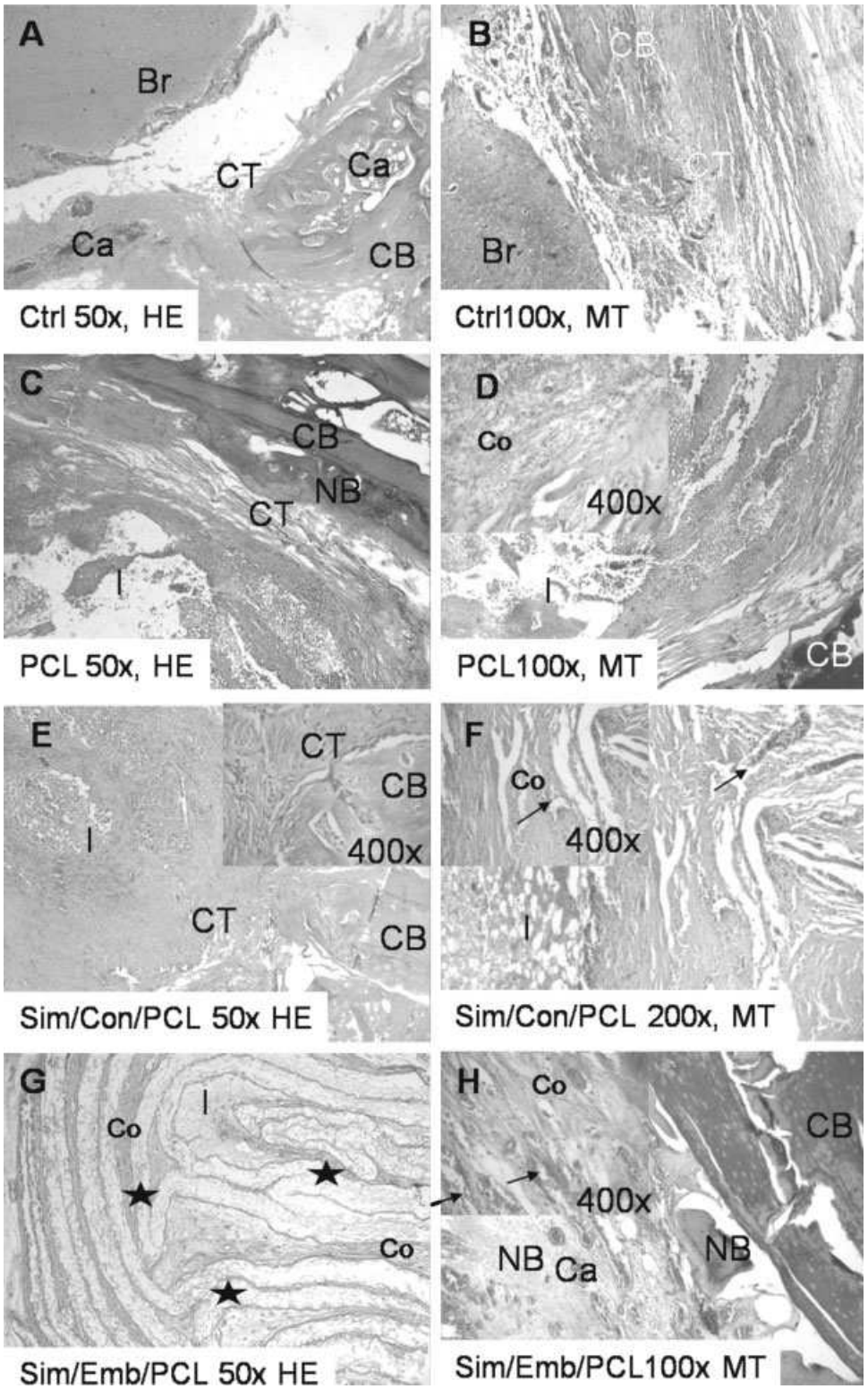

Figure 3. Results at the 1st month: brain (Br) section is observed within the control cavity. The ossification is at a primitive level in that group (A,B). Defect healing process is at a more advanced level in PCL scaffold implanted groups (C–G). Collagen fibers (pink with HE; green with MT) and the blood vessels (arrows) are located within the PCL scaffold macrochannels (star), in close relation with the dissolving implant particles; revealing the biocompatibility and the good guidance of PCL (C–G). HE, hematoxylin and eosin; MT, Masson's trichrome; I, implant (scaffold); CT, connective tissue; BM, bone marrow; CB, compact bone; NB, new bone; Ca, cartilage; Co, collagen fibers. [Color figure can be viewed in the online issue, which is available at www.interscience.wiley.com.]

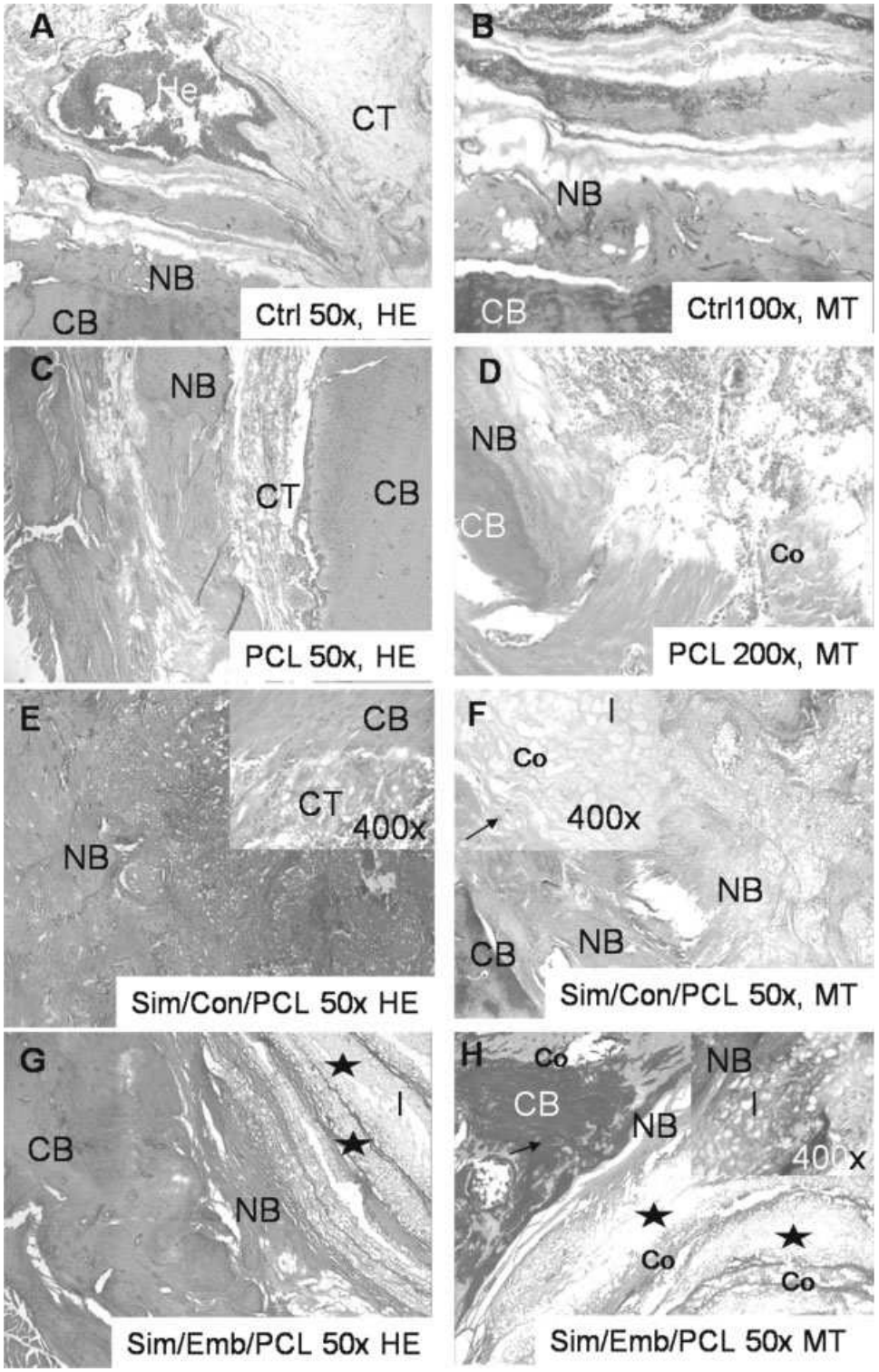

Figure 4. Results at the 3rd month: The control group still exhibits lower level of healing with a disorganized loose connective tissue filling the defect area; when compared with PCL scaffold groups (A,B). An organized thrombus (He) is observed at the bottom of the control cavity (A,B). New bone formation is obvious starting from the cortical edges into the cavity at the "simvastatin-containing PCL scaffolds" group (E,F). Newly apposed bone matrix lined by active osteoblasts appear green, and the maturing bone matrix in red with MT. The macrochannels lined by dissolving biomaterial particles became larger and filled with a highly vascular fibrous callus (G,H). Collagen fibers (pink with HE; green with MT) and the blood vessels are in close relation with the implant (scaffold): HE, hematoxylin and eosin; MT, Masson's trichrome; I, implant (scaffold); CT, connective tissue; BM, bone marrow; CB, compact bone; NB, new bone; Ca, cartilage; Co, collagen fibers. [Color figure can be viewed in the online issue, which is available at www.interscience.wiley.com.]

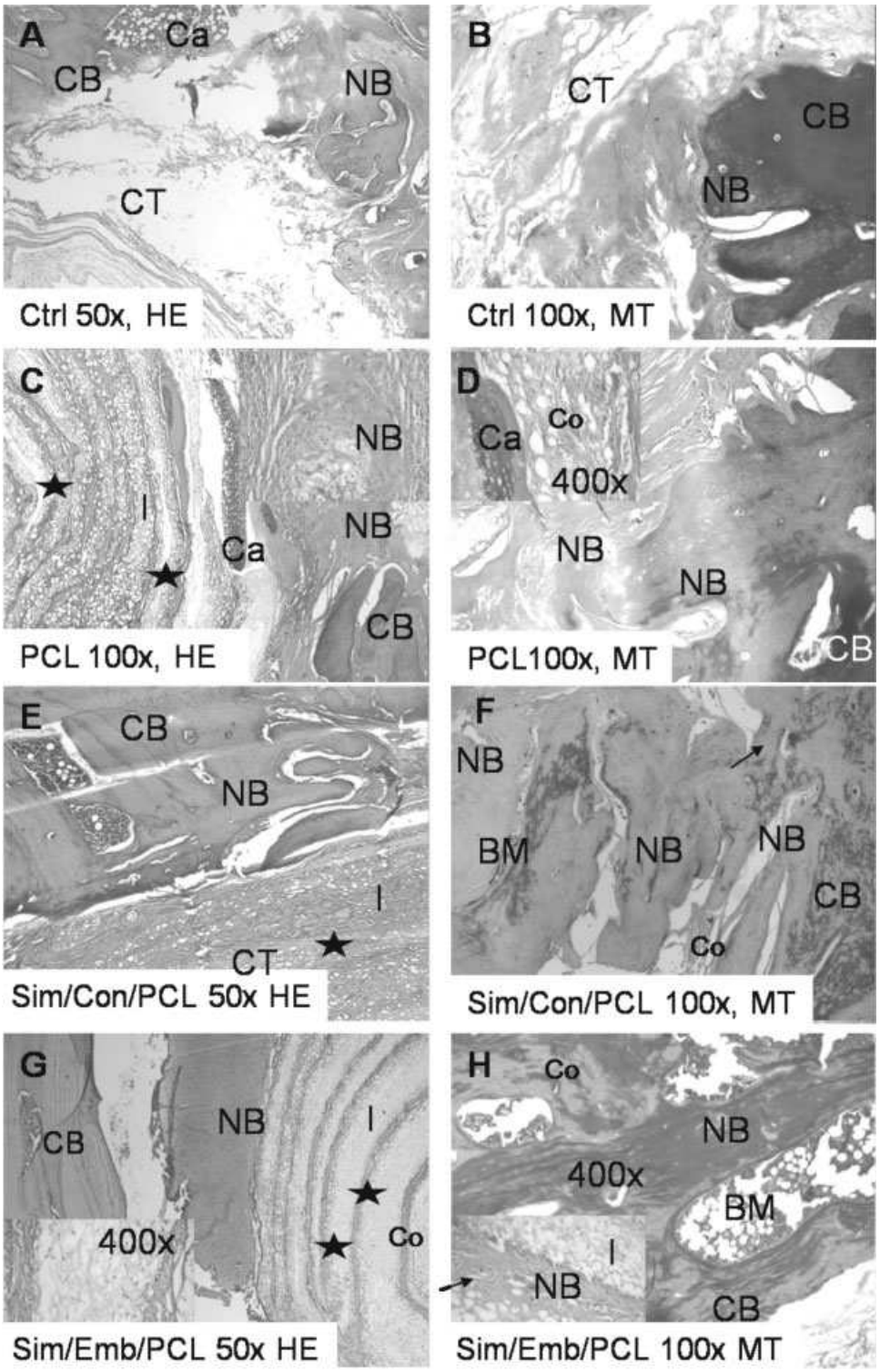

Figure 5. Results at the 6th month: the critical size defect is not totally ossified yet in any of the groups. Control cavity remains to be filled with a scatrice fibrous tissue (A,B). But the healing process is accelerated with PCL scaffolds. The scaffold is degrading from the periphery toward inside; by being divided into smaller compartments with macrochannels (stars) filled with fibrous and osseous callus (C,D). Remodeling of the cortical bone allowed the recovery of the bone marrow elements at "simvastatin-containing PCL scaffolds" group (E–H). HE, hematoxylin and eosin; MT, Masson's trichrome; I, implant (scaffold); CT, connective tissue; BM, bone marrow; CB, compact bone; NB, new bone; Ca, cartilage; Co, collagen fibers. [Color figure can be viewed in the online issue, which is available at www.interscience.wiley.com.]

TABLE III
Histologic Bone Healing and the MicroCT Analysis Data Correlations

Group 1	Month (Spearman's rho 350 − old 350)	Bone Defect Healing		
		R	*p*	*N*
PCL	1.00	0.866	0.058	5
	3.00	0.866	0.058	5
	6.00	0.926	0.008	6
Sim/Con/PCL	1.00	0.866	0.058	5
	3.00	0.975	0.005	5
	6.00	0.949	0.014	5
Sim/Emb/PCL	1.00	0.671	0.215	5
	3.00	0.949	0.014	5
	6.00	0.926	0.008	6

Correlation coefficients (r), p values, and the number of samples (n) for each group are presented.

cant increases in mineralized matrix while others did not, resulting in the large error bar at 3 months (Figs. 6 and 7). This was resolved however at 6 months (Fig. 7).

Results indicate that the introduction of a PCL scaffold alone is not sufficient to result in a mineralized matrix forming within the critical size bone defect. However, simvastatin loading of PCL scaffolds exhibited much better matrix formation, with "simvastatin-containing PCL scaffolds" producing most significant results, most probably as a result of slower release of simvastatin over longer time periods. The release of simvastatin from "simvastatin-embedded PCL scaffolds" exhibits burst release characteristics that do not appear to have a significant effect on the volume of mineralization within the defect area. The 3D-image shows that there is ingrowth of mineralized matrix into the defect area, as is the case with the PCL scaffolds without simvastatin. This suggests that, while not having a significant effect, the PCL scaffolds without simvastatin

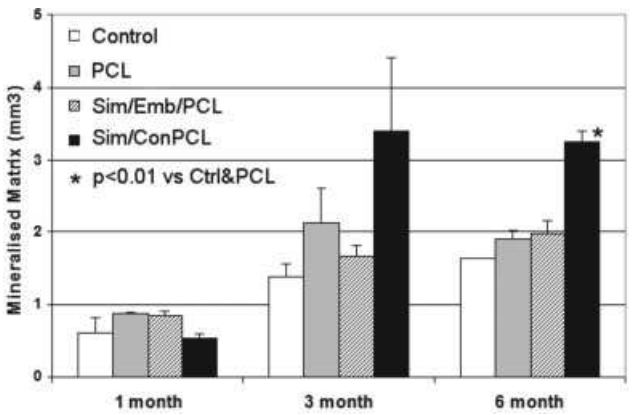

Figure 6. Effect of simvastatin incorporation into PCL scaffolds for repair of critical size defects using microCT analysis.

and the "simvastatin-embedded PCL scaffolds" do promote ingrowth of new bone (mineralized matrix) into an otherwise nonhealing critical-sized bone defect. But only when the simvastatin was present within the scaffold and released over time was it able to have greater effect and allow a significant volume of mineralized matrix to form within the defect area.

CONCLUSIONS

Reconstruction of bone defects is still problematic. It seems that tissue engineering with or without cells but containing bioactive agents to stimulate bone regeneration could be an important therapeutical strategy. Biodegradable scaffolds with highly open and interconnected pore structures and with desirable surface chemistries that would allow cell attachment, migration, and 3D-growth to form the new tissue are needed. In this study, we applied very simple innovative strategies, using blends of high- (for processibility and final mechanical properties) and low- (for faster degradation rates) molecular-weight PCL. Here, we have prepared electrospun PCL by following a straight-forward technique and also prepared nanofibrous membranes. We then simply rolled these membranes into spiral-wound 3D-structures to produce scaffolds with macrochannels and microporosity. To use these scaffolds as "*in situ*" tissue-engineered bone regeneration constructs, we incorporated simvastatin as a novel approach to enhance osteoblastic activity and stimulate new bone formation. The scaffolds with or without simvastatin were implanted into cranial defects of rats for the bone regeneration and harvested after 1, 3, and 6 months. The results of these *in vivo* studies exhibited tissue integration within the implant and functionally stable restoration of the calvarium. Tissue formation was started in the macrochannels in the novel spiral-wound scaffolds. The more successful approach was observed with the "simvastatin-containing PCL scaffolds" in which simvastatin was incorporated into the PCL scaffolds during electrospinning (with slower and long term release). In this group, the bone mineralization was quite significant when compared with the other sample groups. Simvastatin-containing PCL scaffolds resulted in an induced activation-formation in the ARF (activation, resorption, formation) cycle depending on the release behavior. Macrochannels of the scaffolds enhanced the proliferation and attachment of the osteoclasts and osteoblasts from the periphery to the center. In addition, statin induced the dura mater, and periost originated from the preosteoblasts and preosteoclasts to the macrochanneled and nanofibrous

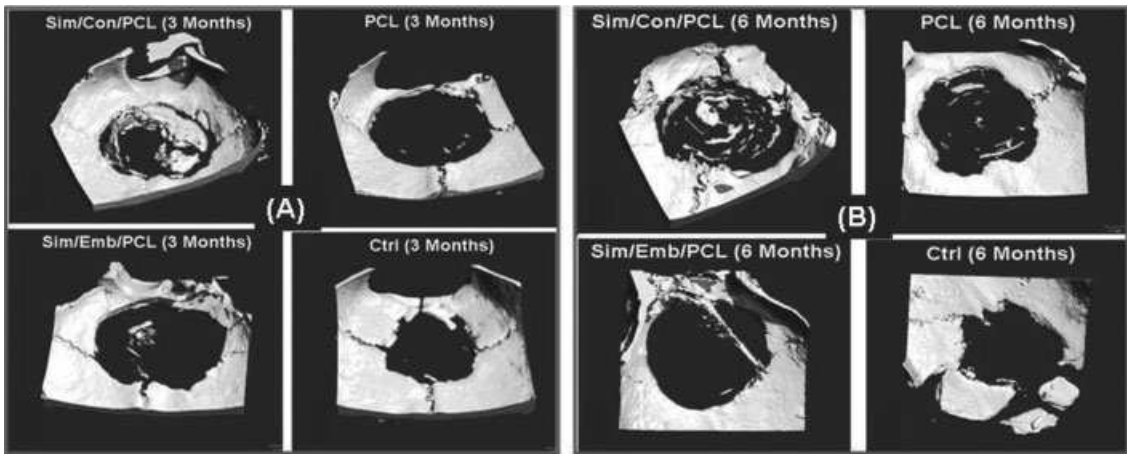

Figure 7. MicroCT 3D-images representing whole sample: "simvastatin-containing PCL scaffolds"; PCL scaffold without simvastatin; "simvastatin-embedded PCL scaffolds"; critical size defect without any scaffold (control group). (A) 3 months; (B) 6 months.

scaffold. The most significant result of this study was the formation of mineralized bone through the macrochannels in 3–6 months. The *in vitro* and *in vivo* degradation studies for longer periods (1 year and more), *in vitro* simvastatin release profiles with different loading strategies, and *in vivo* studies with scaffolds combined with mesenchymal stem cells are under investigation and will be presented in other papers.

This study was performed in the contest of EU-FP6-NoE:Expertissues project and Graduate Programme of Hacettepe University (a part of Ph.D. Thesis of İsmail Alper İşoğlu under the supervision of Prof. Erhan Pişkin).

References

1. Damien CJ, Parsons JR. Bone graft and bone graft substitutes: A review of current technology and applications. J Appl Biomater 1991;2:187–208.
2. Langer R, Vacanti JP. Tissue engineering. Science 1993;260: 920–926.
3. Reddi AH. Role of morphogenetic proteins in skeletal tissue engineering and regeneration. Nat Biotechnol 1998;16:247–252.
4. Tuzlakoğlu K, Bölgen N, Salgado AJ, Gomes ME, Piskin E, Reis RL. Nano- and micro-fiber combined scaffolds: A new architecture for bone tissue engineering. J Mater Sci Mater Med 2005;16:1099–1104.
5. Mistry AS, Mikos AG. Tissue engineering strategies for bone regeneration. Adv Biochem Eng Biotechnol 2005;94:1–22.
6. Alsberg E, Hill EE, Mooney DJ. Craniofacial tissue engineering. Crit Rev Oral Biol Med 2001;12:64–75.
7. Ma PX, Choi JW. Biodegradable polymer scaffolds with well-defined interconnected spherical pore network. Tissue Eng 2001;7:23–33.
8. Bölgen N, Plieva F, Galaev IY, Mattiasson B, Piskin E. "Cryogelation" for preparation of novel biodegradable tissue engineering scaffolds. J Biomater Sci Polym Ed 2007;18:1165–1169.
9. Sharma B, Elisseeff JH. Engineering structurally organized cartilage and bone tissues. Ann Biomed Eng 2004;32:148–159.
10. Caplan AI. Tissue engineering designs for the future: New logics, old molecules. Tissue Eng 2000;6:1–8.
11. Liu X, Ma PX. Polymeric scaffolds for bone tissue engineering. Ann Biomed Eng 2004;32:477–486.
12. Hou QP, Grijpma DW, Feijen J. Porous polymeric structures for tissue engineering prepared by a coagulation, compression molding and salt leaching technique. Biomaterials 2003; 24:1937–1947.
13. Huang ZM, Zhang YZ, Kotaki M, Ramakrishna S. A review on polymer nanofibers by electrospinning and their applications in nanocomposites. Compos Sci Technol 2003;63:2223–2253.
14. Lannutti J, Reneker D, Ma T, Tomasko D, Farson D. Electrospinning for tissue engineering scaffolds. Mater Sci Eng C 2007;27:504–509.
15. Smith LA, Ma PX. Nano-fibrous scaffolds for tissue engineering. Colloids Surf B Biointerfaces 2004;39:125–131.
16. Pişkin E, Bölgen N, Eğri S, İşoğlu İA. Electrospun matrices made of poly(α-hydroxy acids) for medical use. Nanomedicine 2007;2:441–457.
17. Bölgen N, Vargel İ, Korkusuz P, Menceloğlu YZ, Pişkin E. In vivo performance of antibiotic embedded electrospun PCL membranes for prevention of abdominal adhesions. J Biomedical Mater Res B Appl Biomater 2007;81:530–543.
18. Fambri L, Migliaresi C, Kesenci K, Pişkin E. Biodegradable polymers, In: Barbucci R, editor. Integrated Biomaterials Science. New York: Kluwer; 2002. p 119–187.
19. Pişkin E. Biodegradable polymers in medicine. In: Scott G, editor. Degradable Polymers: Principles and Applications. Dordrecht: Kluwer; 2002. p 321–377.
20. Pitt CG. Poly (ε-caprolactone) and its copolymers. In: Chasin M, Langer R, editors. Biodegradable Polymers as Drug Delivery Systems. New York: Marcel Dekker; 1990. p 71–120.
21. Hutmacher DW, Schantz T, Zein I, Ng KW, Teoh SH, Tan KC. Mechanical properties and cell cultural response of polycaprolactone scaffolds designed and fabricated via fused deposition modeling. J Biomed Mater Res 2001;55: 203–216.
22. Ekholm M, Hietanen J, Lindqvist C, Rautavuori J, Santavirta S, Suuronen R. Histological study of tissue reactions to epsilon-caprolactone-lactide copolymer in paste form. Biomaterials 1999;20:1257–1262.
23. Ng KW, Hutmacher DW, Schantz JT, Ng CS, Too HP, Lim TC, Phan TT, Teoh SH. Evaluation of ultra-thin poly(epsilon-caprolactone) films for tissue-engineered skin. Tissue Eng 2001;7:441–455.

24. Li W, Laurencin C, Caterson E, Tuan R, Ko F. Electospun nanofibrous structure: A novel scaffold for tissue engineering. J Biomed Mater Res 2002;60:613–621.
25. Bölgen N, Menceloğlu YZ, Açatay K, Vargel İ, Pişkin E. In vitro and in vivo degradation of non-woven materials made of poly(e-caprolactone) nanofibers prepared by electrospinning at different conditions. J Biomater Sci Polym Ed 2005;16: 1537–1555.
26. Pratt AB, Weber FE, Schmoekel HG, Müller R, Hubbell JA. Synthetic extracellular matrices for in situ tissue engineering. Biotechnol Bioeng 2004;86:27–36.
27. Kim HW, Knowles JC, Kim HE. Hydroxyapatite/poly(epsilon-caprolactone) composite coatings on hydroxyapatite porous bone scaffold for drug delivery. Biomaterials 2004;25: 1279–1287.
28. Hu JJ, Jin D, Quan DP, Zong SZ, Chen JH, Wei KH, Zhao J, Pei GX. Bone defect repair with a new tissue-engineered bone carrying bone morphogenetic protein in rabbits. Di Yi Jun Yi Da Xue Xue Bao 2005;25:1369–1374.
29. Murphy WL, Peters MC, Kohn DH, Mooney DJ. Sustained release of vascular endothelial growth factor from mineralized poly(lactide-*co*-glycolide) scaffolds for tissue engineering. Biomaterials 2000;21:2521–2527.
30. Whang K, Goldstick TK, Healy KE. A biodegradable polymer scaffold for delivery of osteotropic factors. Biomaterials 2000; 21:2545–2551.
31. Babensee JE, McIntire LV, Mikos AG. Growth factor delivery for tissue engineering. Pharm Res 2000;17:497–504.
32. Sugiyama M, Kodama T, Konishi K, Abe K, Asami S, Oikawa S. Compactin and simvastatin, but not pravastatin, induce bone morphogenetic protein-2 in human osteosarcoma cells. Biochem Biophys Res Commun 2000;271:688–692.
33. Garrett IR, Gutierrez G, Mundy GR. Statins and bone formation. Curr Pharm Des 2001;7:715–736.
34. Staal A, Frith JC, French MH, Swartz J, Güngör T, Harrity TW, Tamasi J, Rogers MJ, Feyen JH. The ability of statins to inhibit bone resorption is directly related to their inhibitory effect on HMG-CoA reductase activity. J Bone Miner Res 2003;18:88–96.
35. Hu H, Sung A, Zhao G. Simvastatin enhances bone morphogenetic protein receptor type II expression. Biochem Biophys Res Commun 2006;339:59–64.
36. Yee AJ, Bae HW, Friess D. The use of simvastatin in rabbit posterolateral lumbar intertransverse process spine fusion. Spine J 2006;6:391–396.
37. Shepherd J, Hunninghake DB, Barter P, McKenney JM, Hutchinson HG. Guidelines for lowering lipids to reduce coronary artery disease risk: A comparison of rosuvastatin with atorvastatin, pravastatin, and simvastatin for achieving lipid-lowering goals. J Am Cardiol 2003;91:11–17.
38. Chasman DI, Posada D, Subrahmanyan L, Cook NR, Stanton VP Jr, Ridker PM. Pharmacogenetic study of statin therapy and cholesterol reduction. J Am Med Assoc 2004;291:2821–2827.
39. Furberg CD. Natural statins and stroke risk. Circulation 1999;99:185–188.
40. Jonsson N, Asplund K. Does pretreatment with statins improve clinical outcome after stroke? A pilot case-referent study. Stroke 2001;32:1112–1115.
41. Walter DH, Schachinger V, Elsner M, Mach S, Auch-Schwelk W, Zeiher AM. Effect of statin therapy on restenosis after coronary stent implantation. Am J Cardiol 2000;85: 962–968.
42. Rauch U, Osende JI, Chesebro JH, Fuster V, Vorchheimer DA, Harris K, Harris P, Sandler DA, Fallon JT, Jayaraman S, Badimon JJ. Statins and cardiovascular diseases: The multiple effects of lipid-lowering therapy by statins. Atherosclerosis 2000;153:181–189.
43. Lane NE, Kelman A. A review of anabolic therapies for osteoporosis. Arthr Res Ther 2003;5:214–222.
44. Rogers MJ. Statins: Lower lipids and better bones? Nat Med 2000;6:21–23.
45. Cauley J, Jackson R, Pettinger M, Lacroix A, Bauer D, Chen Z, Daugherty S, Hsia J, Lewis C, McGowan J, McNeeley S, Passaro M. Statin use and bone mineral density (BMD) in older women. J Bone Min Res 2000;15:155.
46. Garrett IR, Mundy G. The role of statins as potential targets for bone formation. Arthr Res 2002;4:237–240.
47. Vogel G. Cholesterol-lowering drugs may boost bones. Science 1999;286:1825–1826.
48. Edwards CJ, Hart DJ, Spector TD. Oral statins and increased bone-mineral density in postmenopausal women. Lancet 2000;355:2218–2219.
49. Bauer DC, Mundy GR, Jamal SA, Black DM, Cauley JA, Ensrud KE, van der Klift M, Pols HAP. Use of statins and fracture: Results of 4 prospective studies and cumulative meta-analysis of observational studies and controlled trials. Arch Intern Med 2004;164:146–152.
50. Toh S, Hernandez-Diaz S. Statins and fracture risk. A systematic review. Pharmacoepidemiol Drug Saf 2007;16:627–640.
51. Wong RWK, Rabie ABM. Statin collagen grafts used to repair defects in the parietal bone of rabbits. Br J Oral Maxillofac Surg 2003;41:244–248.
52. Wong RWK, Rabie ABM. Early healing pattern of statin-induced osteogenesis. Br J Oral Maxillofac Surg 2005;43:46–50.
53. Maritz F, Conradie M, Hulley P, Gopal R, Hough S. Effect of statins on bone mineral density and bone histomorphometry in rodents. Arterioscler Thromb Vasc Biol 2001;21: 1565–1566.
54. Ural E, Kesenci K, Fambri L, Migliaresi C, Pişkin E. Poly(D,L-lactide/ε-caprolactone)/hydroxyapatite composites as bone filler: Preparation and characterization. Biomaterials 2000;21: 2147–2154.
55. İşoğlu, İA. Scaffolds based on electrospun poly(ε-caprolactone) membranes for bone tissue engineering. PhD Thesis. Hacettepe University, Ankara, Turkey, 2007.
56. Burdicka JA, Frankelb D, Dernellb WS, Ansetha KS. An initial investigation of photocurable three-dimensional lactic acid based scaffolds in a critical-sized cranial defect. Biomaterials 2003;24:1613–1620.
57. Jaecques SVN, Van Oosterwyck H, Muraru L, Van Cleynenbreugel T, De Smet E, Wevers M, Naert I, Vander Sloten J. Individualised, micro CT-based finite element modelling as a tool for biomechanical analysis related to tissue engineering of bone. Biomaterials 2004;25:1682–1696.
58. Schantz JT, Teoh SH, Lim TC, Lim TC, Endres M, Lam CX, Hutmacher DW. Repair of calvarial defects with customized tissue-engineered bone grafts. I. Evaluation of osteogenesis in a three-dimensional culture system. Tissue Eng 2003;9:S113–S126.
59. Schantz JT, Hutmacher DW, Lam CXF, Bringmann M, Wong KM, Lim TC, Chou N, Re G, Teoh SH. Repair of calvarial defects with customised tissue-engineered bone grafts. II. Evaluation of cellular efficiency and efficacy in vivo. Tissue Eng 2003;9:S127–S139.
60. Meinel L, Karageorgiou V, Hofmann S, Fajardo R, Snyder B, Li C, Zichner L, Langer R, Vunjak-Novakovic G, Kaplan DL. J Biomed Mater Res Part A 2004;71:25–34.
61. Tuan HS, Hutmacher DW. Application of micro CT and computation modeling in bone tissue engineering. Comput Aid Des 2005;37:1151–1161.
62. Li S, McCarthy S. Further investigations on the hydrolytic degradation of poly(DL-lactide). Biomaterials 1999;20: 35–44.

63. Lu L, Garcia CA, Mikos AG. In vitro degradation of thin poly(DL-lactic-*co*-glycolic acid) films. J Biomed Mater Res 1999; 46:236–244.
64. Grizzi I, Garreau H, Li S, Vert M. Hydrolytic degradation of devices based on poly(DL-lactide) size dependence. Biomaterials 1995;16:305–311.
65. Gan Z, Yu D, Zhong Z, Liang Q, Jing X. Enzymatric degradation of poly(caprolactone)/poly(DL-lactide) blends in phosphate buffer solution. Polymer 1999;40:2859–2862.
66. Pitt CG, Marks TA, Schindler A. Biodegradable drug delivery systems based on aliphatic polyesters: Application to contraceptives and narcotic antagonists. NIDA Res Monogr 1981;28:232–253.
67. Li SM, Liu LJ, Garreau H, Vert M. Lipase-catalysed biodegradation of poly(ε-caprolactone) blended with various polylactide-based polymers. Biomacromolecules 2003;4:373–377.
68. Woodward SC, Brewer PS, Moatamed F, Schindler A, Pitt CG. The intracellular degradation of poly(ε-caprolactone). J Biomed Mater Res 1985;19:437–444.
69. Matlaga BF, Salthouse TN. Ultrastructural observations of cells at the interface of a biodegradable polymer: Polyglactin 910. J Biomed Mater Res 1983;17:185–197.
70. http://www.nibib1.nih.gov/.
71. The internet drug index.www.rxlist.com.

Chemical Engineering Journal 228 (2013) 1057–1065

Contents lists available at SciVerse ScienceDirect

Chemical Engineering Journal

journal homepage: www.elsevier.com/locate/cej

Poly (ε-caprolactone) incorporated bioactive glass nanoparticles and simvastatin nanocomposite nanofibers: Preparation, characterization and *in vitro* drug release for bone regeneration applications

Monireh Kouhi [a,b], Mohammad Morshed [a,*], Jaleh Varshosaz [c], Mohammad Hossein Fathi [b]

[a] Department of Textile Engineering, Isfahan University of Technology, Isfahan 84156-83111, Iran
[b] Biomaterials Group, Department of Materials Engineering, Isfahan University of Technology, Isfahan 84156-83111, Iran
[c] Department of Pharmaceutics, School of Pharmacy and Pharmaceutical Sciences, Isfahan University of Medical Sciences, Isfahan, Iran

HIGHLIGHTS

- Electrospun PCL drug delivery device containing bioactive glass (BG) and simvastatin.
- Incorporation of BG increased tensile strength and crystallinity of nanofibers.
- Nanofiber biodegradation and drug release rate were affected by BG concentration.
- SEM–EDS and XRD analysis showed HA formation on the fiber surface after SBF soaking.
- Composite web exhibited excellent bioactivity and controlled drug release behavior.

ARTICLE INFO

Article history:
Received 7 February 2013
Received in revised form 14 May 2013
Accepted 23 May 2013
Available online 3 June 2013

Keywords:
Nanocomposite nanofiber
Poly ε-caprolactone
Bioactive glass
Simvastatin
Drug release
Bioactivity

ABSTRACT

Poly (ε-caprolactone) (PCL) nanofibers containing bioactive glass (BG) nanoparticles and simvastatin drug was produced by electrospinning. Morphology of as-spun nanofibers was studied using scanning electron microscopy (SEM). Evaluation of the mechanical properties of the nanofibrous webs revealed that there is a limit to the nanoparticle concentration at which BG nanoparticles can improve the tensile strength of the PCL nanofibrous web. Results of *in vitro* degradation tests indicated that the presence of BG led to a faster degradation of the nanofibrous webs. Differential scanning calorimetry (DSC) was employed to determine the effects of BG addition on the crystallinity degree of PCL nanofibers. Based on DSC results, crystallinity of the polymeric nanofibers was also enhanced with increasing BG content. Moreover DSC results showed that drug molecules were present in the amorphous form in the nanofibers. *In vitro* drug release studies performed in the phosphate buffer saline (PBS) at pH 7.4 showed that drug release rate was affected by BG concentration. The assessment of *in vitro* bioactivity of the nanocomposite nanofibers was carried out in the simulated body fluid (SBF). SEM–EDS results and XRD analysis indicated that a hydroxyapatite layer was formed on the surface of the nanofibrous webs after soaking in SBF over different time periods. Generally speaking, this novel nanofibrous web was shown to be able to release simvastatin in a controlled manner and to have the ability to form an apatite layer in the biological fluid on the nanofiber surface, which indicates their good potential for bone regeneration applications.

1. Introduction

Nanofibrous materials are gaining great interest in biomedical fields, such as drug release devices [1] and tissue regeneration matrices [2,3]. In the fields of bone tissue engineering, nanofibrous scaffolds have been widely used in bone regeneration application. Besides the small fiber diameter, nanofibrous scaffolds offer a high surface to volume ratio, the potential for a high porosity and interconnected pores and the enhanced bone regeneration by providing a nanoscale biomimetic structure of natural extracellular matrix (ECM) [1–3].

Electrospinning is regarded as a simple and versatile method to produce ultrafine fibers with diameters ranging from microns down to a few nanometers, by using materials of different compositions from medical materials to degradable polymers and

* Corresponding author. Tel.: +98 311 3915023; fax: +98 311 3912444.
E-mail addresses: monireh.kouhi@ma.iut.ac.ir (M. Kouhi), morshed@cc.iut.ac.ir (M. Morshed), varshosaz@pharm.mui.ac.ir (J. Varshosaz), fathi@cc.iut.ac.ir (M.H. Fathi).

1385-8947/$ - see front matter © 2013 Elsevier B.V. All rights reserved.
http://dx.doi.org/10.1016/j.cej.2013.05.091

bioactive ceramics [1–6]. The basic electrospinning setup includes a polymer solution or melt reservoir, grounded collector, and a high voltage electric field in between. When the voltage is high enough to overcome the surface tension of the polymer solution/melt, a charged jet is generated towards the grounded collector, along which the solvent evaporates/melt solidifies to form solid-state thin fibers [1]. By adopting appropriate process parameters such as solvent, polymer concentration, and flow rate, electrospun nanofibers with various diameters can be obtained [1,2,7–11].

It has been reported that the biological properties for electrospun nanofibrous scaffolds including hydrophilicity, mechanical property, and bioactivity are largely determined by the compositions of the polymers used for making tissue engineering scaffold. In general, a single polymer cannot impart all the required properties to the scaffold. Therefore many studies have been developed to modify or improve the biological properties by simply combining variable components or adjusting the ratios [2–5,7,12,13].

For hard tissue applications, biodegradable synthetic polymers, such as poly (lactide-co-glycolide) (PLGA) [13–15], poly (L-lactic acid) (PLLA) [6,16], poly (ε-caprolactone) (PCL) [5,7,17–21], and their copolymers, have been widely used due to their favorable biocompatibility and degradability. Among these polymers, PCL is a common biodegradable, FDA-approved, and low-price biomaterial that can be easily fabricated and has proper toughness, flexibility, and high compatibility with osteoblasts and, hence, it may be suitable for long-term implant applications. However, most of the polymers including PCL have limitations in bone regeneration applications because of their low stiffness, hydrophobic nature and lack of bioactivity [17,18]. Combination of such polymers with bioactive inorganic phases such as hydroxyapatite (HA), tricalcium phosphate, bioactive glass (BG), and their biphasic mixtures is a promising way to overcome the drawbacks of those biodegradable polymers [5,17–21]. Among the inorganic bioactive phases, BG is a fascinating choice due to excellent bioactivity to form a bone mineral-like hydroxyapatite phase on the material surface which ultimately induces direct bonding with native bone tissue. Efforts have been made to utilize this capability of BG in various composites reinforced with BG particles, such as PLGA/BG, PLLA/BG, PCL/BG, poly (3-hydroxybutyrate) (P (3HB))/BG among others [14,16,21,22]. When compared with microfillers, BG nanofillers with their larger specific surface area have a more favorable influence on organic-based composites, resulting in nanostructured composites with improved bioactivity. Misra et al. [22] reported the successful preparation of (P (3HB))/BG composite containing nano- and microparticles of BG. It has been shown that systematic addition of BG nanoparticles induced surface nanotopography, which improved *in vitro* bioactivity (HA formation), total protein adsorption, wettability and led to a higher water uptake upon immersion in SBF in comparison to the conventional materials (e.g. containing BG microparticles). Hong et al. [16] also studied the effect of nanoparticulate BG-ceramic content on the properties of nanocomposite scaffolds, which exhibited improved mechanical properties.

It has been shown that incorporating drugs into composite implants improves their efficiency. The possibility of introducing drug release systems into the implant site has been widely studied and used. Systems such as biodegradable materials [21,22], bioceramics [23] or ceramic/polymer composites [15,17,19] have been developed and such drugs as antibiotics [8,9,15,24], growth factor [12], chemotherapeutic agents [10], and antiinflammatory drugs [25] have been introduced into the drug delivery systems.

In the present study, a statin drug has been applied as a bone regeneration drug. Statins have recently attracted attention due to their ability to stimulate/trigger bone regeneration. There are several types of commercially available statin drugs widely used in patients as cholesterol-reducing agent [26,27]. A number of *in vitro* and *in vivo* studies suggest that statins have an anabolic and antiresorptive effect on bones [28–31]. Piskin et al. [30] investigated the use of simvastatin (SIM) (a widely used statin) in spiral-wound polycaprolactone scaffolds. Their results exhibited osseous tissue integration within the implant and mineralized bone restoration of the calvarium. Thylin et al. [31] incorporated 2.2 mg of simvastatin into methylcellulose gels prior to implantation into a murine calvarial model. After 22 and 44 days, a significant increase (up to 180%) was observed in bone formation with the statin eluting group in comparison to the gel only controls.

A number of studies have been reported in the literature that focused on PCL composite containing different forms of bioactive materials. However, to the best of our knowledge, the present one is the first dealing with electrospun PCL nanofibers containing BG nanoparticles and SIM to evaluate their bioactivity and drug release properties. For this purpose the electrospinning technique was used to fabricate a novel nanocomposite nanofibrous web from PCL solution incorporating BG nanoparticles and SIM for drug delivery systems in bone regeneration applications. The morphological and mechanical properties of the nanofibrous web were investigated and its *in vitro* bioactivity and drug release characteristic were evaluated in simulated body fluids.

2. Materials and methods

2.1. Materials

Poly (ε-caprolactone) PCL (average Mw: 80,000) was purchased from Aldrich Company (US). BG nanoparticles, with the properties as described in Ref. [32] were the courtesy of the Biomaterials Research Group, Isfahan University of Technology, Iran. SIM was kindly provided by Amin Pharmaceutical Co. (Iran). Chloroform and methanol (Aldrich, US) were used as received.

2.2. Nanocomposite nanofibers fabrication

BG nanoparticles were dispersed in the mixtures of chloroform/methanol with ratios of 1/1, 2/1, 3/1 and 4/1 v/v and stirred for 6 h with a magnetic stirrer. Into these nanoparticles dispersions was added and dissolved the weighed amount of PCL to obtain 7.5, 8.5 and 9.5 wt% polymer composite solutions, which were then stirred overnight. The percentage of the nanoparticles added was varied from 0 to 20 wt% of the PCL content. The composite solution thus prepared was sonicated for 20 min for further dispersion and SIM, which is freely soluble in chloroform/methanol, was added just before electrospinning to the composite solution (SIM concentration in all samples was 6 wt% of the PCL content) which was drawn into a syringe having a needle gauge 23. Elecrospinning was carried out at a flow rate of 1.32 ml/h using a high DC voltage of 16 kV at a distance of 22 cm and the nanofibers were collected on the rotating drum. The electrospun nanofibrous web was dried in a vacuum oven for 24 h and then kept in the desiccator.

2.3. Viscosity measurement

Viscosity measurements were accomplished using the Rheometer (BROOKFIELD DV-IIPRO, USA) at 25 °C and 5 rpm and results were reported as the average and standard deviation of three measurements.

2.4. Morphology characterization

The morphology of as-spun nanofibers was studied using scanning electron microscopy (SEM) (AIS-2100, SERON TECH, Korea 2008). Samples were coated with gold using an automatic sputter

coater and their morphology was observed by SEM. The average diameter of electrospun nanofibers was determined by measurement of 100 single nanofibers from the SEM image using Microstructure Measurement software.

2.5. Differential scanning calorimetry (DSC)

DSC can be employed to determine the effects of BG concentration on the melting point and the crystallinity degree of PCL nanocomposite nanofibers as well as the state of the drug in the nanofibers. DSC measurements were taken using a TA-INSTRUMENT 2010 (USA) instrument. The sample was heated from 0 °C to 200 °C at a constant temperature increment of 10 °C/min and purged with nitrogen gas at 30 ml/min.

Crystallinity degree, X_C, was calculated as:

$$X_C = \Delta H_m\ (\mathrm{J/g}) / \Delta H_{m^\circ}\ (\mathrm{J/g})$$

where ΔH_m (J/g) is the enthalpy of melting derived from DSC curves, and ΔH_{m° (J/g) is the enthalpy of melting 100% crystalline polymer. For PCL, ΔH_{m° (J/g) is 139.5 J/g [33].

2.6. Mechanical characterization

Nanofibrous webs were cut into the rectangular dimensions of 10 mm width and 60 mm length. Tensile test of nanofibrous webs was conducted by Zwick 1446-60 tensiometer with a 40 mm gauge length. For each formulation, five samples at the cross-speed head of 50 mm/min were tested and tensile strength and strain at break were calculated based on the stress–strain curves of each sample. Results were reported as an average and standard deviation of five measurements.

2.7. Degradation measurements

In vitro degradation of nanofibrous web was studied by measuring the weight loss of each specimen after submerging in the phosphate buffer saline (PBS) over the test periods. The buffer solution was prepared from 0.2 M potassium phosphate monobasic and a small amount of NaOH in order to simulate the physiological environment. In these experiments, nanocomposite nanofibrous webs with dimensions of 250 mm × 250 mm were placed in a plastic container filled with PBS (pH = 7.4) at 37 °C over different time periods. The initial weight of the specimens was measured prior to immersion tests (W_0). After each degradation period, the sample was washed, dried in a vacuum oven at room temperature for 24 h, and weighed (W_t). The weight loss percentage was calculated as follows:

$$\text{Weight loss}\% = 100 \times (W_0 - W_t)/W_0 \quad (1)$$

An average of three measurements was taken for each sample.

2.8. In vitro drug release studies

The electrospun nanofibrous webs were cut into specimens of 250 mm × 250 mm which were then accurately weighed and placed in 10 ml of pre-warmed PBS (pH = 7.4) at 37 °C. At predetermined time periods, 3 ml of PBS release media was removed for sampling and replaced with fresh PBS. The amount of released drug was determined spectrophotometrically using a Shimadzu UVmini 1240 spectrophotometer (Japan) at a wavelength of 238 nm (wavelength of maximum absorbance of SIM in PBS). Three samples in each condition were used for the *in vitro* drug-release tests, and the data were represented as means value and standard deviation.

The calibration curve of SIM in PBS was determined by taking absorbance versus SIM concentration between 0 and 32 μg ml^{-1}. For this interval, the calibration curve fits the Lambert and Beers' law:

$$A = 0.0441C + 0.0717,$$

where A is absorbance and C designates concentration (μg ml^{-1}).

2.9. In vitro bioactivity assessment

The assessment of *in vitro* bioactivity of nanocomposite nanofibers was carried out in the SBF. The SBF has a composition and ionic concentration similar to those of human body plasma (containing NaCl, $NaHCO_3$, KCl, $MgCl_2$, HCl, $CaCl_2$, Na_2SO_4, Na_2HPO_4 and $(CH_2OH)_3(CNH)_2$ as the buffering agent) which was prepared according to the procedure described in Kokubo et al. [34]. SBF was buffered at pH 7.4 with tris (hydroxymethyl aminomethane) and 1 M hydrochloric acid at 37 °C. Nanofibrous webs were cut into samples of 10 × 10 mm^2 and subsequently immersed in 100 ml SBF in a polyethylene bottle at 37 °C for different time periods (7, 14, and 28 days). After soaking, the nanofibrous webs were removed from SBF, rinsed with distilled water, and dried at room temperature. Formation of bone like apatite layer on the surface of nanocomposite webs was determined by X-ray diffraction (XRD), scanning electron microscopy coupled with energy dispersive spectroscopy (SEM–EDS). XRD patterns of the nanofiber surface were made using a Philips Xpert MPD system (Netherlands). The diffractometer was operated at 40 kV and 30 mA at a 2θ range of 0–50° employing a step size of 0.02.

2.10. Statistical analysis

Statistical significance in this study was evaluated using a one-way ANOVA analysis with a post hoc Least Square Difference (LSD) test. A value of $p < 0.05$ was considered to be statistically significant.

3. Results and discussion

3.1. Preparation and characterization of nanofibers

This study focuses on the electrospinning of nanocomposite nanofibers with the objective of assessing their bioactivity and drug release capability as indicators of their potential application for bone tissue regeneration. Electrospinning of PCL has been suc-

Table 1
Dependence of nanofiber morphology on PCL concentration and solvent ratio.

Chloroform/methanol ratio (v/v)	Polymer concentration (wt%)	Nanofiber morphology
1/1	7.5	Fiber formation failure
	8.5	Fiber formation failure
	9.5	Fiber formation failure
2/1	7.5	Beaded nanofiber with non-uniform diameter
	8.5	Beaded nanofiber
	9.5	Beaded nanofiber with non-uniform diameter
3/1	7.5	Nanofiber with non-uniform diameter
	8.5	Bead-free nanofiber with uniform diameter
	9.5	Beaded nanofiber with non-uniform diameter
4/1	7.5	Fiber formation failure
	8.5	Beaded nanofiber
	9.5	Beaded nanofiber

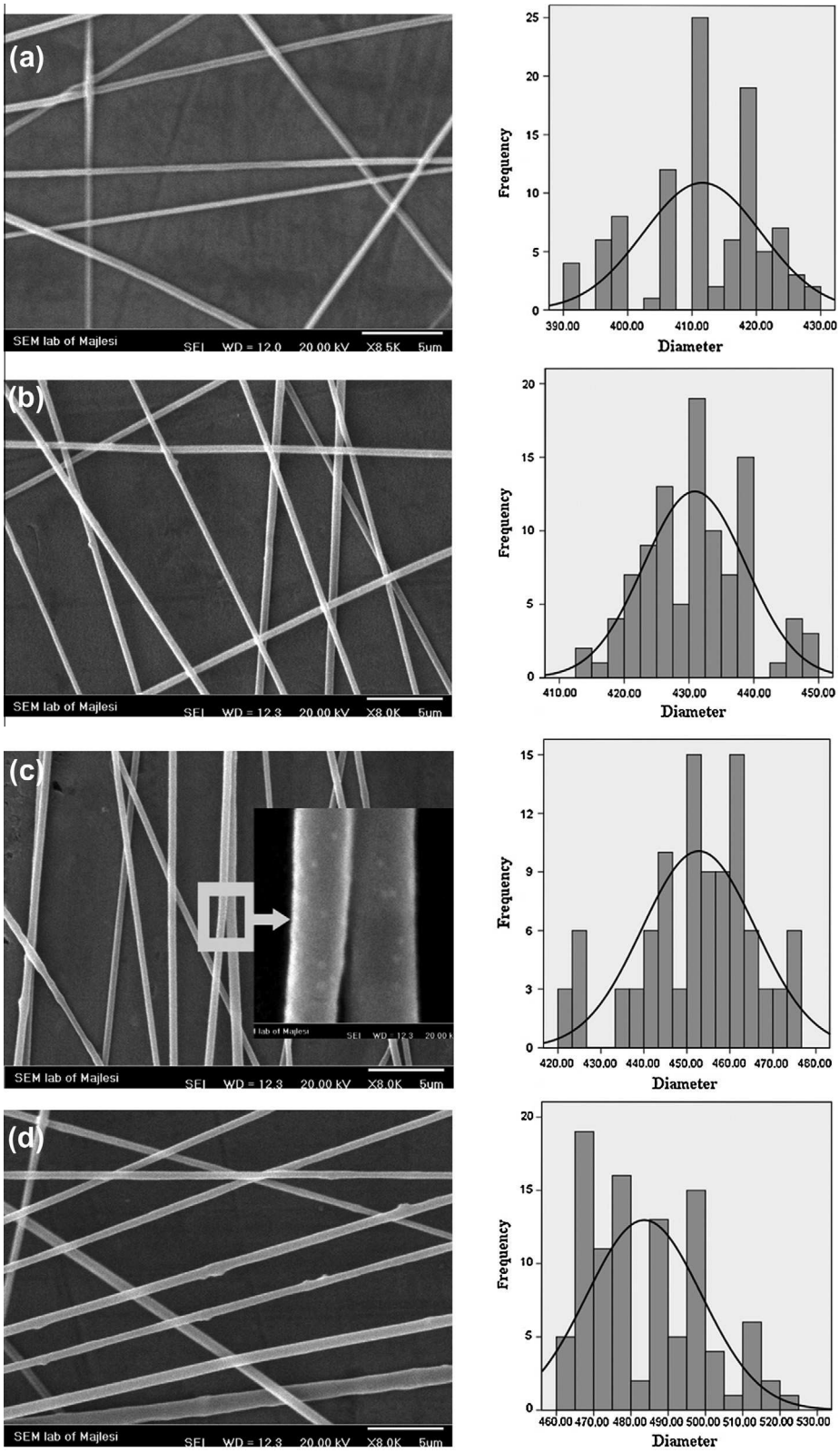

Fig. 1. Selected scanning electron micrographs of as-spun nanofibers from PCL nanocomposite containing 6 wt% SIM and (a) 0%, (b) 5%, (c) 15% and (d) 20% BG.

cessfully carried out in various solvents such as dichloromethane/DMF, chloroform/ethanol and dichloromethane/methanol [5,9–11]. In the present work, due to the good solubility of SIM in methanol, a mixture of chloroform and methanol was used as the solvent for the preparation of PCL/BG solutions as well as for the preparation of PCL/SIM and PCL/SIM/BG mixtures for electrospinning. At first, in order to optimize PCL concentration and chloroform/methanol ratio, electrospinning of solutions with different PCL concentration at different solvent ratios were carried out. The results of these experiments are summarized in Table 1. As

Table 2
Solution viscosity and nanofiber diameter with different BG contents.

Sample	Solution viscosity (cp)	Average diameter (nm)
PCL/SIM/0%BG	134.4 ± 0.15	411.59 ± 0.09
PCL/SIM/5%BG	156.6 ± 0.22	430.89 ± 0.07
PCL/SIM/15%BG	159 ± 0.22	452.78 ± 0.13
PCL/SIM/20%BG	170.4 ± 0.13	483.57 ± 0.15

Table 3
Thermal properties of neat PCL and PCL nanocomposite web derived from DSC thermograms.

Sample	T_m (°C)	ΔH_m (J/g)	X_C (%)
PCL/SIM/0%BG	60.04	80.82	57.89
PCL/SIM/5%BG	63.06	82.77	59.29
PCL/SIM/15%BG	61.55	90.93	65.13

shown in this table, fiber forming ability (spinnability) was increased by increasing chloroform/methanol ratio from 1/1 to 3/1 v/v and also bead-free nanofiber with uniform diameter can be obtained only at 8.5 wt% PCL and chloroform/methanol ratio of 3/1 v/v. Therefore the solvent ratio of 3/1 v/v and polymer concentration of 8.5 wt% were selected as optimum parameters for further experiments. Thus PCL polymeric solutions containing 6 wt% SIM and different concentrations of BG (0–20 wt% with respect to PCL) in the mixture of chloroform/methanol (3/1 v/v) were successfully electrospun to produce nanofibers. Fig. 1 shows selected SEM images of as-spun nanofibers of PCL containing different concentrations of BG and 6 wt% SIM. The effects of BG nanoparticle concentration on solution viscosity and on the diameter of the resulting nanofibers are shown in Table 2. According to this table, increasing nanoparticle content significantly ($p < 0.05$) increased solution viscosity from 134.4 cp to 170.4 cp. Similar results have been reported by Fujihara and coworkers [35]; they prepared PCL nanofibers containing $CaCO_3$ nanoparticles and observed that by increasing the nanoparticle concentration compared to that of PCL, solution viscosity and, consequently, fiber diameter increased. Einstein [36] pointed out that the presence of rigid particles increased the shear viscosity of dilute suspensions compared to that of neat liquids. Solution viscosity determined by polymer concentration and additives has a significant effect on the final fiber diameter and morphology. This is revealed by the measurement results in Table 2 and SEM images and fiber diameter distribution shown in Fig 1; average diameter of nanofibers increased significantly ($p < 0.05$) from 411 to 483 nm by increasing BG concentration from 0 to 20 wt% of the PCL content. This must be the result of the increased viscosity of the spinning solution due to the presence of the nanoparticles. As shown in Fig 1c, some BG nanoparticles could be observed on the nanofiber surface without any agglomeration, however according to these figures, by increasing BG concentration from 15 to 20 wt%, the fiber morphology changed from a smooth and uniform fiber structure to a non-uniform fiber structure and agglomeration of nanoparticles appear to have taken place.

3.2. Differential scanning calorimetry (DSC)

DSC studies were also performed on the PCL/BG, PCL/SIM and PCL/SIM/BG nanofibers to investigate the effect of BG nanoparticles on the structural properties of PCL matrix as well as the physical state of SIM in the electrospun nanofibers. As seen in Fig. 2, the PCL nanofiber without BG has an endothermic peak at around 60 °C which is associated with the melting point of the PCL polymer [21,37]. The same peak is also seen in the PCL nanofibers containing BG thermograms, with the difference that its place has slightly shifted but the change does not follow any particular pattern. It is well accepted that mechanical and physical properties of crystalline polymers are governed by the supra molecular morphology which is, in turn, controlled by the crystallization process [5]. Thus, it is necessary to study the crystallization behavior of the nanocomposite fibers in order to establish their structure/property correlations. The results of DSC analysis are summarized in Table 3. It is clear that when nanoparticles were incorporated into the nanofibers, the melting enthalpy (ΔH_m J/g) of PCL nanofibers increased from 80.82 J/g to 82.77 J/g and 90.93 J/g and crystallinity degree (X_C %) increased from 57.89% to 59.29% and 65.13% for BG concentration of 5% and 15 wt%, respectively. These results show that the presence of nanoparticles increases the crystallinity of PCL due to the nucleating properties of nanoparticles in the polymer matrix.

In Fig. 3, DSC thermograms are shown for SIM drug, nanocomposite nanofibers without SIM, and nanocomposite nanofibers containing SIM. As can be seen, SIM thermogram has an endothermic peak at about 140 °C that is related to SIM's melting point [30], but the peak, corresponding to crystalline drug, disappears in the thermogram of nanofibers containing SIM. These findings suggest that SIM was molecularly dispersed or dispersed in an amorphous state in the nanofibers.

3.3. Mechanical properties

Analysis of the mechanical properties of the nanocomposite fibrous webs is necessary for understanding their performance in

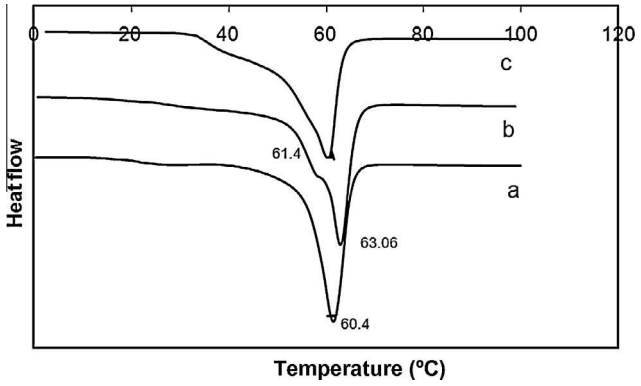

Fig. 2. DSC thermograms of PCL nanofibers containing 6 wt% SIM and (a) 0%, (b) 5%, and (c) 15% BG nanoparticles.

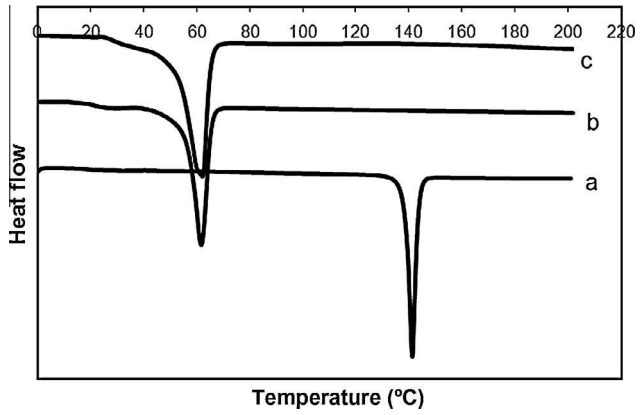

Fig. 3. DSC thermograms of (a) pure SIM, (b) pure PCL nanocomposite nanofibers, and (c) 6 wt% SIM-loaded PCL nanocomposite nanofibers.

the bone regeneration scaffold. In this work, the mechanical properties of PCL nanocomposite webs were measured in both tensile and strain modes and then compared with those of neat PCL. Table 4 summarizes tensile strength and strain at break. According to the table, tensile strength for PCL without BG was 2.3 MPa, which significantly ($p < 0.05$) increased to 3.45 MPa by increasing the nanoparticles concentration to 15 wt% due to the reinforcement effect of BG (ceramic materials have stiffer mechanical properties than polymers) within the polymer matrix while the tensile strain at break decreased. Any further increase in the nanoparticle content up to 20% resulted in a decrease in strength (although it was still higher than that of neat PCL nanofibers), suggesting that there is a threshold limit for BG concentration beyond which the nanoparticles caused a defective situation rather than reinforcing the polymer matrix, so that the nanocomposite became more brittle. These results are in good agreement with those reported in studies on electrospun nanohybrids [13,14,19,20]. It may be concluded that there is a limit to the nanoparticle concentration at which BG nanoparticles can improve the mechanical properties of the PCL nanofibrous web.

3.4. Degradation measurement

In vitro biodegradation was studied by measuring the weight loss of the nanofibrous web in PBS at 37 °C during incubation time. The results of biodegradation measurements are demonstrated in Fig. 4 in which weight loss % (calculated from Eq. (1)) is plotted versus incubation time for both the neat and PCL nanocomposite nanofibrous webs. As shown in this figure, after 28 days, the weight loss was only 4% in the case of PCL without BG, while it was higher in the case of the nanocomposite nanofibers over the same period. Increasing BG concentration (from 5% to 20%) led to the increased weight loss from 21% to 40% in the nanocomposite nanofiber after 28 days. Generally, polymer degradation kinetics is affected by their chemical and structural characteristics. As PCL is a hydrophobic and highly crystalline polyester, it does not allow fast water penetration into the PCL bulk. Though the mechanism of PCL degradation is known to be a random hydrolytic chain scission of the ester linkage [20,33], the degradation rate is relatively low. Incorporation of a glass phase in the polymer matrix increases its capacity to absorb water during the incubation period and, consequently, increases its hydrolytic degradation [19] so that the weight loss of the PCL nanocomposite nanofibrous webs will be higher than that of neat PCL nanofibrous web.

3.5. In vitro drug release

Fig. 5 shows SIM release profiles of both neat PCL nanofibers and nanocomposite nanofibrous webs containing 6 wt% drug. In the neat PCL nanofiber, two phases can be observed in the release behavior, an initial rapid release followed by very slow release. In the first phase, 47.3% of the SIM was released into the PBS medium after 36 h, and in the second release phase, only 8.8% of the loaded drug was released within 144 h. PCL is a hydrophobic and semi-crystalline polymer and, as shown in previous section, it exhibits a low degradation rate. On the other hand, as also indicated by the DSC results, SIM, being a hydrophobic drug (its solubility in water is about 0.03 g/l), was molecularly dispersed in the PCL polymer matrix (SIM has a good compatibility with PCL). The release of hydrophobic drugs from hydrophobic polymers is a very slowly process; hence, the rather slow release of total SIM from PCL.

Miyajima et al. [38,39] suggested that the drug would undergo a biphasic release stage, including an initial diffusion phase from the polymeric matrix and a second diffusion phase from the aqueous pores formed in the polymer. For the PCL nanofibers without nanoparticles, initial release rate was high in the first stage due to the high concentration of the drug near the nanofiber surface, but the diffusional release rate through the pores in the second stage was very low due to both the low PCL degradation rate and the low pore formation rate; hence, the total quantity of drug released during the test was minimal.

As shown in Fig. 5, increased quantities of the nanoparticles led to the decreased rate of the initial release while over prolonged periods, the total quantity of the drug released increased; i.e., the total SIM released during the 180 h increased from 56.1% to 88% when BG content increased from 0% to 20%. According to the results from diameter measurement, the presence of BG nanoparticles in nanofibers increased their diameter and, consequently, the release path through the nanofibers increased. On the other hand,

Table 4
Mechanical properties of PCL nanofibrous web containing different concentrations of BG.

Sample	Tensile strength (MPa)	Strain at break (%)
PCL/SIM/0%BG	2.3 ± 0.16	119.04 ± 0.16
PCL/SIM/5%BG	2.97 ± 0.17	103.45 ± 0.19
PCL/SIM/10%BG	3.31 ± 0.08	108.06 ± 0.03
PCL/SIM/15%BG	3.45 ± 0.15	96.09 ± 0.23
PCL/SIM/20%BG	2.66 ± 0.26	70.43 ± 0.24

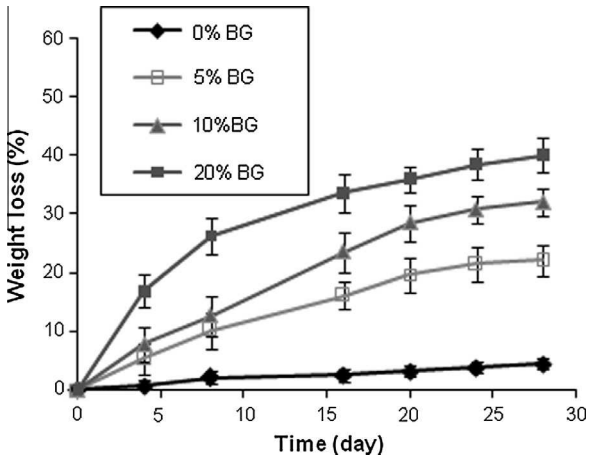

Fig. 4. Weight loss of the PCL nanofiber containing different concentrations of BG after incubation in PBS.

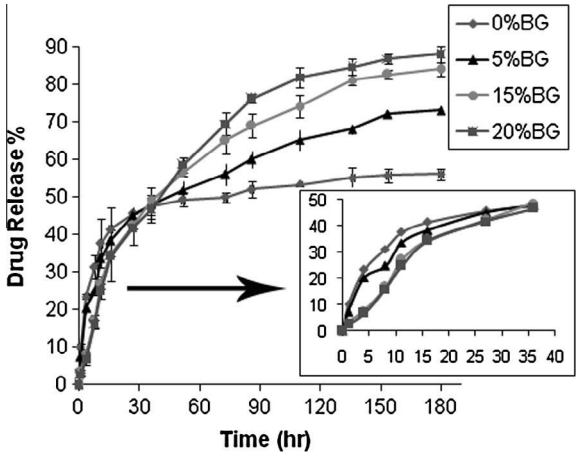

Fig. 5. Influence of BG content on the drug release profile of PCL nanofibers after incubation in PBS. The inset shows a magnification of the first 40 h.

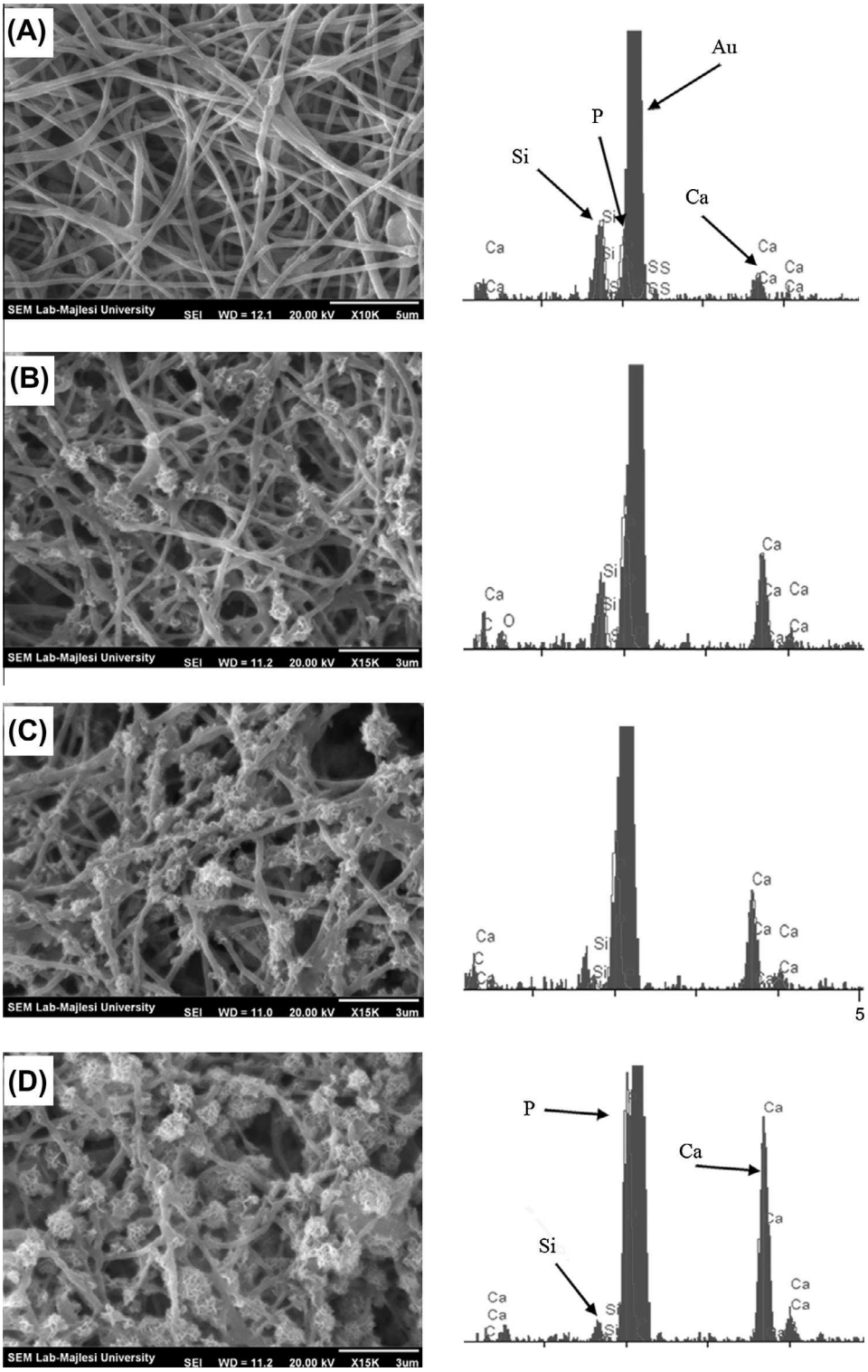

Fig. 6. SEM–EDS micrographs of nanocomposite nanofibers containing 15 wt% BG, (A) before and after, (B) 7, (C) 14 and (D) 28 days soaking in SBF.

DSC results showed that crystallinity of the nanofibers increased when nanoparticles were added to nanofibers. Drugs may be incorporated into the amorphous regions of semicrystalline polymers such as PCL, and therefore, drug release occurs firstly from these regions [11]. Thus, the higher crystallinity of PCL nanofibers containing BG supports the lower release rate. Increasing BG nanoparticle concentration, therefore, decreases the initial release rate (diffusion from the polymeric matrix). Since BG nanoparticles are hydrolyzed in the biological fluid, water uptake by the electrospun nanofiber is, therefore, enhanced and, indicated by the biodegradation test results, PCL degradation rate is increased. Water uptake and degradation rate play crucial roles in drug release as the process can be a direct one via material degradation. With higher water uptake, the structure would be more openly spaced and easier for drugs to diffuse out. Material degradation also accelerates drug diffusion by offering big open channels. Therefore, addition

of BG nanoparticles enhances drug release from the nanocomposite nanofibers over prolonged periods.

The results of this study show that this novel nanocomposite nanofibrous web can release SIM in a controlled manner, making it especially suitable as a controlled drug delivery device.

3.6. In vitro bioactivity

The inorganic part of the human bone is hydroxycarbonate apatite, and a significant characteristic of bioactive materials is their ability to bond with living bone through the formation of an apatite interface layer [21]. The mechanisms of apatite formation upon contact of bioactive glass with SBF or PBS have been discussed extensively in the literature. The process involves five stages which occur very rapidly on the surface of bioactive glass particles because of fast ion exchange of alkali ions with hydrogen ions from the liquid medium (stage 1), glass network dissolution (stage 2), silica-gel polymerization (stage 3), and chemisorption and crystallization of the carbonated hydroxyapatite layer (stages 4 and 5). The detailed analysis of the reactions involved has been presented by Hench [40]. In the present study, bioactive glass nanoparticles were incorporated in PCL nanofiber to form the nanocomposite nanofibrous web and its bioactivity was investigated in SBF. SEM–EDS images of the nanocomposite nanofibrous web surface before and after soaking in SBF at 37 °C over different incubation times (7, 14, and 28 days) are shown in Fig. 6. After soaking for 7 days, the surface morphology of the nanocomposite nanofiber changed and some new tiny materials appeared on the nanofiber surface. After prolonged immersion of 2 and 4 weeks, these new materials grew and the surface of the nanofibers was almost totally covered with the precipitates. This morphology is typical of hydroxyapatite, which has been reported to grow on the surface of bioactive glass/polymer composite scaffold after incubating in SBF [14,21,34]. EDS analysis of nanofibrous web surface before and after soaking in SBF allows the relative concentration (in mol%) of silicon, calcium and phosphorus to be determined. Both a decrease in silicon peak height and an increase in calcium and phosphorus peak height were observed as the immersion times in SBF increased (Fig. 6), an observation which confirms the formation of a calcium phosphate layer [14,41] (the Au peak came from the sputtering before SEM characterization and overlaps with the phosphorus peak).

The apatite formed on the surfaces of the nanofiber was confirmed by XRD. XRD may be used to analyze crystalline materials and has been extensively used for apatite and other biomedical materials. Fig. 7 shows the XRD patterns of the nanocomposite nanofibrous webs before and after soaking in SBF over different time periods. As shown in Fig. 7, there are two diffraction peaks observed in all the samples related to the crystalline phase of PCL (PCL is a semicrystalline polymer with two diffraction peaks, around 21° and 23° [17,18]). After soaking in SBF, two more crystalline peaks at $2\theta = 26°$ and $2\theta = 32°$ started to appear which increased with immersion time, indicated by the increase in peak height and the peaks becoming more resolved. These two peaks could be assigned to the reflection of an apatite phase [14,41,42].

As mentioned above, SEM images showed that new materials formed on the nanofiber surfaces after soaking in SBF and XRD patterns confirmed that these new materials are hydroxyapatite. Data obtained by means of SEM–EDS and XRD point to the formation of a hydroxyapatite layer on the surface of the nanocomposite nanofibers when they were soaked in SBF; this is a very interesting property for bone tissue engineering applications.

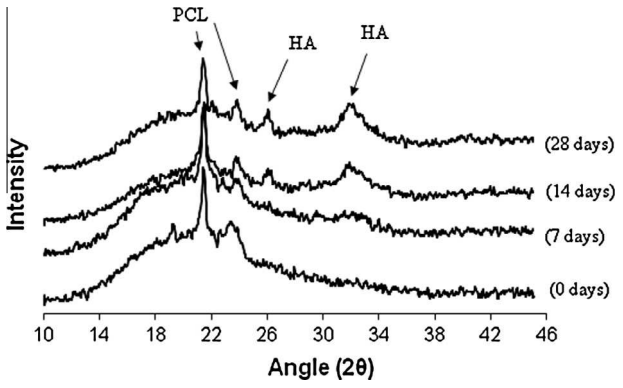

Fig. 7. XRD patterns of the nanocomposite nanofibers containing 15 wt% BG before and after soaking in SBF for different time periods.

4. Conclusion

A novel PCL nanocomposite nanofibrous web containing BG nanoparticles and SIM drug with controlled drug release has been fabricated using the electrospinning technique. The viscosity of the spinning solution and the electrospun fiber diameter increased with the addition of increasing amounts of the nanoparticles. Incorporation of BG nanoparticles significantly increased tensile strength but decreased strain at break of the nanocomposite web. The presence of BG nanoparticles increased the crystallinity degree of PCL nanofibers, and DSC results also showed that SIM was dispersed in the molecular state through the PCL matrix. Nanofiber biodegradation and drug release rate were found to be affected by BG nanoparticles concentration; the initial SIM release rate from nanocomposite nanofiber decreased as compared to that from neat nanofibers; however, more SIM was released from the nanocomposite nanofibers over prolonged incubation periods. Based on the release results, PCL nanofibers containing BG could release SIM in a controlled manner. The nanocomposite nanofibrous web demonstrated excellent bioactivity, inducing the precipitation of bone like apatite mineral on its surface under a simulated physiological medium. It is concluded that prepared novel nanocomposite nanofibrous web may be used as a potential scaffold in such applications as controlled drug release and bone tissue regeneration.

Acknowledgments

The authors express their sincere gratitude to the Isfahan University of Technology for the financial support. This project was also supported by the Isfahan Pharmaceutical Sciences Research Center.

References

[1] Z. Zhang, J. Hu, P.X. Ma, Nanofiber-based delivery of bioactive agents and stem cells to bone sites, Adv. Drug Deliv. Rev. 65 (2012) 1129–1141.
[2] A. Abdal-hay, L.D. Tijing, J.K. Lim, Characterization of the surface biocompatibility of an electrospun nylon 6/CaP nanofiber scaffold using osteoblasts, Chem. Eng. J. 215–216 (2013) 57–64.
[3] H.R. Pant, P. Risal, C.H. Park, L.D. Tijing, Y.J. Jeong, C.S. Kim, Core–shell structured electrospun biomimetic composite nanofibers of calcium lactate/nylon-6 for tissue engineering, Chem. Eng. J. 221 (2013) 90–98.
[4] N.A.M. Barakat, M.F. Abadir, F.A. Sheikh, M.A. Kanjwal, S.J. Park, H.Y. Kim, Polymeric nanofibers containing solid nanoparticles prepared by electrospinning and their applications, Chem. Eng. J. 156 (2010) 487–495.
[5] A. Bianco, E.D. Federico, I. Moscatelli, A. Camaioni, I. Armentano, L. Campagnolo, et al., Electrospun poly(ε-caprolactone)/Ca-deficient hydroxyapatite nanohybrids: microstructure, mechanical properties and cell response by murine embryonic stem cells, Mater. Sci. Eng. C 29 (2009) 2063–2071.
[6] H.W. Kim, H.H. Lee, G.S. Chun, Bioactivity and osteoblast responses of novel biomedical nanocomposites of bioactive glass nanofiber filled poly (lactic acid), J. Biomed. Mater. Res. A 85 (2008) 651–663.

[7] F. Yang, J.G.C. Wolke, J.A. Jansen, Biomimetic calcium phosphate coating on electrospun poly (e-caprolactone) scaffolds for bone tissue engineering, Chem. Eng. J. 137 (2008) 154–161.
[8] N. Charernsriwilaiwat, P. Opanasopit, T. Rojanarata, T. Ngawhirunpat, Lysozyme-loaded, electrospun chitosan-based nanofiber mats for wound healing, Int. J. Pharm. 427 (2012) 379–384.
[9] Z.M. Huang, C.L. He, A. Yang, Y. Zhang, X.J. Han, J. Yin, et al., Encapsulating drugs in biodegradable ultrafine fibers through co-axial electrospinning, J. Biomed. Mater. Res. A 77 (2006) 169–179.
[10] M. Zamani, M. Morshed, J. Varshosaz, M. Jannesari, Controlled release of metronidazole benzoate from poly e-caprolactone electrospun nanofibers for periodontal diseases, Eur. J. Pharm. Biopharm. 75 (2010) 179–185.
[11] E.L. Van, L. Grondahl, K.N. Chua, K.W. Leong, V. Nurcombe, S.M. Cool, Controlled release of heparin from poly(e-caprolactone) electrospun fibers, Biomaterials 27 (2006) 2042–2050.
[12] L.C. Ionescu, G.C. Lee, B.J. Sennett, J.A. Burdick, R.L. Mauck, An anisotropic nanofiber/microsphere composite with controlled release of biomolecules for fibrous tissue engineering, Biomaterials 31 (2010) 4113–4120.
[13] M.V. Jose, V. Thomas, K.T. Johnson, D.R. Dean, E. Nyairo, Aligned PLGA/HA nanofibrous nanocomposite scaffolds for bone tissue engineering, Acta Biomater. 5 (2009) 305–315.
[14] A.R. Boccaccini, V. Maquet, Bioresorbable and bioactive polymer/bioglass composites with tailored pore structure for tissue engineering applications, Compos. Sci. Technol. 63 (2003) 2417–2429.
[15] J. Schnieders, U. Gbureck, R. Thull, T. Kissel, Controlled release of gentamicin from calcium phosphate-poly(lactic acid-co-glycolic acid) composite bone cement, Biomaterials 27 (2006) 4239–4249.
[16] Z. Hong, R.L. Reis, J.F. Mano, Preparation and *in vitro* characterization of scaffolds of poly(L-lactic acid) containing bioactive glass ceramic nanoparticles, Acta Biomater. 4 (2008) 1297–1306.
[17] H.W. Kim, J.C. Knowles, H.E. Kim, Effect of biphasic calcium phosphates on drug release and biological and mechanical properties of poly(e-caprolactone) composite membranes, J. Biomed. Mater. Res. A 70 (2004) 467–479.
[18] P. Fabbri, F. Bondioli, M. Messori, C. Bartoli, D. Dinucci, F. Chiellini, Porous scaffolds of polycaprolactone reinforced with in situ generated hydroxyapatite for bone tissue engineering, J. Mater. Sci: Mater. Med. 21 (2010) 343–351.
[19] H.W. Kim, E.J. Lee, I.K. Jun, H.E. Kim, J.C. Knowles, Degradation and drug release of phosphate glass/polycaprolactone biological composites for hard-tissue regeneration, J. Biomed. Mater. Res. B: Appl. Biomater. 75B (2005) 34–41.
[20] F. Causa, P.A. Netti, L. Ambrosio, G. Ciapetti, N. Baldini, S. Pagani, et al., Poly-e caprolactone/hydroxyapatite composites for bone regeneration: *in vitro* characterization and human osteoblast response, J. Biomed. Mater. Res. A 76 (2006) 151–162.
[21] X. Li, J. Shi, X. Dong, L. Zhang, H. Zeng, A mesoporous bioactive glass/polycaprolactone composite scaffold and its bioactivity behavior, J. Biomed. Mater. Res. A 84 (2008) 84–91.
[22] S.K. Misra, D. Mohn, T.J. Brunner, W.J. Stark, S.E. Philip, I. Roy, et al., Comparison of nanoscale and microscale bioactive glass on the properties of P(3HB)/bioglass composites, Biomaterials 29 (12) (2008) 1750–1761.
[23] N. Singh, A. Karambelkar, L. Gu, K. Lin, J.S. Miller, C.S. Chen, et al., Bioresponsive mesoporous silica nanoparticles for triggered drug release, J. Am. Chem. Soc. 133 (2011) 19582–19585.
[24] D.S. Jones, C.P. McCoy, G.P. Andrews, Physicochemical and drug diffusion analysis of rifampicin containing polyethylene glycol–poly (e-caprolactone) networks designed for medical device applications, Chem. Eng. J. 172 (2011) 1088–1095.
[25] M.J. Webber, J.B. Matson, V.K. Tamboli, S.I. Stupp, Controlled release of dexamethasone from peptide nanofiber gels to modulate inflammatory response, Biomaterials 33 (2012) 6823–6832.
[26] D.I. Chasman, D. Posada, L. Subrahmanyan, N.R. Cook, V.P. Jr Stanton, P.M. Ridker, Pharmacogenetic study of statin therapy and cholesterol reduction, J. Am. Med. Assoc. 291 (2004) 2821–2827.
[27] U. Rauch, J.I. Osende, J.H. Chesebro, V. Fuster, D.A. Vorchheimer, K. Harris, et al., Statins and cardiovascular diseases: the multiple effects of lipid-lowering therapy by statins, Atherosclerosis 153 (2000) 181–189.
[28] D.S. Benoit, C.R. Nuttelman, S.D. Collins, K.S. Anseth, Synthesis and characterization of a fluvastatin-releasing hydrogel delivery system to modulate hMSC differentiation and function for bone regeneration, Biomaterials 27 (2006) 6102–6110.
[29] F. Adah, H. Benghuzzi, M. Tucci, G. Russell, B. England, Cholesterol production inhibitor (statin) increased bone healing in surgically created femoral defect in an animal model, Biomed. Sci. Instrum. 43 (2007) 95–103.
[30] E. Piskin, A. Isoglu, N. Bolgen, I. Vargel, S. Griffiths, T. Cavusoglu, et al., In vivo performance of simvastatin-loaded electrospun spiral-wound polycaprolactone scaffolds in reconstruction of cranial bone defects in the rat model, J. Biomed. Mater. Res. A 90 (2009) 1137–1151.
[31] M.R. Thylin, J.C. McConnell, M.J. Schmid, R.R. Reckling, J. Ojha, I. Bhattacharyya, et al., Effects of simvastatin gels on murine calvarial bone, J. Periodontol. 73 (2002) 1141–1148.
[32] M.H. Fathi, A. Doostmohammadi, Bioactive glass nanopowder and bioglass coating for biocompatibility improvement of metallic implant, J. Mater. Process. Technol. 209 (2009) 1385–1391.
[33] C.G. Pitt, F.I. Chasalow, Y.M. Hibionada, D.M. Klimas, A. Schindler, Aliphatic polyesters I. The degradation of poly(e-caprolactone) in vivo, J. Appl. Polym. Sci. 26 (1981) 3779–3787.
[34] T. Kokubo, H. Takadama, How useful is SBF in predicting in vivo bone bioactivity?, Biomaterials 27 (2006) 2907–2915
[35] K. Fujihara, M. Kotaki, S. Ramakrishna, Guided bone regeneration membrane made of polycaprolactone/calcium carbonate composite nano-fibers, Biomaterials 26 (2005) 4139–4147.
[36] A. Einstein, Annu. Phys. 19 (1906) 289–306.
[37] S. Yang, K. Leong, C. Chua, The design of scaffolds for use in tissue engineering. Part 1. Traditional factors, Tissue Eng. 7 (2001) 679–689.
[38] M. Miyajima, A. Koshika, J. Okada, A. Kusai, M. Ikeda, Factors influencing the diffusion-controlled release of papaverine from poly(l-lactic acid) matrix, J. Control. Release 56 (1998) 85–94.
[39] M. Miyajima, A. Koshika, J. Okada, M. Ikeda, Mechanism of drug release from poly(l-lactic acid) matrix containing acidic or neutral drugs, J. Control. Release 60 (1999) 199–209.
[40] L.L. Hench, Bioceramics: from concept to clinic, J. Am. Ceram. Soc. 74 (1991) 1487–1510.
[41] M. Vallet-Regí, A.M. Romero, C.V. Ragel, R.Z. LeGeros, XRD, SEM–EDS, and FTIR studies of *in vitro* growth of an apatite-like layer on sol–gel glasses, J. Biomed. Mater. Res. 44 (1999) 416–421.
[42] I. Rehman, J.C. Knowles, W. Bonfield, Analysis of *in vitro* reaction layers formed on bioglass using thin-film X-ray diffraction and ATR–FTIR microspectroscopy, J. Biomed. Mater. Res. 41 (1998) 162–166.

Journal of Dispersion Science and Technology

ISSN: 0193-2691 (Print) 1532-2351 (Online) Journal homepage: https://www.tandfonline.com/loi/ldis20

Preparation and Characterization of Microparticles Containing Simvastatin Solid Dispersions in Eudragit E 100 and Poly(3-Hydroxybutyrate)

Bianca R. Pezzini , Sacha K. Schucko , Iára C. Schmücker , Melissa Zétola , Theodoro M. Wagner , Gilmar S. Erzinger & Giovana C. Bazzo

To cite this article: Bianca R. Pezzini , Sacha K. Schucko , Iára C. Schmücker , Melissa Zétola , Theodoro M. Wagner , Gilmar S. Erzinger & Giovana C. Bazzo (2013) Preparation and Characterization of Microparticles Containing Simvastatin Solid Dispersions in Eudragit E 100 and Poly(3-Hydroxybutyrate), Journal of Dispersion Science and Technology, 34:11, 1603-1608, DOI: 10.1080/01932691.2012.681998

To link to this article: https://doi.org/10.1080/01932691.2012.681998

Published online: 23 Oct 2013.

Journal of Dispersion Science and Technology, 34:1603–1608, 2013

ISSN: 0193-2691 print/1532-2351 online
DOI: 10.1080/01932691.2012.681998

Taylor & Francis
Taylor & Francis Group

Preparation and Characterization of Microparticles Containing Simvastatin Solid Dispersions in Eudragit E 100 and Poly(3-Hydroxybutyrate)

Bianca R. Pezzini, Sacha K. Schucko, Iára C. Schmücker, Melissa Zétola, Theodoro M. Wagner, Gilmar S. Erzinger, and Giovana C. Bazzo

Department of Pharmacy, University of Joinville Region, Joinville, Brazil

GRAPHICAL ABSTRACT

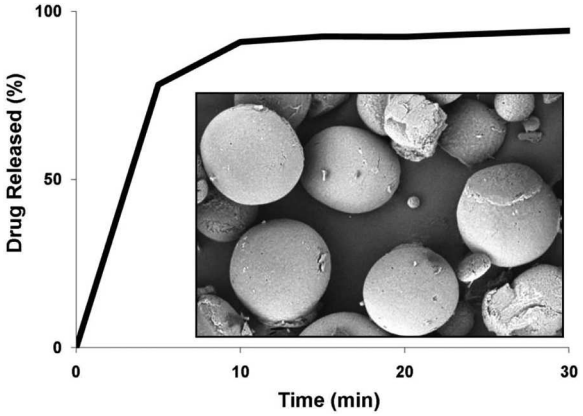

The aim of this study was to prepare fast-dissolving microparticles containing solid dispersions of simvastatin (SIM) in Eudragit E 100 (EU) and poly(3-hydroxybutyrate) (PHB) and to characterize them using the dissolution test, scanning electron microscopy, x-ray powder diffractometry, and infrared spectroscopy. Four formulations of microparticles were obtained by the emulsion-solvent evaporation method using different proportions of EU and PHB. All formulations caused a significant increase in the SIM dissolution rate, the best performance being obtained with that containing SIM/EU/PHB in the ratio of 1:3.8:0.6. The characterization of the formulations showed that SIM was in the amorphous state, which increases the drug dissolution.

Keywords Eudragit E 100, microparticles, PHB, simvastatin, solid dispersion

INTRODUCTION

Oral drug delivery is the simplest and easiest way to administer medicines. However, this route requires the dissolution of the drug in the gastrointestinal fluids prior to absorption, this process being indispensable for drug bioavailability and therapeutic effect.[1] This principle is critical for drugs belonging to class II of the Biopharmaceutical Classification System (BCS), that is, those with low water solubility and high gastrointestinal permeability, the bioavailability of which can be enhanced by improving the dissolution profile.[1,2]

Solid dispersions, one of the most efficient systems used to improve the water solubility of drugs, involve the dispersion of a hydrophobic drug in hydrophilic carriers in solid state,[3,4] polyvinylpyrrolidone and polyethylene glycol being the most commonly used carriers.[1,5,6]

The main techniques applied to obtain solid dispersions are melting the drug and carrier, followed by cooling and pulverization of the molten mixture, or dissolving the drug and carrier in a volatile solvent and then evaporating it.[1,5,6] However, there are some limitations associated with these methods, such as the use of high melting

Received 26 January 2012; accepted 6 March 2012.

Financial support from the Conselho Nacional de Desenvolvimento Científico e Tecnológico (CNPq) and Fundo de Apoio à Pesquisa da UNIVILLE is gratefully acknowledged.

Address correspondence to Bianca R. Pezzini, Departamento de Farmácia, Universidade da Região de Joinville, Rua Paulo Malschitzki no.10, Campus Universitário, Zona Industrial, CEP. 89219-710, Joinville-SC, Brazil. E-mail: bianca.ramos@univille.br

temperatures, which can lead to the degradation of the drug or the use of large amounts of organic solvents, which are difficult to subsequently reduce to an acceptable level.[1,7]

It is also difficult to scale up the preparation of final products from solid dispersions. The soft and tacky properties of solid dispersion powders result in poor flow, mixing and compaction characteristics, which may complicate the operations and result in poor reproducibility of the physicochemical properties of the final products.[7]

In this context, several modifications of melting and solvent evaporation methods and the use of alternative carriers have been proposed in order to solve manufacturing difficulties and stability problems.[1,7]

A poorly explored technique is microencapsulation by emulsion-solvent evaporation, which involves: 1) dissolution of the hydrophobic drug in an organic solvent containing the polymeric carrier; 2) emulsification of this organic phase in an aqueous phase; 3) solvent extraction by evaporation, transforming droplets of the internal phase of the emulsion into solid particles; and 4) recovery and drying of microparticles to eliminate the residual solvent.[8]

Eudragit E 100 (EU) is a cationic polymer based on dimethylaminoethyl methacrylate and other neutral methacrylic acid esters applied in the pharmaceutical field as a tablet coating for protection and taste masking.[9] Poly(3-hydroxybutyrate) [PHB] is a biosynthetic polyester that is very useful in the drug delivery field due to its biodegradability and biocompatibility.[10]

The present study aimed to obtain fast-dissolving microparticles containing solid dispersions of simvastatin (SIM), a class II drug according to the BCS, in EU and PHB. EU was selected as a carrier material due to its high solubility in acidic medium, since the aim was that the microparticles dissolve as soon as they reach the stomach. PHB was added to the formulations to improve the physical and morphological characteristics, based on preliminary studies. The obtained microparticles were characterized using the dissolution test, scanning electron microscopy, infrared spectroscopy, and powder x-ray diffractometry.

EXPERIMENTAL

Materials

SIM was purchased from Henrifarma (São Paulo, SP, Brazil) and poly(vinylalcohol) (PVA) was obtained from Vetec (Rio de Janeiro, RJ, Brazil). EU was donated by Almapal (São Paulo, SP, Brazil) and poly(3-hydroxybutyrate) by PHB Industrial (Serrana, SP, Brazil). All of the other chemicals were of analytical grade.

Preparation of Solid Dispersions

Solid dispersions containing SIM were prepared by the emulsion solvent-evaporation method, with varying ratios of SIM/EU/PHB, as shown in Table 1. The drug and polymers were dissolved in 10 mL of dichloromethane (organic phase) and then slowly added to the aqueous phase (200 mL of 0.15% w/v PVA) under stirring at around 1000 rpm. The emulsion was kept under magnetic stirring at room temperature for 24 hours until complete evaporation of dichloromethane and formation of microparticles. The microparticles were washed three times with distilled water and dried at room temperature.

TABLE 1
2^2 factorial design that originated the formulation compositions of F1 to F4

	Factors[a]		Composition (g)		
Formulations	A	B	SIM	EU	PHB
F1	−	−	0.400	0.750	0.125
F2	+	−	0.400	1.500	0.125
F3	−	+	0.400	0.750	0.250
F4	+	+	0.400	1.500	0.250

[a]Factors: (A) SIM:EU ratio; (B) SIM:PHB ratio.
Levels: A: (−) 1:1.9 (+) 1:3.8; B: (−) 1:0.3 (+) 1:0.6.

Factorial Design

Four formulations (F1–F4) of solid dispersion microparticles containing SIM, EU, and PHB were obtained according to a 2^2 factorial design (Table 1), aiming at elucidating the effects of the SIM:EU ratio (factor A: levels 1:1.9 or 1:3.8) and SIM:PHB ratio (factor B: levels 1:0.3 or 1:0.6) on SIM release. The amount of drug dissolved in 15 minutes ($Q\%_{15min}$) was used to evaluate the rate of drug dissolution. The main effects of the factors were analyzed and those which were statistically significant were identified by ANOVA ($\alpha = 0.05$).[11,12] Calculations were carried out using Microsoft Office Excel software.

Drug Content and Loading Efficiency

An amount of microparticles equivalent to 5 mg of SIM was accurately weighed and then dissolved and diluted in dichloromethane to achieve a drug concentration of 10 mg/L. The solution was analyzed in a UV-visible spectrophotometer (Shimadzu 1601 PC, Kyoto, Japan) at 240.5 nm and the SIM content present in the microparticles was obtained from a calibration curve. The loading efficiency (LE%) was obtained using Equation (1). The experiments were carried out in triplicate.

$$LE\% = \frac{drug\ found\ in\ microparticles\ (mg)}{drug\ initially\ added\ to\ the\ formulation\ (mg)} \times 100 \quad [1]$$

In Vitro Dissolution Studies

Hard gelatin capsules were filled with isolated SIM (5 mg), the SIM/EU/PHB physical mixture (PM), and SIM microparticles (equivalent to 5 mg of the drug). Dissolution tests were performed using the basket apparatus at 100 rpm and 500 mL of 0.1 N HCl, pH 1.2, at 37°C. At predetermined time intervals (5, 10, 15, 20, 40, and 60 minutes), a 10 mL sample of the medium was taken, centrifuged and the drug concentration in the solution was determined using a UV-Visible spectrophotometer (Shimadzu 1601 PC, Kyoto, Japan) at 238.5 nm. Experiments were carried out in triplicate.

Scanning Electron Microscopy (SEM)

Microparticles were mounted onto stubs using double-sided adhesive tape and coated with gold. Samples were analyzed using a Zeiss DSM 940 A scanning electron microscope (Oberkochen, Germany) to observe the surface and cross-section morphology. Images were captured at an excitation voltage of 20 kV at several magnifications.

The arithmetic mean diameter (spherical microparticles) or the arithmetic mean ratio between length and width (irregular microparticles and spherical microparticle fragments) was measured on micrographs obtained by SEM. Results are expressed as mean ± standard deviation (SD) or median ± quartile deviation of 100 determinations.

The Kolmogorov-Smirnov test was used to establish whether the samples came from populations with a normal size distribution (Easy Fit Professional Software, version 5.5, Mathwave Technologies, Dnepropetrovsk, Ukraine). The Grubbs' test was performed to detect the presence of outliers (Graph Pad Software, Quick Calcs–Online Calculators for Scientists, GraphPad Software, Inc., San Diego, CA, USA).

X-Ray Powder Diffraction Analysis (XRPD)

Diffractograms were recorded from 5° to 80° (2θ) at a scanning speed of 2° min^{-1} with an x-ray powder diffractometer (Shimadzu XRD-6000, Kyoto, Japan). Cu Kα radiation was used as the x-ray source and the equipment was operated at a voltage of 40 kV and a current of 30 mA.

Infrared Spectroscopy

Samples were mixed thoroughly with KCl (1:8w/w).The mixtures were then compressed in a hydraulic press (Til Macron MPH-30, SP, Brazil), producing the sample disks. Scans were taken from 400 to 4000 cm^{-1}, using a Perkin Elmer 1420 spectrometer (Norwalk, CT, USA).

RESULTS AND DISCUSSION

Microparticle Size and Morphology

Shape and size are very important properties of particles since they affect the flowability and packability of powders, consequently affecting the manufacturing process of solid dosage forms. In order to achieve uniformity, for example, in terms of the tablet weight, the feed particles must flow and pack smoothly into the die cavity of the tablet machine.[13]

It is generally accepted that the larger the particles, the better the flow. Thus, particles larger than 250 μm are usually free flowing; particles smaller than 100 μm become cohesive; and particles less than 10 μm are extremely cohesive.[13,14]

In addition, powders with similar particle sizes but dissimilar shapes can have markedly different flow properties owing to differences in interparticle contact areas. It is generally believed that the flowability of powders decreases as the shapes of particles become more irregular.[13]

On the basis of the above information, it can be concluded that the preparation of solid dispersions as spherical microparticles would improve the scalability of the manufacturing process of the final product.

In our preliminary studies, brittle microparticles and large agglomerates were obtained when EU was used alone for SIM microencapsulation. Thus, we used PHB to improve the physical and morphological characteristics of the microparticles.

The SEM micrographs and particle size distribution are shown in Figures 1 and 2. Microparticles of the F1 and F4 formulations had a spherical shape, with mean particle sizes of 86 ± 25 μm and 141 ± 50 μm, respectively. F2 showed high particle size variation, exhibiting agglomerates formed by small intact microspheres and fragments of large microspheres with mean particle size of 68 ± 48 μm. The particle sizes of F1, F2, and F4 had

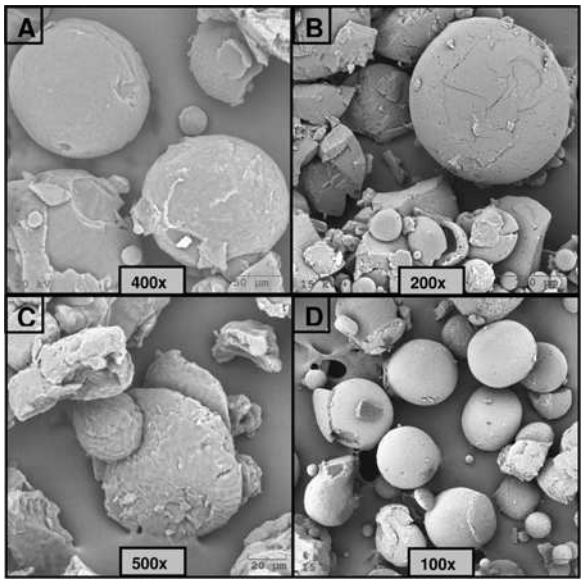

FIG. 1. Scanning electron micrographs of SIM/EU/PHB microparticles: (A) F1, (B) F2, (C) F3 and (D) F4. (Figure available in color online.)

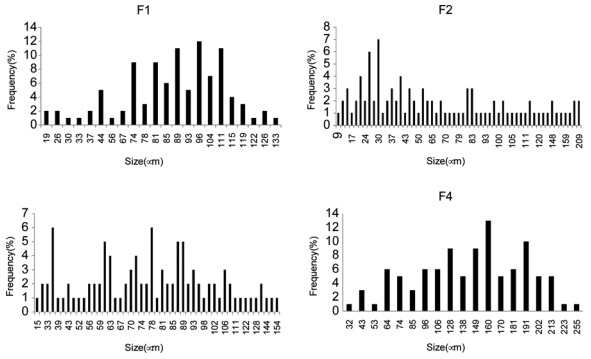

FIG. 2. Histograms of particle size distribution of F1 to F4 microparticle formulations.

normal distributions ($p > 0.05$) and no outliers were detected ($p > 0.05$). F3 had an irregular shape, with a particle size of 78 ± 16 μm, expressed as the median ± quartile deviation since the particle size of this formulation did not have a normal distribution ($p < 0.05$).

The difference in the microparticle size could be caused by the concentration of polymers in the internal phase of the emulsion.[15] In this case, F4 microparticles showed a larger size than the other formulations because of the higher concentration of polymers in the internal phase, which made the solution more viscous and therefore less easily fragmented into small droplets.

The surface morphologies observed for the microparticle formulations were: F1 (porous and wrinkled), F2 (porous and cracked), F3 (wrinkled and heterogeneous), and F4 (homogeneous and smooth). Also, there was an absence of SIM crystals at the surface and in the cross-section of the microparticles of F1 to F4, suggesting that the drug was present in an amorphous state.

Our findings led us to believe that the spherical shape and larger particle size of F4 could favor the production of solid dosage forms such as tablets, in comparison with F1 to F3.

Drug Content and Loading Efficiency

The loading efficiency and SIM content of the microparticles are presented in Table 2. All formulations had loading efficiencies of between 90 and 103%, indicating that the process conditions used to prepare the solid dispersion microparticles were efficient in obtaining high drug contents.

In Vitro Dissolution Studies

Dissolution profiles of isolated SIM and the F1 to F4 microparticle formulations are shown in Figure 3. All formulations displayed a considerably higher drug dissolution compared with the isolated SIM. The best result was achieved for F4, which released more than 90% of the drug in 15 minutes, while the dissolution of isolated SIM was only 26.6% in 1 hour. The simple association of the drug and the polymers could not have been responsible for the dissolution performance of F4 microparticles, since the dissolution profile of the corresponding physical mixture (PM) showed a $Q\%_{15\text{min}}$ of 19.7% and 46.5% of drug dissolved over 1 hour (Figure 3). These results clearly indicate that microencapsulation with EU and PHB strongly improved the dissolution profile of SIM.

TABLE 2
Loading efficiency of SIM in the microparticles

Formulation	Loading efficiency (%)[a]
1	90.1 ± 5.6
2	101.2 ± 1.3
3	101.5 ± 4.6
4	103.3 ± 3.9

[a]The loading efficiency was calculated in relation to isolated SIM used to prepare the microparticles, which was considered 100% in content.

Results expressed as the mean ± SD of three determinations.

The statistical analysis of the main effects of the SIM:EU (factor A) and SIM:PHB (factor B) ratios on the drug release are shown in Figure 4. These data, together with the ANOVA ($\alpha = 0.05$) results shown in Table 3, indicate that both factors caused significant positive effects on $Q\%_{15\text{min}}$ (extracted from the dissolution curves) and that, of these two factors, the SIM:PHB ratio was the main factor that influenced the response. Also, they indicate that there was no significant effect of the interaction between the studied factors on the drug release.

Several approaches to enhancing the dissolution rate of SIM have been investigated, two of them being reported by Jun et al.[16] and Zhang et al.[17] In the first study, tablets containing a SIM/hydroxypropyl-β-cyclodextrin inclusion complex showed 73.6% of drug dissolved in 10 minutes

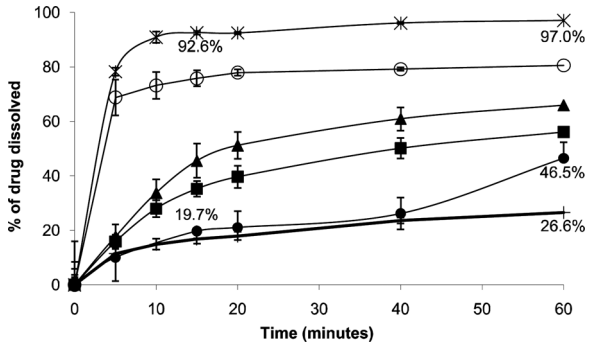

FIG. 3. Dissolution profiles of (+) SIM, (■) F1, (▲) F2, (○) F3, (∗) F4, and (●) physical mixture (PM). Each data point represents the mean ± SD of three determinations.

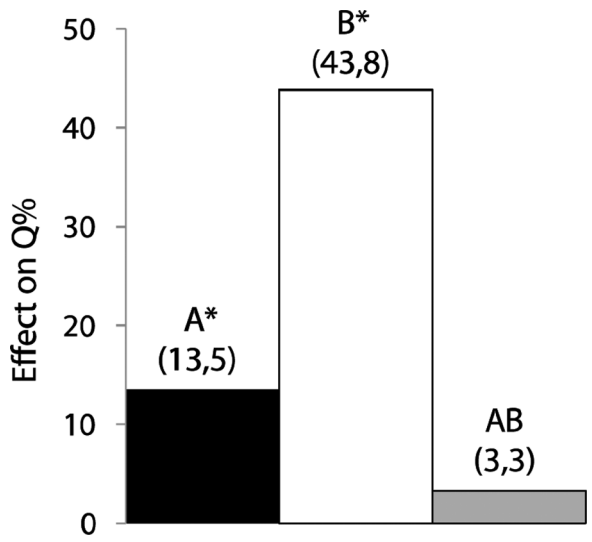

FIG. 4. Analysis of the effect of (A) SIM:EU ratio and (B) SIM:PHB ratio on Q% at 15 minutes. *Statistically significant ($P < 0.05$).

and 84.2% in 30 minutes, while tablets containing isolated SIM presented corresponding values of 4.1 and 13.3%.[16] In the second study, spherical mesocellularfoam nanoparticles loaded with SIM showed 89% of drug dissolved in 20 minutes, while the dissolution of isolated SIM was 17% in 1 hour.[17] In both studies, the in vitro drug release study was conducted using the paddle apparatus at 100 rpm and 900 mL of phosphate buffer (pH = 6.8) as the dissolution medium.

A comparison of the results obtained in this study with those reported by Jun et al.[16] and Zhang et al.[17] indicated that the F4 microparticle formulation presented an excellent drug dissolution profile, although the dissolution studies were conducted under different conditions.

Solid state characterization of microparticles was carried out by infrared spectroscopy and XRPD to explain the considerable enhancement of the drug dissolution attained in the present study.

TABLE 3
Summary of analysis of variance results obtained using the amount of drug released in 15 minutes ($Q\%_{15min}$) as the dependent variable

Source	SS[a]	df[b]	MS[c]	$F_{calculated}$	$F_{critical}$	P-value
A	548.1	1.0	548.1	35.3	5.3	$P < 0.05$
B	5750.9	1.0	5750.9	370.2		
AB	32.3	1.0	32.3	2.1		
Error	124.3	8.0	15.5			
Total	6455.7	11.0	586.9			

$F_{calc} > F_{crit}$ = statistically significant effect.
[a]SS (sum of squares); [b]df (degrees of freedom); [c]MS (mean square).

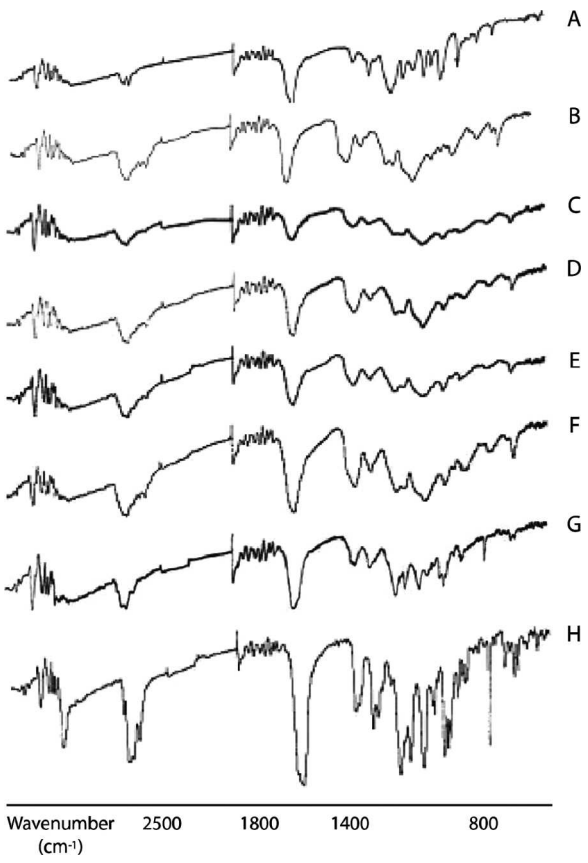

FIG. 5. Infrared spectra of (A) PHB, (B) EU, (C) F1, (D) F2, (E) F3, (F) F4, (G) physical mixture, and (H) isolated SIM.

Infrared Spectroscopy

The infrared spectra for the SIM, EU, PHB, physical mixture (SIM/EU/PHB proportion equivalent to F4) and the F1 to F4 solid dispersion microparticles can be observed in Figure 5. The SIM peak corresponding to the stretching vibration at 780 cm^{-1} was selected to characterize SIM in the microparticles because it was not overlapped with the polymer peaks. This specific peak was observed on the infrared spectrum for the physical mixture but was not found in the case of the spectra for the F1 to F4 microparticles, suggesting an interaction between SIM and the polymers in all microparticle formulations, which could lead to the amorphization of the drug.

X-Ray Powder Diffraction Analysis

XRPD was used to evaluate the crystallinity of the SIM, the physical mixture (SIM/EU/PHB proportion equivalent to F4) and the F1 to F4 solid dispersion microparticles, and the diffractograms are compared in Figure 6. Many diffraction peaks with high intensity at 2θ of 9.3°, 17.2°,

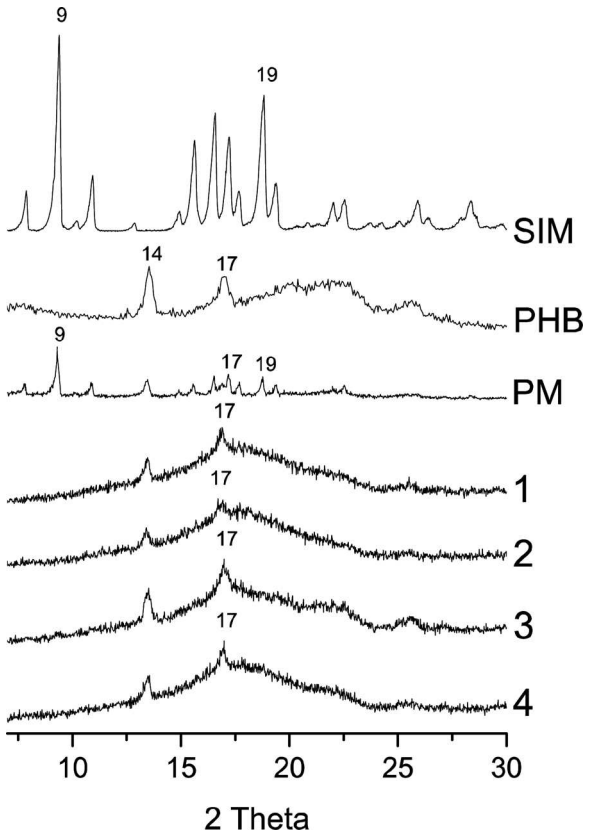

FIG. 6. X-ray powder diffraction patterns for isolated SIM, PHB, physical mixture and F1 to F4 microparticle formulations.

18.8°, and 22.6° can be seen in the diffraction pattern for the pure SIM due to its crystalline state, as reported in the literature.[17] On the other hand, the characteristic peaks of SIM at 2θ of 9.3° and 18.8° present on the diffractogram for the SIM/EU/PHB physical mixture were not present on those for F1 to F4, confirming that SIM was present in the amorphous form in the microparticles. The peaks at 2θ of 13.5° and 16.9° on the diffractograms for the physical mixture and the F1 to F4 microparticles correspond to the crystalline structure of PHB, which presents a high degree of crystallinity.[18] Other studies have confirmed that the crystallinity of PHB is maintained when it is used to prepare microparticles through the emulsion solvent evaporation technique,[18,19] as observed in this study.

CONCLUSIONS

The association of Eudragit E 100 and poly(3-hydroxybutyrate) as inert carriers in solid dispersion microparticles promoted the fast dissolution of simvastatin. The ratio between SIM:EU and SIM:PHB influenced the drug dissolution rate, the optimal performance being obtained for a proportion of SIM:EU:PHB corresponding to 1:3.8:0.6. The considerable SIM dissolution enhancement observed for the microparticles in comparison with isolated SIM was explained by the drug being in the amorphous state in the solid dispersion, which is more soluble compared with the crystalline state.

SIM:EU:PHB (1:3.8:0.6) microparticles also had spherical shape and mean particle size of $141 \pm 50\,\mu m$, characteristics that could favor the production of solid dosage forms. Considering the final dosage form of the solid dispersion microparticles, the tablet is the most appropriate in terms of the advantages related to its production and application. Thus, in the next step of our research we will attempt to develop tablets from these solid dispersion microparticles.

REFERENCES

[1] Vasconcelos, T., Sarmento, B., and Costa, P. (2007) *Drug Discov. Today*, 12: 1068–1075.
[2] Waard, H., Hinrichs, W.L.J., Visser, M.R., Bologna, C., and Frijlink, H.W. (2008) *Int. J. Pharm.*, 349: 66–73.
[3] Craig, D.Q.M. (2002) *Int. J. Pharm.*, 231: 131–144.
[4] Li, P. and Zhao, L. (2007) *Int. J. Pharm.*, 341: 1–19.
[5] Leuner, C. and Dressman, J. (2000) *Eur. J. Pharm. Biopharm.*, 50: 47–60.
[6] Van den Mooter, G., Weuts, I., Ridder, T., and Blaton, N. (2006) *Int. J. Pharm.*, 316: 1–6.
[7] Sun, N., Wei, X., Wu, B., Chen, J., Lu, Y., and Wu, W. (2008) *Powder Technol.*, 182: 72–80.
[8] Li, M., Rouaud, O., and Poncelet, D. (2008) *Int. J. Pharm.*, 363: 26–39.
[9] Quinteros, D.A., Rigo, V.R., Kairuz, A.F.J., Olivera, M.E., Manzo, R.H., and Allemandi, D.A. (2008) *Eur. J. Pharm. Sci.*, 33: 72–79.
[10] Zinn, M., Witholt, B., and Egli, T. (2001) *Adv. Drug Delivery Rev.*, 53: 5–21.
[11] Bolton, S. (1997) *Pharmaceutical Statistics: Practical and Clinical Applications*; Nova York: Marcel Dekker.
[12] Montgomery, D.C. (1997) *Design and Analysis of Experiments*; New York: John Wiley & Sons.
[13] Nokhodchi, A., Maghsoodi, M., Hassan-Zadeh, D., and Barzegar-Jalali, M. (2007) *Powder Technol.*, 175: 73–81.
[14] Liu, L.X., Marziano, I., Bentham, A.C., Litster, J.D., White, E.T., and Howes, T. (2008) *Int. J. Pharm.*, 362: 109–117.
[15] Thompson, C.J., Hansford, D., Higgins, S., Rostron, C., Hutcheon, G.A., and Munday, D.L. (2007) *Int. J. Pharm.*, 329: 53–61.
[16] Jun, S.W., Kim, M., Kim, J., Park, H.J., Lee, S., Woo, J., and Hwang, S. (2007) *Eur. J. Pharm. Biopharm.*, 66: 413–421.
[17] Zhang, Y., Zhang, J., Jiang, T., and Wang, S. (2011) *Int. J. Pharm.*, 410: 118–124.
[18] Martin, M.A., Miguens, F.C., Rieumont, J., and Sanchez, R. (2000) *Colloids Surf. B*, 17: 111–116.
[19] Bidone, J., Melo, A.P.P., Bazzo, G.C., Carmignan, F., Soldi, M., Pires, A.T.N., and Lemos-Senna, E. (2009) *Mater. Sci. Eng. C*, 29: 588–593.